Electronic Nose Instrumentation for Biomedical Applications

By

Siavash Esfahani

Dissertation Submitted for the Degree of

Doctor of Philosophy

School of Engineering

February 2018

Content

List of Figures

List of Tables

Declaration

This thesis is submitted to the University of Warwick in support of the application for the degree of Doctor of Philosophy. It has not been submitted in part, or in whole, for a degree or other qualification at any other University. Parts of this thesis are published by the author in peer-reviewed research papers listed. Apart from commonly understood and accepted ideas, or where reference is made to the work of others, the work described in this thesis is carried out by the author in School of Engineering of the University of Warwick.

Siavash Esfahani

2014-2018

To mum and dad

Khorso & Setareh

تقدیم به پدر و مادر عزیز و مهربانم

که در سختی‌ها و دشواری‌های زندگی همواره یاری دلسوز و

فداکار و پشتیبانی محکم و مطمئن برایم بوده‌اند.

خسرو و ستاره

همراهان همیشگی و پشتوانه های زندگیم.

Acknowledgement

First, I would like to thank my PhD supervisor, Prof James Covington, without whom this PhD would not have been possible. Undertaking this PhD in the exciting field of Electronic Nose, has provided me with experience that I am hugely grateful for, and, without doubt, James is the sole recipient of this gratitude. Again, thank you James, I sincerely hope that our professional relationship can continue in the future.

For their technical wisdom, I must thank Frank Courtney, Ian Griffith, and Gavin Downs who helped me immensely throughout my PhD studies. Without their technical support it would not have been possible to develop the systems.

I would also like to specially thank Dr Christos Mias, who's enthusiasm for and knowledge of electronics was a huge inspiration for me and his support during my PhD studies at the University of Warwick was invaluable.

Special thanks go to my colleagues and friends Samuel Agbroko, Dr Chris Purssell, Akira Tile, Dr Emma Daulton, Wangi Pandan Sari, Alfian Wicaksono, Rhys Jones, Erfan Bashar and Dr Simon Leigh for all the support and happiness that you brought. Huge thanks go to my old friends Sadra Mobayyen, Saber Poustchi, Vahid Mehri, Omid Doustdar, Soroush Afyouni, Habib Ganjgahi, Golnaz Nematbakhsh and Faraneh Ardian for all your encouragements and support.

I would also like to thank my second family Manijeh, Siamak, Roxanna, Roozbeh, Aydin and Zarina who were always there for me and supported me through hard times.

In the end, unreserved thanks and gratitude must go to my lovely family. I can't find any word to thank my mum, Nahid and dad, Mohammad Taghi for their unconditional love and support throughout my life. I would also like to thank my brother, Khosro and sister, Setareh for supporting me constantly and caring for me.

Lastly, but obviously not least, I would also like to thank my partner, Yeganeh, for being with me all the time, supporting and encouraging me during my PhD and without her, I wouldn't be able to finish this thesis. Thanks for being with me.

Publication List

1. **Esfahani, S.**; Sagar, N.M.; Kyrou, I.; Mozdiak, E.; O'Connell, N.; Nwokolo, C.; Bardhan, K.D.; Arasaradnam, R.P.; Covington, J.A. "Variation in gas and volatile compound emissions from human urine as it ages, measured by an electronic nose". *Biosensors* 2016, *6*, 4.

2. Tiele, A.; **Esfahani, S.**; Covington, J. A.; "Design and development of a low-cost, portable, monitoring device for indoor environment quality". Journal of Sensors, Accepted 25 December 2017

3. **Esfahani, S.**; Covington, J.A. In Low cost optical electronic nose for biomedical applications, Multidisciplinary Digital Publishing Institute Proceedings, 2017; p 589.

4. **Esfahani, S.**; Skinner, J.; Savage, R.; O'Connell, N.; Kyrou, I.; Nwokolo, C.; Bardhan, K.; Arasaradnam, R.; Covington, J. A rapid discrimination of diabetic patients from volunteers using urinary volatile and an electronic nose. ISOEN conference, 2015, 51-52

5. Chapter 4 and 6 of this thesis are in progress of publication in Elsevier journal.

Abstract

The growing rate of diabetes and undiagnosed diabetes related diseases is becoming a worldwide major health concern. The motivation of this thesis was to make use of a technology called the 'electronic nose' (eNose) for diagnosing diseases. It presents a comprehensive study on metabolic and gastro-intestinal disorders, choosing diabetes as a target disease. Using eNose technology with urinary volatile organic compounds (VOCs) is attractive as it allows non-invasive monitoring of various molecular constituents in urine. Trace gases in urine are linked to metabolic reactions and diseases. Therefore, urinary volatile compounds were used for diagnosis purposes in this thesis. The literature on existing eNose technologies, their pros and cons and applications in biomedical field was thoroughly reviewed, especially in detecting headspace of urine.

Since the thesis investigates urinary VOCs, it is important to discover the stability of urine samples and their VOCs in time. It was discovered that urine samples lose their stability and VOCs emission after 9 months. A comprehensive study with 137 diabetic and healthy control urine samples was done to access the capability of commercially available eNose instruments for discrimination between these two groups. Metal oxide gas sensor based commercial eNose (Fox 4000, AlphaMOS Ltd) and field asymmetric ion mobility spectrometer (Lonestar, Owlstone Ltd) were used to analyse volatiles in urinary headspace. Both technologies were able to distinguish both groups with sensitivity and specificity of more than 90%.

Then the project moved onto developing a Non-dispersive infrared (NDIR) sensor system that is non-invasive, low-cost, precise, rapid, simple and patient friendly, and can be used at both hospitals and homes. NDIR gas sensing is one of the most widely used optical gas detection techniques. NDIR system was used for diagnosing diabetes and gastro related diseases from patient's wastes. To the best of the authors' knowledge, this is the first and only developed tuneable NDIR eNose system. The developed optical eNose is able to scan the whole infrared range between 3.1μm and 10.5 μm with step size of 20 nm.

To simulate the effect of background humidity and temperature on the sensor response, a gas test rig system that includes gas mixture, VOC generator, humidity generator and gas analyser was designed to enable the user to have control of gas flow, humidity and temperature. This also helps to find out system's sensitivity and selectivity.

Finally, after evaluating the sensitivity and selectivity of optical eNose, it was tested on simple and complex odours. The results were promising in discriminating the odours. Due to insufficient sample batches received from the hospital, synthetic urine samples were purchased, and diabetic samples were artificially made. The optical eNose was able to successfully separate artificial diabetic samples from non-diabetic ones.

List of Abbreviations

Electronic Nose	eNose
Analogue Front End	AFE
Appropriate Operational Code	APC
Area Under Curve	AUC
Bile Acid Diarrhoea	BAD
Carbon Dioxide	CO2
Central Wavelength	CW
Colorectal cCancer	CRC
Control Voltage	CV
Counter Electrode	CE
Crohn's Disease	CD
Diarrhoea-Predominant IBS	D-IBS
Differential Absorption LIDAR	DIAL
Differential Optical Absorption Spectroscopy	DOAS
Digital to Analogue Convertor	DAC
Drift-Tube Ion Mobility Spectrometry	DT-IMS
Electrochemical	EC
Electron Capture Detectors	ECD
Fabry-Perot Filter	FPF
Fabry-Pérot Interferometry	FPI
Fasting Plasma Glucose	FPG
Field Asymmetric Ion Mobility Spectrometry	FAIMS
Fisher Discriminant Analysis	FDA
Flame Ionization Detectors	FID
Gas Chromatography	GC
Gas Chromatography Mass Spectrometry	GCMS
Gastroesophageal Reflux Disease	GERD
Gastrointestinal	GI
Glycated Protein	A1C

High-Density Lipoprotein	HDL
Impaired Glucose Tolerance	IGT
Infectious Diarrhoea	ID
Inflammatory Bowel Disease	IBD
Infrared	IR
Interdigital Transducers Deposited	ITD
Intra-Cavity Absorption Spectrometry	ICAS
Ion Mobility Spectrometry	IMS
Irritable Bowel Syndrome	IBS
Light Detection and Ranging	LIDAR
Linear Discriminant Analysis	LDA
Linear Discriminant Function	LDF
Maple Syrup Urine Disease	MSUD
Mass Flow Controller	MFC
Mass Flow Meter	MFM
Mass Spectroscopy	MS
Metal Oxides Semi-conducting	MOS
Metal-Oxide	MOX
Methane	CH4
Microcontroller	MCU
National Diabetes Audit	NDA
Negative Predictive Value	NPV
Neural Network	NN
Non-dispersive infrared	NDIR
Operational Code	OPC
Oral Glucose Tolerance Test	OGTT
Osmetech Microbial Analyzer	OMA
Partial Least Square–Discriminant Analysis	PLS-DA
Parts Per Billion	PPB
Parts Per Million	PPM
Positive Predictive Value	PPV
Principal Component Analysis	PCA
Principal Component Analysis	PCA

Process Variable	PV
Quartz Crystal Microbalance	QCM
Random Plasma Glucose	RPG
Receiver Operator Curve	ROC
Reference Electrode	RE
Relative Humidity	RH
Setpoint	SP
Signal to Noise Ratio	SNR
Split Flow Box	SFB
Surface Acoustic Wave	SAW
Surface Acoustic Wave	PID
Thermal Conductivity Detectors	TCD
Travelling-Wave Ion Mobility Spectrometry	TW-IMS
Trimethylaminuria	TMAU
Tunable Diode Laser Absorption Spectroscopy	TDLAS
Type 2 Diabetes Mellitus	T2DM
Ulcerative Colitis	UC
Universal Asynchronous Receiver-Transmitter	UART
Universal Windows Application	UWA
University Hospital Coventry and Warwickshire	UHCW
Urinary Tract Infections	UTI
Volatile Organic Compounds	VOCs
Working Electrode	WE

List of Symbols

A	Amount of absorption
α	Compound specific values
b	Path length
ß	Compound specific values
c	Molar concentration
c_v	Gas concentration
CV	Control voltage
E	Electric field
ε	Molar absorptivity
e(t)	Difference between process variable and control voltage
F_{sa}	Sample flow
i	Concentration
K	Low field mobility
K_d	Differential constant
K_h	High field mobility
K_i	Integral constant
K_{pa}	Pressure in Kilopascal
K_p	Coefficient of partition / proportional constant
N	Carrier gas density number
PR	Permeation rate
P_{tot}	Total pressure
P_w	Water vapour pressure
P_{ws}	Saturation water vapour pressure
R	Current resistance of sensor
R_0	Initial resistance
R_b	Baseline resistance of sensor
R_T	Sensor's conductance value
S	Sensitivity
v	Velocity
ΔR	Sensor resistance difference
Δf_p	Frequency changes
ρ_p	Density of the coating polymer membrane

Chapter

1 Introduction

1.1 Introduction

The idea of imitating the mammalian olfactory system was introduced by Dodd and Persaud in the early 1980s [1]. Further developments in miniaturised gas sensing technology, electronics, biochemistry and artificial intelligence made it possible to make electronic nose (eNose) instruments that are able to repeatedly sniff aromas, identify and classify them in different groups [2]. Similar to the human and animal olfaction system, eNose technology can detect the chemical species as a whole, based on pattern/fingerprint approach, but is not able to identify individual chemicals. Fig. 1.1[3] illustrates the principal operation of an eNose, from the odour being presented to the classification point and decision making.

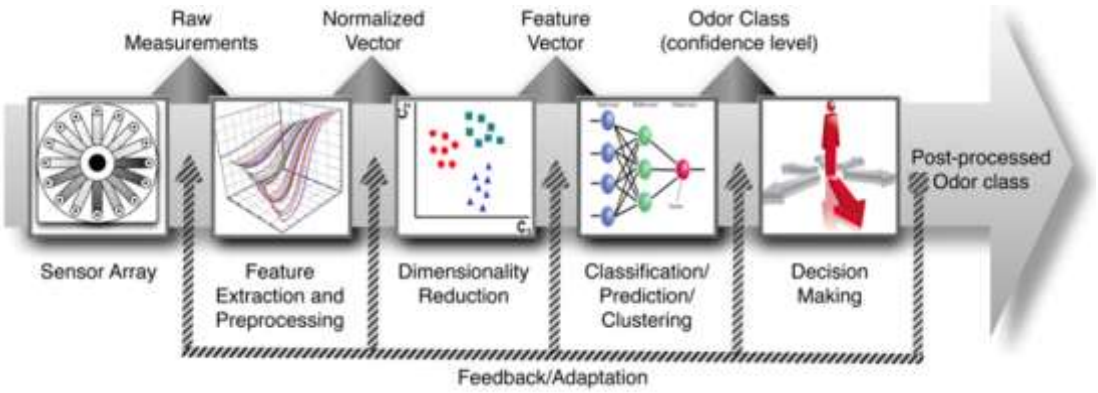

Fig. 1.1 Principle operation of eNose technology [3]

The first commercial eNose was produced almost 25 years ago and since then they have become relatively common within the market place [4]. However, the total number of presently available commercial instruments still remains low at under 10. There have also been several types of experimental eNose instruments developed in different laboratories, but these have not made it into the market place. Fig. 1.2 shows a few examples of commercially available eNose instruments. Fig. 1.2.a illustrates the handheld Sensigent Cyranose-320 eNose (US), which contains a nanocomposite sensor array with 32 sensors and can detect low ppm levels[5]. Fig. 1.2.b shows the Airsense PEN3, eNose (German), which contains 10 different metal oxide single thick film sensors. The operating temperature of this eNose is between 350°C and 500°C [6]. Fig. 1.2.c shows the RoboScientific eNose (UK), which has a flexible number of sensors (between 6 and 12 individual sensors depending on their application). The sensor arrays used in this instrument are organic semiconductor sensors[7]. eNose technology has been explored in many applications including agricultural, biomedical, environmental, food, manufacturing, military and many other research areas[2].

Fig. 1.2 Commercially available portable eNose instruments. a) Cyranose 320, b) PEN3, c) RoboScientific VOC analyser [5,6,7]

1.2 Smell in Medicine

For centuries, using the sense of smell for diagnosing diseases was an important tool in medical practice. This goes back to 2000 BC when the ancient Greek and Chinese used to smell the patient's waste or body to diagnose diseases. In 400 BC, Hippocrates discovered that samples (urine, breath, sweat, stool) from patients with different

diseases had a specific smell[8, 9]. In recent decades, several studies have been done on using human and animals (particularly dogs, but also rats and bees). Human sense of smell, for diagnosing diseases, is not repeatable and it is different from person to person. Dogs have a very sensitive sense of smell, but it requires special training for different diseases, thus requires specific expertise and this is time consuming. In addition, having animals in a healthcare setting (such as a hospital) could be considered unhygienic. As eNose technology doesn't have these issues, it is very attractive for medical applications.

Analytical instruments were first used for analysing gas phase biomarkers emanating from human waste for diagnosing diseases. Analytical instruments can identify the chemicals/volatile organic compounds (VOCs) generated from samples and thus the biomarkers for different diseases. This was established after the development of gas chromatography (GC) and mass spectroscopy (MS) instruments in the 1950s. The disadvantages of these instruments, including the operational cost, requirement for trained staff, not portable and time consuming data processing steps, have made them unpractical for many clinical applications [10].

eNose technology has the potential to overcome these disadvantages. They have good sensitivity and specificity, down to single parts per million (ppm) or even parts per billion (ppb) levels depending on the sensors selected for the sensor array. They provide rapid results because of rapid response of gas sensors. Moreover, data analysis for eNose instruments is often not as complicated compared to other analytical devices.

eNose instruments are less expensive, easier and cheaper to operate compared to most analytical instruments. Thus, this creates the potential to design and develop low cost eNose's for specific medical applications. eNose instruments do not need trained staff and are small, portable devices, which require less space in either a primary or secondary care setting [2, 10, 11]. On the other hand, current eNose instruments suffer from intolerance to temperature and humidity on the sensors response, recovery of the sensors, and reproducibility after multiple tests. However, eNose instruments are still considered as a promising diagnostic tool for a variety of diseases, including different types of cancers, metabolic disorders, urinary and intestinal-tract infections, and related physiological monitoring of diseases [10, 12, 13].

1.3 Diabetes

Currently, one of the urgent public medical issues is the fast-growing number of people with diabetes. According to statistics, the number of people worldwide with diabetes in 2015 was 415 million and it is estimated to reach to 642 million in 2040 in the world. According to estimation, 1 of 2 adults with type 2 diabetes are not diagnosed[14] . In the UK, the number of people with type 2 diabetes are estimated around 4.5 million people. Thus roughly 1.1 million are without a proper diagnosis [14, 15]. It is a major health concern. Even in the under 20s, the number of diabetic children is rapidly increasing. In the UK alone, around 31,500 patients under the age of 19 have diabetes [14]. According to the National Diabetes Audit (NDA) report, 24,000 patients suffering from diabetes have early death each year (65 patients a day)[16]. From a financial cost point of view, 10% of NHS budget is spent on diabetes. In 2010/11 diabetes

costs in the UK was around £23.7 billion and this value is estimated to reach £39.8 billion in 2035⁄36 [17].

Diabetes can cause many other diseases, but one of the more common ones is Gastrointestinal (GI) disorders[18]. Around 75% of diabetic people in clinics reported significant GI symptoms [19, 20]. The whole GI tract from the oral cavity to the large bowel and anorectal region, can be affected by diabetes. These complications and their symptoms are a consequence of diabetic autonomic neuropathy involving the GI tract[20]. The most common GI tract diseases associated with diabetes are ulcer disease, gallstones, irritable bowel syndrome, Candida infections, Pancreatic exocrine dysfunction, gall bladder, and fatty liver [20, 21].

A few methods that are currently being used to diagnose the GI tract conditions are colonoscopy, tissue biopsies, and microbial-culture tests[22]. These are invasive techniques, which take a long time, are costly, not patient friendly and not practical to use for huge number of disease monitoring purposes. Thus, researchers have focussed on using an eNose approach to GI disease diagnosis, by detecting diseases through chemical VOCs emanating from human waste. The class of metabolic VOCs discharged from different GI diseases depends on how and where these metabolites are released in the body and which organs are involved [23]. eNose technology makes GI diseases diagnosis non-invasive and it helps in having a more effective treatment, faster patient recuperation, and shorter more affordable stays at hospital [12]. eNose instruments have been shown to work in specific GI tract diseases including colorectal cancer (CRC), inflammatory bowel disease (IBD) (Crohn's Disease (CD) and ulcerative colitis (UC)),

irritable bowel syndrome (IBS), infectious diarrhoea (ID), coeliac disease, necrotizing enterocolitis, and cholera[24].

The number of undiagnosed people with diabetes, the growing rate of diabetes between young and adult people and the effect of late diagnosing, is worrying. Hence scientists are trying to find easy, fast, non-invasive and patient friendly ways for the early diagnosis of diabetes. Several studies found out that early diagnosis and the treatment of type 2 diabetes can reduce Cardiovascular morbidity, mortality, have more effective treatments and reduces NHS costs [25].

Right now, there are six different methods for diagnosing diabetes, specifically urinary glucose, fasting plasma glucose (FPG), random plasma glucose (RPG), the oral glucose tolerance test (OGTT), capillary glucose, and glycated protein (A1C)[26]. A1C is considered as the gold standard for monitoring glucose control. It is easy to purchase, does not require fasting, and is used as a point of care monitoring. But, there is potential for nonglycemic causes of error and it is not sensitive to impaired glucose tolerance (IGT)[26]. A1C, is a blood test, which gives evidence about the person's average levels of blood glucose, over the past 3 months. Hemoglobin A1c and HbA1c are the other names for A1C test[27].

Although, HbA1c is a gold standard, it is not appropriate for all children and young people, patients with diabetes symptoms for less than 2 months, high risk patients with actual illness, medication, which led quick glucose growth, patients with serious pancreatic injury, and pregnant women [28].

Currently eNose technology is showing promising results in detecting GI diseases through VOCs generated from digestion system. Urine is one end of the digestion system, in patients with type 2 diabetes, the level of glucose in urine increases due to abnormal high blood sugar, but in comparison to glucose in blood, this is very small. This means that high levels of sugar in urine changes the smell to sweet or fruity[29]. Hence, this has prompted the idea of using an eNose instrument to diagnose diabetes from healthy volunteers by directly analysing gases and vapours existence above urine samples in vial after heating it (headspace). Using the eNose will provide advantages of rapid processing time, inexpensive and does not require blood samples.

1.4 Research Aims

There is a need for a new tool for the early diagnosis of diabetes – a condition which is rapidly expanding and causing many other disorders (mainly GI disorders). This tool should have the ability to rapid diagnose the disease, be inexpensive, portable and patient friendly.

The aim of this study was to investigate a potential, innovative, non-invasive low-cost method of identifying individuals suffering from metabolic disorders and gastrointestinal diseases with urine sample.

The eNose technology which was used in this study was designed in a way to overcome some of the disadvantages of current available eNose instruments. Most of the available eNose technologies suffer from cross sensitivity, drift, selectivity and

effect of humidity and temperature due to the chosen sensor technology. The novel eNose system designed in this study, includes tuneable optical sensors as the sensor array and is able to cover the whole infrared range of 3.1 μm to 10.5 μm. Other advantages of the system are high flexibility in terms of the substances measurement, identification of unknown substances, using chemometric approaches for multi-component analysis, and measurement of known compositions with overlapping bands. In addition, since optical sensors were used in this eNose, the system will not suffer from common eNose disadvantages such cross sensitivity, temperature and humidity dependence. This eNose system is called the "Warwick Optical eNose". Warwick Optical eNose was tested as early point-of-care solution for diagnosing diabetes. The biological sample used in this study was urinary VOCs as novel non-invasive diagnostic biomarker for diabetes[30].

1.5 Overview of Dissertation

The structure of this thesis is listed below.

Chapter 2: State of The Art. This chapter reviews current gas sensors technology used in eNose instruments. It then continues with addressing commercially existing eNose instruments and their applications. This chapter follows with discussions of eNose instruments specifically developed for biomedical applications, especially lower gastro-intestinal diseases using urinary VOCs.

Chapter 3: Urine Stability Study with eNose. This chapter investigates the effect of storage time on stability and reproducibility of total gas/vapour emissions from diabetic urine samples, using an eNose instrument.

Chapter 4: Discrimination of Diabetes from Control Sample Using eNose Technology. This chapter presents a comparative experimental study on using two commercially-available eNose instruments (AlphaMOS Fox 4000, Owlstone Lonestar) for diagnosing diabetes from healthy control patients by urinary volatile organic compounds.

Chapter 5: Development & Construction of Gas Test Rig. Chapter 5 addresses the design, construction and development of the gas test rig system. The test rig consists of gas controller, volatile generator, humidity generator, and gas analyser. It is designed and developed for verifying the sensitivity and selectivity of the eNose instrument (chapter 6) and monitoring the effect of humidity on the system.

Chapter 6: Development & Construction of NDIR Optical eNose Instrument. This chapter describes the development and construction of a novel eNose instrument by using tuneable optical sensors, which covers the wavelength range of 3.1 μm to 10.5 μm. This eNose provides the possibility to scan the whole range of 3.1 μm to 10.5 μm and choose fixed frequency measurements as "virtual sensors". It is developed as a test platform to study the possibility of using tuneable optical sensors array eNose instruments for biomedical applications.

Chapter 7: Experimental Testing of Warwick Optical eNose Instrument. Chapter 7 presents the experimental results of the developed NDIR optical eNose instrument and addresses its ability to perform as a diagnostic tool and compare its results with commercial available eNose instruments.

Chapter 8: Conclusions and Further Work. This chapter concludes the dissertation and presents a summary of overall results discussions with an overview of the future research application of optical eNose technology on biomedical application.

Chapter

2 State of The Art

2.1 Introduction

This chapter will provide an overview of the eNose, its principle of operation and the different types of gas sensors that have been used within these instruments. This will include discussion on current and past commercial eNose's and their applications in routine use. Finally, this chapter will consider medical uses of eNoses, with special focus on metabolic/gastro disorders.

Human olfaction is a particularly difficult sense to replicate and understand. Even now, food quality, drinks and even in disease diagnosis, the human nose has been and is still being used for a wide variety of analytical processes. This assessment is usually based on a group of experts, sniffing an odour and then completing a

questionnaire about the item or product. Though this method might be considered convenient, it is still subjective and depends on individual perceptions of a smell. To overcome some of these issues and to make a more analytical assessment, techniques such as gas chromatography and mass spectrometry technology are often employed[31-33]. Although these methods are sensitive and can produce constant results, they are hard to link to human perception. In addition, these instruments are generally expensive, bulky, time consuming, hard to use, and usually require trained experts [32-34].

In an attempt to fill the gap between high-end analytical instruments and human olfaction, the eNose was invented at Warwick University in 1980s [35, 36]. Since this point in time, there have been continuous developments, brought about by improvements in sensor technologies, instrumentation, method development and data analysis, which have resulted in instruments being made cheaper, smaller in size and more reliable for different applications.

The eNose is cost effective, when compared to traditional GCMS, portable and can give real time results[37]. Presently, eNose technology is being utilised in a variety of applications including, industrial construction (e.g., harmful gaseous substances detection)[38-41], automotive industry (e.g., detection of polluting gases from vehicles)[42-46] , medical applications (using VOCs produced from human waste)[10, 47-51] , indoor air quality supervision (e.g., detection of carbon monoxide)[52, 53] , environmental studies (e.g., greenhouse gas monitoring)[54-57], agricultural and forestry (e.g., cell culture, plant identification) [58, 59], and military [60].

2.2 Principle Operation of eNose

eNose has been defined as “an instrument, which comprises an array of electronic chemical sensors with partial specificity and an appropriate pattern-recognition system, capable of recognising simple or complex odours” in 1988 by Gardner and Bartlett[61]. The eNose is designed to replicate the mammalian olfactory system in being able to detect a variety of different volatile compounds, Fig. 2.1[61, 62]. Unlike techniques, such as GCMS, the eNose is designed to classify and identify complex odours as a whole without the identification of each individual chemical [63-66].

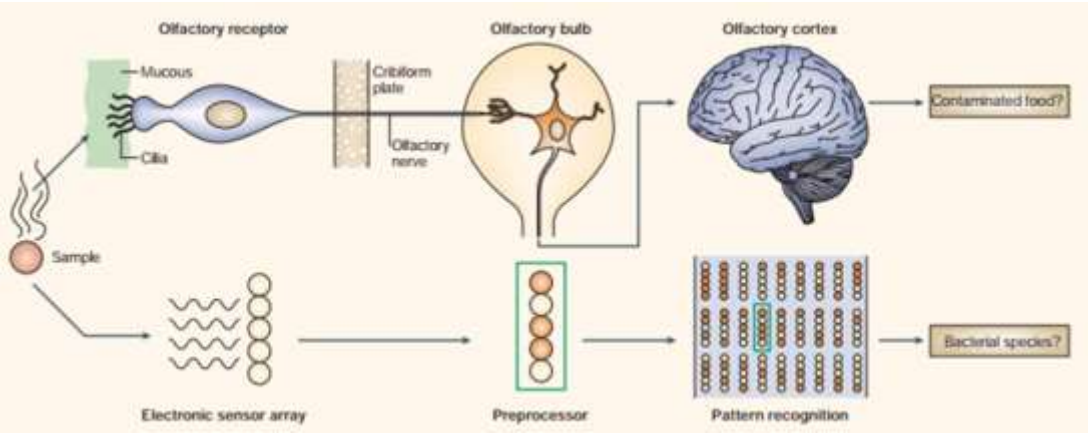

Fig. 2.1 Comparing human olfactory system with electronic nose [61]

The eNose is composed of an aroma delivery system (or a sample handler), sensor array in a gas chamber, measurement electronics and some form of pattern recognition system [67, 68]. ‘Sample handling’ are techniques that draw the gas molecules of the

sample to the sensor array of the electronic nose. This can be by headspace sampling, diffusion methods, bubblers etc. [31, 69]. The sensor array and electronic measurements will be explained in detail later in this chapter. To produce a pattern recognition from the sensor's responses, several multivariate statistical analysis techniques can be used. The two most common analysis are Principal Component Analysis (PCA) and Linear Discriminant Analysis (LDA)[29, 70]. PCA is a linear feature extraction technique, and works based on reducing the dimensionality of the data and removing the lowest ranking variable[29, 70]. LDA uses an algorithm to discover a linear discriminant function (LDF), which is a linear combination of features that characterises or separates two or more classes of the original variables, aiming to achieve maximum separation [70].

The term eNose covers a large number of different approaches that can accomplish the same result. The sensor array is one of the most critical and important parts of the eNose. The main difference between these instruments is the core gas sensing technology used. The majority of eNoses use an array of between 6 and 12 chemical sensors. By far the most popular is to use an array of chemoresistive metal-oxide sensors. [71-74], however other instruments use electrochemical gas sensors [75], chemoresistive polymers [76, 77], mass surface acoustic wave [78, 79] and photo-optical absorbance [80].

In the presence of the sample's vapour, chemical/physical characteristics of the sensing material changes, which is detected as a change in some electrical property (signal), such as resistance[81]. Fig. 2.2 shows the typical response of a p-type metal-

oxide gas sensor used in FOX4000 eNose (AlphaMOS, France) where the resistance varies with presence of a gas. Phase (a) in the Fig. 2.2 indicates the baseline of sensor (reference gas), phase (b) shows the resistance changes in presence of gas (response time) and phase (c) is the recovery time when there is no gas.

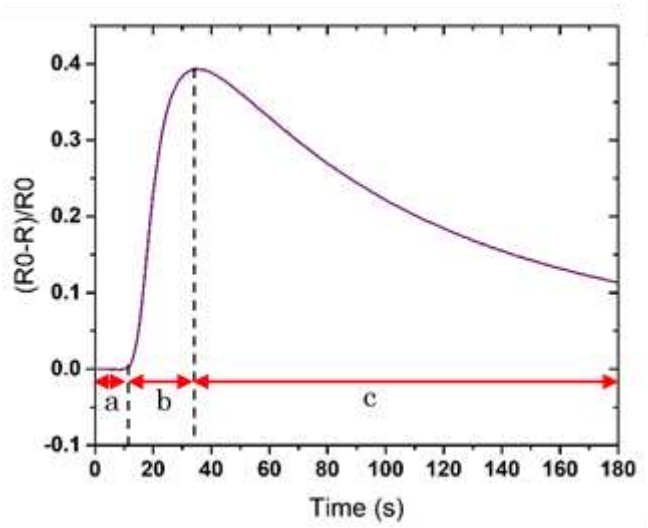

Fig. 2.2- Typical response of p-type metal oxide gas sensor; part (a) baseline or reference gas, (b) presence of target gas, (c) recovery time

In an eNose, each sensor in the array acts in a similar way to a biological receptor, where each responds broadly to a family of odours [82]. These instruments are formed of an array of such sensors that are different in some way (usually a different sensing material). When they are exposed to a complex odour, each sensor responds different to the chemical components within it. These different responses can then by analysed by some form of pattern recognition algorithm, so that if the sample is presented to the sensor array again it is able to identify it. Since it is the gas sensor that is at the heart of the eNose instrument, it is important to understand the different sensing properties,

what their sensitivity and selectivity levels are and what are the advantages and disadvantages of each. In general, gas sensing methods can be divided into two main groups, the first group is based on an electrical variation, such as metal oxide semiconductors, conducting polymers, electrochemical and carbon nanotubes. The second group is based on other kinds of variation such as optic, acoustic, gas chromatograph [83] and calorimetric methods [84]. In most eNose instruments, an array of metal oxide [71, 72], polymer, quartz crystal microbalance [85], surface acoustic wave [78], electro-chemical, and optical [80] sensors have been used.

2.2.1 Common Data Analysis Methods of eNose

The analysis of electronic nose data can be divided into two parts. The first part is reviewing the data mathematically, where mathematical methods are employed to distinguish different groups from each other. The second part is related to machine learning, where the accuracy of mathematical classifications is analysed and compared to real data acquired from medics.

When data acquisition is done by eNose, it is time to extract the features. In the context of eNoses, the maximum sensor responses are the features that are typically considered. Feature selection is the method of classifying the most effective subset of the original features to use in the classification process that result in the lowest classification error. Filter methods are the most common feature selection methods in the context of eNoses which work independently to eliminate features without knowing

the outcome on the classification algorithm. Usual linear methods used are principal component analysis (PCA) and linear discriminant analysis (LDA) [70].

Principal component analysis (PCA) a.k.a. the Karhunen-L_oeve expansion or singular value decomposition (SVD) is an unverified multivariate process and is a renowned linear data compression and feature extraction method. The scores produced could be plotted in two or three dimensions to review the data. PCA obtains new, uncorrelated variables that are linear combinations of the original variable set well-organized by reducing variability. It is mostly used to decrease the dimensionality of a data set while keeping as many data as possible by removing the lowest ranking variables [70].

Linear discriminant analysis (LDA) looks for a linear discriminant function (LDF) which is a linear combination of the original variables, so that the ratio between-class scatter and within-class scatter is maximized[86].

A receiver operating characteristic curve (ROC) is a statistical plot which shows the classifier ability in diagnosing diseases. Plotting the true positive rate (TPR) against false positive rate (FPR) creates the ROC curve. When the prediction result is positive as well as the real value, it is considered as true positive (TP). But, if the real value is negative it is considered as false positive (FP). On the other hand, if the prediction result is negative and real value is negative it is called true negative (TN). Moreover, if real value is positive it is considered as false negative (FN).

In ROC curve TPR is considered as sensitivity which can be calculated by dividing the TP over all positive conditions.

FPR is equal to 1 minus TNR value. TNR is called specificity which is equal to TN value over all negative conditions.

After plotting the ROC curve, the area under curve (AUC) shows how good the classification and predictions are. The maximum value for AUC is 1. There isn't any threshold value for AUC to decide if the prediction is good or bad.

2.3 Common Gas Sensors in eNose

This section describes the principle operation of the common gas sensors, which have been used in eNose instruments and highlights the advantages and disadvantage of each type.

2.3.1 Conductivity Sensors

The three most common sensing materials used as conductivity sensors are conducting polymer composites, intrinsically conducting polymers and metal oxides[31]. These materials are described as chemoresistive, as they change their resistance when exposed to a target molecule. In these sensors, the sensing material is

deposited onto a set of electrodes, often formed of gold, which interfaces to the sensing layer to assist in measuring its resistance.

Fig. 2.3 [31] shows the typical structure of the conductivity sensor, with a set of electrodes and a sensing layer. If a metal oxide material is used, it requires very high temperatures (>200C) to operate and therefore the structure also includes a heater [87].

The next two following sections (2.3.2 & 2.3.3) explain the different sensing materials that have been used in conductivity sensors in detail.

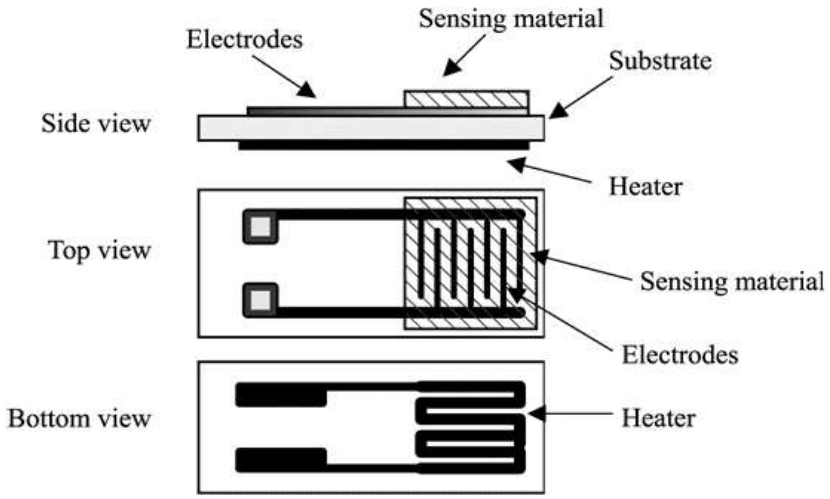

Fig. 2.3 Typical construction of a conductivity sensor [31]

2.3.2 Metal Oxide Sensors

Metal oxide sensing materials having received a considerable amount of attention for gas sensing applications since their invention. The reason is simple, they have a low-cost of production, can be made very small (miniaturised), can be integrated into modern electronics, are easy to use and respond to a wide range of molecules [55, 88]. This method of detection strongly relies on surface reactions. A large number of metal oxide materials are used in active layers of gas sensors such as Cr_2O_3, Mn_2O_3, Co_3O_4, NiO, CuO, SrO, In_2O_3, WO_3, TiO_2, V_2O_3, Fe_2O_3, GeO_2, Nb_2O_5, MoO_3, Ta_2O_5, La_2O_3, CeO_2, and Nd_2O_3 [89, 90]. However, only SnO_2, WO_3, ZnO and La_2O_3 are commercially in use. In metal oxide sensors, the oxide conductance changes in the presence of the target gas and the amount of change is proportional (though non-linear) to the target gas concentration [91]. MOX sensors have very high sensitivity from ppm to ppb depending on the target gases. In general, a metal oxide sensor's response (ΔR – change in resistance) can be positive or negative depending on the sensor type. MOX sensors are divided into two groups; n-type and p-type. Table 2.1 shows the response of n-type and p-type sensors[31, 92].

Table 2.1 MOX Sensor response to variation in gas atmosphere

Classification	Oxidising Gases	Reducing Gases
n-type	Resistance increase	Resistance decrease
p-type	Resistance decrease	Resistance increase

The local sensitivity of the MOX gas sensors can be calculated using equation 2.1[93].

$$S = \frac{{}^{\Delta R}/_{R_b}}{Concentration\ of\ gas} \qquad (2.1)$$

Where S is sensitivity, $R_b$is baseline resistance of sensor, and R is the resistance of sensor in presence of gas. If the gas is oxidising $\Delta R = R - R_b$; and if the gas is reducing, then $\Delta R = R_b - R$.

Sensing performance requirements, such as sensitivity, selectivity, response time and, reliability requirements, such as drift, stability and cross sensitivity are all related to humidity, temperature and factors that are influencing the surface reactions of the sensing material[88, 90, 94].

Overall, the response time of a MOX sensor, with gas concentration up to 400 ppm, is between 5 to 35 seconds for operating temperature range of 250 °C to 500°C and recovery time between 15 to 70 seconds [95, 96].

2.3.3 Polymer Sensors

The Conducting polymers sensors are the second most widely used sensor technology in electronic noses after MOX [97]. MOX sensors need a high temperature of operation, which means high power consumption. Therefore, in some applications polymer gas sensors could be more suited [84]. The main advantages are improved specificity, and reversible physicochemical properties at ambient temperatures [98, 99]. Response of the sensors for same volatile compound depends on the physicochemical

and chemical modification of polymers. They come in two forms, either electrically conducting polymers or composite polymers, where an insulating material is combined with a conducting nano-material (such as carbon) to form a semi-conducting composite.

NH_3, NO_2 and H_2S sensors were the first polymer sensors that were applied to eNose's using poly(3,4-ethylenedioxythiophene)(PEDOT) [100]. Many conducting polymer sensors have since been used and several reports indicate success of these sensor functionality in different applications, such as beer flavour monitoring[101], identification of microorganisms from samples headspace [102],testing food quality in food industries and detecting mite infestation in wheat [103].

Commercial Cyranose 320 which includes 32 polymers carbon black composite polymer sensors were used in classifying bacteria [104] and cigarette brand identification[105]. However, the first and biggest issue with polymer sensors is their sensitivity to humidity, which in turn can affect the total sensitivity[106]. Their other issues are drift and poor repeatability. Due to the random nature of the polymer, the reproducibility of the these sensors is another challenge [107]. For these reasons, they remain less common in electronic nose instruments.

2.3.4 Acoustic Wave Sensors

The Acoustic wave detection is based on vibration of crystals (typically Quartz), which is coated with a polymer sensing material. This technology is divided to two main types. The first one is surface acoustic wave (SAW) and second is quartz crystal

microbalance (QCM). SAW sensors produce a surface wave, which moves along the surface of the crystal. QCM sensors produce a wave that moves through the bulk of the sensor. Both SAW and QCM sensors work with the same principle of operation. In the presence of the target gas, the mass of the sensing material, coated onto the piezoelectric sensor, changes causing the resonant frequency to change [108]. In this type of sensor, the coating material and its thickness plays an important role in selectivity and sensitivity in detecting volatile compounds [109]. To detect different VOCs the coating chemical composition needs to be different [108, 110].

The structure of a SAW device is shown in Fig. 2.4.[111] It contains two interdigital transducers (IDTs) deposited, one as an input and the other one as an output, with a coated sensitive membrane in between them.

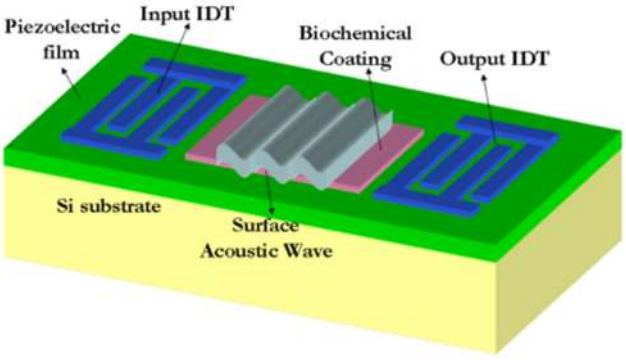

Fig. 2.4 A SAW sensor structure [111]

2-dimensional waves propagate on the surface of the sensor by applying ac signal across the input IDTs. When molecules of the target gas absorb onto the coating, the mass changes and this in turn causes a frequency change. The difference in frequency change can be calculated by:

$$\Delta f = \Delta f_p c_v K_p / \rho_p \quad (2.2)$$

Where Δf_p is the frequency changes from membrane, c_v is gas concentration, K_p is coefficient of partition, and ρ_p is the density of the coating polymer membrane[31, 112].

There have been several reports on SAW based eNose instruments in different applications, such as food quality monitoring[113], detecting lung cancer[114], and detecting the adulteration of virgin coconut oil [115].

2.3.5 Electrochemical Sensor

The principle operation of electrochemical (EC) sensors is based on an electrochemical oxidation or reduction of gas molecules at the sensor's catalytic electrode surface[2, 116]. Some of the electrochemical sensors have two and some have three electrodes. Figure 2.5 shows the three-electrode electrochemical sensor schematic. Any three-electrode sensor can be changed to the two electrodes, by connecting the Counter and reference electrodes together. The main operation of the EC sensor depends on the working electrode (WE) consisting of a catalytic material. In presence of the gas, the catalytic material starts to react, and it produces current at the WE terminal. The counter electrode (CE) keeps the sensor electrically neutral. Normally CE has equal or opposite current to replace the excess or deficit of electrons. Reference electrode (RE) measures the electrolyte potential without allowing a current to pass through it[117]. Porous support avoids liquid electrolyte from leaking.

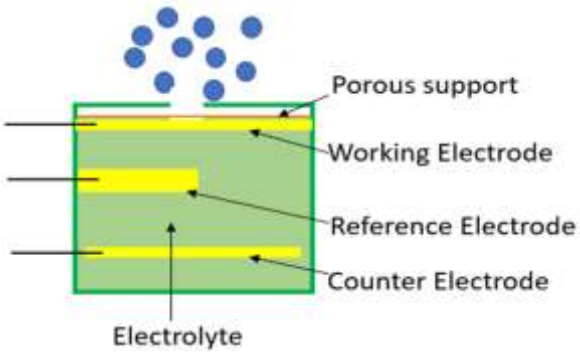

Fig. 2.5 Schematic design of electrochemical sensor

The advantages of EC sensors are their room temperature operation, being very robust, relatively low-cost and low power consumption, with the biggest disadvantage being their size, which is bulky (due to the need for an electrolyte sack and the size of the electrodes). EC sensors are sensitive to electrochemically active gases, particularly toxic gases (such as CO and NO_2), so have been used in tunnelling and mining operation and industrial applications, however these sensors are not sensitive to several compounds particularly simple aromatic hydrocarbons [97, 118]. However, EC sensors have shown a promising solution for detecting VOCs such as ammonia, ethylene oxide, glutaraldehyde and ethanol for low concentration up to ppb level[119].

2.3.6 Optical Sensors

The Optical gas sensor have a simpler operating principle, with good sensitivity, selectivity (especially to gases such as CO_2 and CH_4) and longer life time compared to other gas sensor types [84]. Since optical sensor principle is based on spectroscopy and

not related to chemical reaction, environmental changes have less effect on the response of the sensor, with the exception of pressure. Optical sensors can be used as a real-time detection method since it has short response time compared to other methods. However, they usually have a higher unit cost and miniaturization of optical sensor in gas detection technology is difficult [84]. Compared to other gas sensor technology, optical gas sensors have had less commercial success (probably due to cost), with CO_2 detection being the main success for mass markets. Optical sensors work based on absorption and emission spectrometry. The amount of absorption depends on gas concentration at a wavelength related to that specific gas. The absorption frequency for different gases can be found from the HITRAN database [120]. The amount of absorption can be calculated by the Beer-Lambert law shown in the equation below [121].

$$A = \varepsilon * b * c \qquad (2.3)$$

Where A is amount of absorption, ε is molar absorptivity, b is path length, and c is molar concentration [121]. There are different methods that can be applied to basic optical sensor principle to increase the absorption spectrometry. These methods are "Differential Optical Absorption Spectroscopy (DOAS) [122], Tunable Diode Laser Absorption Spectroscopy (TDLAS) [123], Raman Light Detection and Ranging (LIDAR)[124], Differential Absorption LIDAR (DIAL) [125], Intra-Cavity Absorption Spectrometry (ICAS) [126]" [84] and Non-Dispersive Infrared (NDIR). Infrared (IR) source and optical gas sensors operate based on the molecular absorption spectrometry and are widely used in gas sensing applications. In presence of IR radiation, each gas

has its own absorption frequencies, this absorption fingerprint is unique. Fig. 2.6 shows absorption frequency of some important gases in the range of 2.8 μm and 5.2 μm [127].

NDIR detection system contains three main parts: IR detector, gas flow path, and IR radiation source. As shown from Fig. 2.7, IR source emits the broadband radiation, this should include the wavelength absorption of the target gas. When a gas is inside the gas cell, gas molecules will absorb this radiation. The filter on the optical sensor will only let the radiation wavelength related to the target gas to pass.

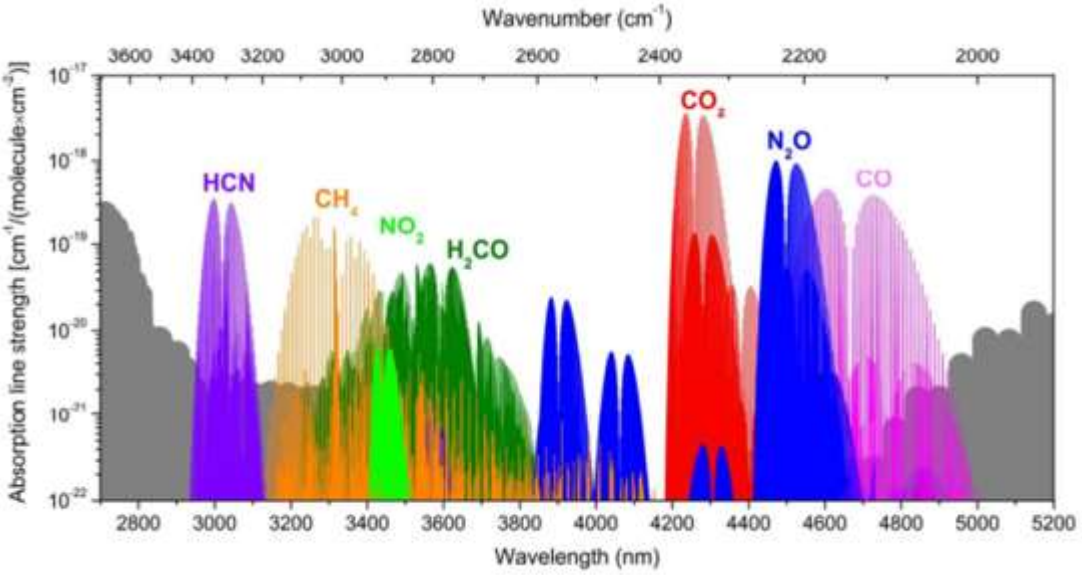

Fig. 2.6 Absorption frequency of some of the important gases in between 2.8um and 5.2um [127]

The IR source plays an important role in the NDIR gas detection method because of the selection of the IR wavelength range. The mid-infrared spectrum (3 μm to 50 μm) is more applicable compare to near-infrared, as it has stronger molecular absorption [84]. IR frequency band has two main advantages compared to the other frequency bands. Firstly, IR radiation is less scattered in the presence of steam, mist, or smoke compared to visible radiation, due to its longer wavelength[84, 128]. Secondly, the miniaturization of infrared sources and detectors is possible by using MEMS technology.

The NDIR sensors have been widely used in air quality monitoring and gas leakage monitoring systems, with high sensitivity [128, 129] . CO_2 is the easiest gas to detect due to its large absorption frequency at 4.2 μm[130-132].

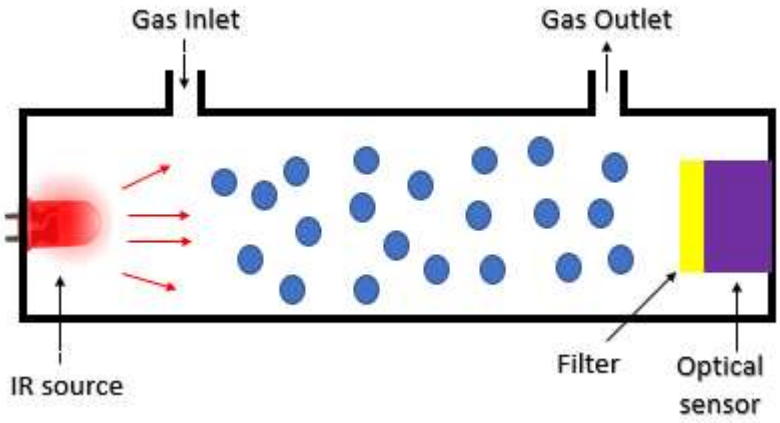

Fig. 2.7 NDIR gas sensor detection principle

2.3.7 Summary of Gas Sensor

This section has summarised the most common sensor technology that have been used in eNose instruments. The sensor types, the sensitive materials that have been used, and their detection method is summarised in Table 2.2 [2, 84]. The pros and cons of each sensor technology with their applications is briefly describe in Table 2.3 [2, 84].

Table 2.2 The summary of common eNose gas sensors' types and their principle of operation [2,84]

Sensor type	Sensitive material	Detection principle
Metal oxides semi-conducting (MOS)	Doped semi-conducting metal oxides (SnO2, GaO)	Resistance change
Conducting polymer sensors	Modified conducting polymers	Resistance change
Acoustic sensors: QMB, SAW, BAW	Organic or inorganic film layers	Mass change (frequency shift)
Electrochemical sensors	Solid or liquid electrolytes	Current or voltage change
Optical sensors	Photodiode, light-sensitive	Light modulation, optical changes
Infrared sensors	IR-sensitive detector	Infrared-radiation absorption

Table 2.3 The Summary of Common eNose gas Sensors' pros, cons and applications [2,84]

Sensor type	Advantages	Disadvantage	Application
Metal oxides semi-conducting (MOS)	Very high sensitivity, limited sensing range, rapid response, low cost, wide range of target gases, long lifetime	High temperature operation, slow recovery times high power consumption, sulphur & weak acid poisoning, limited sensor coatings, sensitive to humidity, poor precision	Industrial applications and civil use
Conducting polymer sensors	Ambient temperature operation, sensitive to many VOCs, short response time, diverse sensor coatings, inexpensive, resistance to sensor poisoning, low energy consumption	Sensitive to humidity and temperature, sensor life is limited, long time instability, irreversibility, poor selectivity	Indoor air monitoring, Storage place of synthetic products as paints, wax or fuels, Workplaces like chemical industries.
Surface acoustic wave (SAW)	High sensitivity, good response time, diverse sensor coatings, small, inexpensive, sensitive to virtually all gases	Complex circuitry, temperature sensitive, specificity to analyte groups affected by polymeric- film sensor coating	Air quality monitoring
Electrochemical sensors (EC)	Ambient temperature operation, low power consumption, very sensitive to diverse VOCs	Bulky size, limited sensitivity to simple or large mol. wt. gases	Environmental analysis, food analysis, and clinical analysis
Optical sensors	Very high sensitivity selectivity and stability, capable of identifications of individual compounds in mixtures, multi-parameter detection capabilities, long lifetime, insensitive to environment change	Complex sensor-array systems, more expensive to operate, low portability due to delicate optics and electrical components, miniaturization difficulty	Remote air quality monitoring, Gas leak detection systems with high accuracy and safety, High-end market applications.

2.4 Other Methods of Gas Detection

Gas sensors are not the only way to detect VOCs. There are several other methods for analysing gases based on the chemical and physical reaction of molecules. Some of the methods that have been used in detecting VOCs are: ion mobility spectrometry, gas chromatography, and photoionization detectors.

2.4.1 Ion Mobility Spectrometry (IMS)

Another promising technology in detecting complex vapours is ion mobility spectrometry. This method provides more information about the content and physical measurement of complex vapour than many traditional eNose instruments based on a sensor array [133]. There are three main methods of IMS: Drift-Tube Ion Mobility Spectrometry (DT-IMS), Travelling-Wave Ion Mobility Spectrometry (TW-IMS), and Field Asymmetric Ion Mobility Spectrometry (FAIMS)[134].

DT-IMS method contains a long drift tube with a constant electric field in parallel with the ions direction. The sample gas is ionized and then flowed through a drift tube. A buffer gas is that sent the other way through the drift tube and larger molecules are slowed down as they collide more with the buffer gas as shown in Fig. 2.8 [135]. TW-IMS has the same principle, but instead of having a constant electric field it has a positive and zero electric field. As FAIMS has been used in this study, it has been

introduced in more detail in section 2.4.2. Comparing these methods shows that FAIMS has the highest sensitivity followed by TW-IMS and DT-IMS respectively[134].

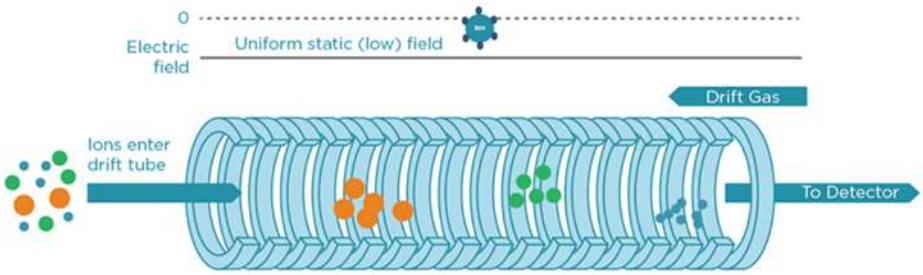

Fig. 2.8 Drift tube IMS schematic [134]

2.4.2 Field Asymmetric Ion Mobility Spectrometry (FAIMS)

FAIMS (or sometimes called Differential Mobility Spectrometry—DMS), has been seen as a useful means of separating gases and vapours since its conception in the 1980s [136]. They come in two basic configurations using either a cylindrical or (as in our case) planar design [137]. Such technology has found favour in the security area for the detection of chemical warfare agents [138], but has been used for a range of other applications either on its own or in combination with mass-spectrometry [139-141]. FAIMS carries similar advantages in use to many electronic noses, it undertakes headspace analysis, it uses air as the carrier gas, is relatively portable, is simple to operate, costs a similar amount to existing commercial electronic noses and importantly, as it relies on a physical measurement of a chemical, it suffers less from

drift/poisoning than most electronic nose instruments. Sensitivity strongly depends on proton affinity of the chemical of interest, but ranges between parts per million and parts per trillion[142], and in use compares well with techniques such as gas chromatography- mass spectrometry (GCMS) [143]. It is worth noting that FAIMS is far more sensitive than a standard GCMS system and the latter would require the use of a sophisticated pre-concentration system (such as absorbent tubes) to reach similar sensitivity levels. FAIMS is composed of three stages, ionization, filtration/separation and detection. In use, the sample headspace is drawn into the instrument (in our case using a dynamic sampling methodology) where it is ionized (for example a Ni-63 source) and mixed with a carrier gas of clean/dry air. The total sample is then pushed between two separator plates to which an oscillating asynchronous waveform is applied (up to GHz, with an amplitude up to hundreds of volts). The plates are subjected to a high positive potential for a short period of time, followed by a small in magnitude negative potential for a much longer period of time, but where the amplitude x time is the same in both cases. The Lonestar (as used in this study) employs a silicon-based separator with a sub 50 μm electrode spacing to create very high electric fields of up to 100 kV/cm. In use, the short/high potential is ramped through a series of values, described as the "dispersion field" from 0 up to the systems maximum value. Ionised molecules that enter the separation stage are then attracted, repelled or not affected by the electric field, depending upon the mobility difference between high- and low-field regimes (as shown in Fig. 2.9). Any ion that touches one of the separator plates, loses its charge and

is not detected. However, those ions that pass between the plates then exit the system where they collide with a detection plate and their charge measured.

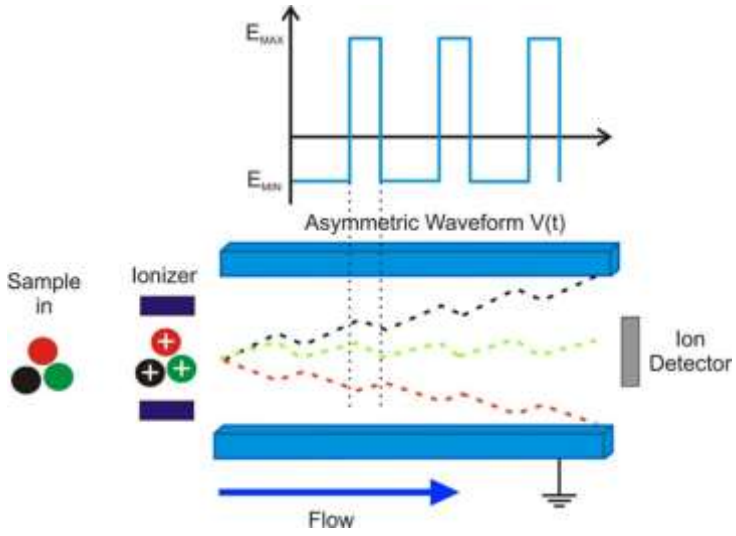

Fig. 2.9 Asymmetric waveform applied in field-asymmetric ion mobility spectrometry (FAIMS) and ions being separated by an asymmetric waveform. EMAX and EMIN are the differences in generated electric fields to the applied waveform V(t). The coloured lines between the plates show an example of possible paths depending on the molecules differential mobility

To increase the chemical detection range, a DC compensation voltage is applied to the plates, which is used to remove the ion movement towards one of the plates. This compensation voltage (normally a single figure voltage) is swept between a positive and negative potential and therefore for a certain compensation voltage, only chemicals with a specific differential mobility will be detected. The mobility of an ion depends on the mass, charge, size and shape since the field and the velocity are constant and are related by the equation below.

$$v = KE \quad (2.4)$$

where v and K are the velocity and mobility of ion respectively, and E is the electric field strength. Since velocity change is not proportional to the electric field intensity variations, at higher electric fields the ion mobility can be expressed by the following equation:

$$K_h = K[1 + \alpha\,(\frac{E}{N})^2 + \beta\,(\frac{E}{N})^4\,] \quad (2.5)$$

where K_h and K are the high-field mobility and low-field mobility respectively. α and β are compound specific values, which account for high-field mobility effect, N is carrier gas density number, and E is the electric field strength. More details of this process can be found in [142-144].

2.4.2.1 Gas Chromatography

Another common method of detecting, separating, and analysis of volatile organic compounds is gas chromatography (GC)[145]. A GC has six parts: carrier gas, pressure control, injector for injecting sample, column, detector, and data system (Fig. 2.10 [146]).

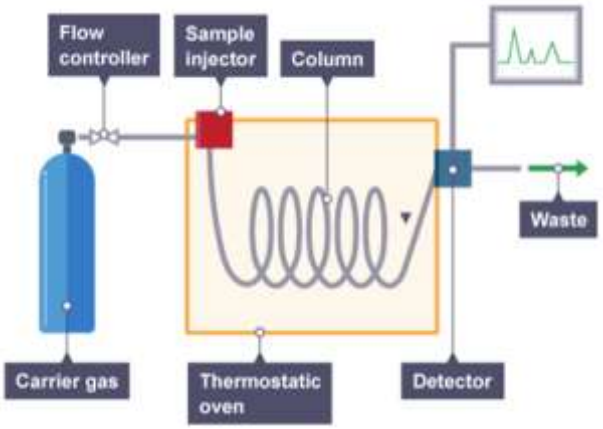

Fig. 2.10 Gas Chromatography system [146]

The carrier gas is usually argon, hydrogen, nitrogen or helium. Both the sample vapour and carrier gas are heated and then moved to the column. The inside of the column is coated with a chemically sensitive material, which interacts with the molecules inside the sample, so some of the molecules move faster compared to others. The molecules with low interaction (for example have lower boiling point or lower weight compared to the molecules with high interaction), exit the column first, with those with high interactions being released later. The vapour pressure, polarity, length, diameter, polarity and temperature of the column, carrier gas flow rate, and material injection amount are important factors in separation of the molecules [147]. A detector at the end of the column shows the amount of vapour reaching to it. There are five types of detector which are normally used in GC. There are Flame ionization detectors (FID), Thermal conductivity detectors (TCD), Electron capture detectors (ECD), Photo-ionization detectors (PID) and mass spectrometer (MS) [145, 147]. The outcome of this method is series of peaks. The size (height) of the peaks is directly related to the amount of each vapour component. To identify each peak, it is needed to compare to the chromatogram from a standard mixture [145].This method offers high performance in sensitivity and selectivity, but it usually has been used in laboratory and is expensive [84].

2.5 Commercial eNose in Market

There have been many eNose instruments, which have been commercially developed for several applications, including quality control, medical, security, safety, and many others. A summary of commercial eNose's are listed in Table 2.4 [2, 31, 97, 148-151] (both previously and currently available). This table also provides the core sensing technology used by the instrument.

Table 2.4 Commercial eNose instrument and their technology principle

Instrument type	manufacturer	Model	Technology principle
Single-technology (e-nose sensors only)	Airsense Analytics	i-Pen, PEN2, PEN3	MOX sensors
	Alpha MOS	FOX 2000, 3000, 4000	MOX sensors
	Applied Sensor	Air quality module	MOX sensors
	Chemsensing	ChemSensing Sensor array	Colorimetric optical
	CogniScent Inc.	ScenTrak	Dye polymer sensors
	CSIRO	Cybernose	Receptor-based array

Single-technology (e-nose sensors only)	Dr. Födisch AG	OMD 98, 1.10	MOX sensors
	Forschungszentrum Karlsruhe	SAGAS	SAW sensors
	Gerstel GmbH Co.	QSC	MOX sensors
	GSG Mess- und Analysengeräte	MOSES II	MOX gas sensors
	Illumina Inc.	oNose	Fluorescence optical
	Microsensor Systems Inc	Hazmatcad, Fuel Sniffer, SAW MiniCAD mk II	SAW sensors
	Osmetech Plc	Aromascan A32S	Conducting polymers
	Sacmi	EOS 835, Ambiente	Gas sensor array
	Scensive Technol.	Bloodhound ST214	Conducting polymers
	Sensigent	Cyranose 320	Carbon black-polymers

	Sysca AG	Artinose	MOX sensors
	Technobiochip	LibraNose 2.1	QMB sensors
Combined-technology (eNose + analytical instrument)	Airsense Analytics	GDA 2	MOX, EC, IMS, PID
	Alpha MOS	RQ Box, Prometheus	MOX, EC, PID, MS
	Electronic Sensor Technology	ZNose 4200, 4300, 7100	SAW, GC
	Environics Industry	MGD-1	Ion-mobility
	HKR Sensorsysteme	QMB6	Quartz-crystal microbalance, mass spectrometry-based
	IMSPEX	FlavourSpec	Ion Mobility Spectrometry (IMS)
		BreathSpec	Ion Mobility Spectrometry
		GC-IMS	Ion Mobility Spectrometry with chromatographic pre-separation

Combined-technology (eNose + analytical instrument)		GC-IMS-SILOX	Gas Chromatography – Ion Mobility Spectrometry (IMS)
	Microsensor Syst.	Hazmatcad Plus	SAW, EC
		CW Sentry 3G	SAW, EC
	OWLSTONE MEDICAL	Lonestar VOC Analyser	Field-Asymmetric Ion Mobility Spectrometry
		Ultra FAIMS	Ion mobility & mass spectrometers
	Rae Systems	Area RAE monitor	CB, O_2, EC, PID
		IAQRAE	Thermistor, EC, PID, CO_2, humidity
	RST Rostock	FF2, GFD1	MOX, QMB, SAW
	SMart Nose	Smartnose-300	Mass spectrometry-based

2.6 Medical Applications of eNose

One application that has seen considerable researcher effort is in the area of biomedicine. The human body emits volatile organic compounds (VOCs) from different parts, such as breath, skin, blood, faeces, spit and urine. A person's daily odour fingerprint can be changed if he/she has an infection or metabolic disorder. The disorder may produce new VOCs or changes the ratio of the normal VOCs emitted [152]. The relation between unusual smell of human and disease probability was raised by the father of medicine, Hippocrates, around 400BC[153]. Similarly, in traditional Chinese medicine the olfactory sense was used in diagnosis of disease[154]. Existence of microbial types in a body leads changes in production of VOCs in human waste, as the microbial interacts with organic media and biological fluids[152]. Investigations of abnormal chemicals in human fluids started from the development of GC and MS in late 20th century. For example, there was a study in 1988 investigating 189 strains of 33 bacterial species using GC and they concluded that strains of species produced wide range of VOCs, but it wasn't possible to distinguish strains of species completely[10]. However, even now GC-MS has yet to make it into routine medical diagnosis due to their high operating costs, time-consuming procedure, sample-preparation methods, and need for training and expertise for effective operation and data interpretation [155, 156]. For this reason, there has been interest in using eNose instruments that are cheaper, simpler and more user-friendly [10].

Gibson et al.[102] reported an accuracy of 93.4% using an eNose containing an array of 16-sensors to identify and classify twelve different bacteria and one pathogenic yeast. In parallel, Chandiok et al. [157] reported the positive predictive value of 61.5% for screening bacterial vaginosis with using AromaScan eNose. The accuracy of this study in the classification of bacteria was 99.69%[158]. In a similar study on Escherichia coli and Staphylococcus aureus bacteria, Gardner et al. [159] used an eNose with six different metal oxide semiconducting gas sensors for classification of these bacteria and it could successfully classify 100% of unknown S. aureus samples and 92% of the unknown E. coli samples. Many studies have been undertaken with eNose's for early disease diagnoses Table 2.5 summarises some of the commercial eNose that have been successfully used for diagnosing a wide range of diseases.

Table 2.5 commercial eNose instrument which showed success in diagnosing disease

eNose instrument	Manufacturer	sensor	Disease diagnosis	source	references
Bloodhound BH-114	Roboscientific	14 Conducting Polymers	Early detection of TB	culture sputum	[160]
			Urinary tract infections	urine	[161]
Cyranose C320	Cyrano Sciences	32 Conducting Polymers	Bacterial & SA infections	Eye fluid	[104]
			Pneumonia score prediction	breath	[162]
			Lung cancer detection	breath	[163]
			Bacteria identifications	Blood urine	[164]
DE 101	Experimental model	3 MOS	Detect renal dysfunction	sweat	[165]
Fox 2000	Alpha MOS	6 MOS	Diagnose diseases	breath	[166]
FOX4000	Alpha MOS	18 MOS	Diabetes	urine	[50]
Lonestar VOC Analyzer	OWLSTONE	FAIMS	Colorectal cancer	urine	[167]
			Inflammatory bowel disease	breath	[168]
			Pelvic radiation disease	Stool	[169]

2.7 Using Urinary VOCs in Diagnosing Diseases

In this study, we have focused primarily on investigating urine as the biological waste of choice, as it provides an integrated physiological signal that is stable, can be provided on demand and, in our experience, is the most “user friendly” of biological samples for both the patient and the investigation team when compared with blood, breath and faeces.

One end of the metabolic pathways product is urine that contains a wide diversity of elements, such as ketone, alcohol, furan, pyrrole, and sulphide. Any of these elements can lead to a specific odour[152]. In some cases, the urine odour can be linked to a particular disease. Since urine has previously been used for diagnosing diseases, urine profiles and components have been well characterised [170]. As there have been many diseases diagnosed from body fluids, it is difficult to bring all of them together in a small section. Therefore, in this chapter, we are focusing on diagnosing diseases from urinary VOCs among all body fluids for metabolic and gastro disorders.

Urine is considered as a highly complex fluid from chemical perspective because it’s composition can be affected by a large number of elements such as, gender, age, physical activity and so on[171, 172]. There are several researches were done about identification of biomarkers in urine[171, 173]; however using highly trained dogs as

discriminator are showing the most promising results[174, 175]. In 2015, there was a study on detecting prostate cancer using two female highly trained dogs by sniffing the urinary VOCs and they achieved a sensitivity and specificity of over 97% in diagnosing patients sample from control ones[176]. Table 2.6 shows the important urinary biomarkers that link to specific disease that have the potential to be diagnosed by the eNose.

The metabolic disorder called maple syrup urine disease (MSUD) prevents the breakdown of certain amino acids in body. This causes growth in the level of amino acids in the blood. Thus, this particular disease can lead to smells of maple syrup in urine[177, 178]. Tanaka et al. described a disease in infants, led to the emission of sweaty feet smell from urine[179]. Trimethylaminuria (TMAU) disorder preventing body metabolism from converting trimethylamine into trimethylamine N-oxide. This causes accumulation of trimethylamine in the urine so urine smells fishy[177]. Some of the primary use of aromas emits from human urine in diagnosing disease are summarised in Table 2.7.

Table 2.6 Potential eNose applications for disease diagnoses via detection of urinary VOCs

Disease	Associated biomarkers	References
Anaerobic bacterial infections	Isobutylamine, acetic acid, butyric acid	[161, 180, 181]
Bacteriuria	Specific complex mixture of VOCs	[182]
Haematuria	Specific complex mixture of VOCs	[183]
Metabolic disorders	Isovaleric acid	[184]
Renal dysfunction and failure	Specific complex mixture of VOCs	[183]
Sweaty feet syndrome	Butyric acid, hexanoic acid; trans-3-methyl-2 hexenoic acid	[185]
Urinary tract infection	Isovaleric acid, alkanes, Specific complex mixture of VOCs	[161, 186]
	Benzaldehyde, isobutyraldehyde, isovalaraldehyde; sulfides	[187]
	Dimethyl sulphide, methyl mercaptan	[187]
	Trimethylamine, ethyl acetate	[188]
	Isobutanol, isopentyl acetate ketones, I-undecene	[184, 189]
Gastrointestinal diseases	Trimethylamine, ethyl acetate	[188]

Table 2.7 - early use of urine smell in diagnosing diseases

Disease	Descriptive aroma	References
Azotemia (prerenal)	Concentrated urine odour	[190]
Bladder infection	Ammonia	[177]
Maple syrup urine disease	Maple syrup, burnt sugar	[177]
Sweaty feet syndrome	Foul acetic	[185]
Trimethylaminuria	Fishy	[177]
Tubular necrosis (acute)	Stale water	[190]

2.7.1 Diagnosing Metabolic disorder/ Gastrointestinal diseases with eNose

A person with a metabolic disorder normally has three or more of the following factors: abdominal obesity, elevated triglycerides, low high-density lipoprotein (HDL) cholesterol, high blood pressure, and high fasting glucose [191, 192]. Metabolic disorders attract more attention, since it can lead to cardiovascular and other chronic conditions. Obesity is one of the main diseases caused by metabolic disorders, which then leads to many gastrointestinal diseases[192]. US and western countries are suffering from a rapid increase of numbers of people with gastroesophageal reflux disease (GERD) and obesity[193, 194]. Gastrointestinal diseases cover all conditions associated with the gastrointestinal (GI) tract. Irritable bowel syndrome (IBS), hemorrhoids, diverticular disease, colon polyps, colon cancer, and inflammatory bowel disease are the most common GI example[195]. Early diagnosis of metabolic disorders are important, because it helps with earlier and more operative treatments, more rapid

recovery, which mean short stay in hospital and subsequent reduced costs[196]. Since early diagnosis of metabolic disorders are important, eNose instruments have been used extensively for different studies (using urine) such as, IBD[22, 168], colorectal cancer[22], and prostate cancer[197]. Our group have previously shown the utility of the electronic nose to detect and monitor a range of gastroenterological and metabolic disorders[168, 198].

2.7.1.1 Bacterial Cultures

eNose technology has also been used in the discrimination of the different bacterial strains, using the VOCs produced from them. In a study, Pavlou et al. [199], used an eNose instrument with 14 conducting polymer sensors to distinguish anaerobic bacteria such as Clostridium and Bacteroides fragilis using headspace of samples. They used PCA statistical analysis and obtained 94% seperation between these two groups. Bruins et al. [200] used experimental eNose called the "Mono-nose" (manufactured by C-it, Zutphen, The Netherlands) for the separation of 9 different bacterial species. They used Sliding Window-Minimum Variance matching adaptation of the Dynamic Time Warping algorithm for data analysis and achieved 87% of average identification. In another study Aathithan et al. [182] used Osmetech Microbial Analyzer (OMA, Osmetech plc, Crewe, UK), an eNose instrument based on multiple conducting polymer sensors, to diagnose bacterial infection in urine by VOCs. 534 urine samples were collected, where 21.5% of them had a considerable bacteria load and the eNose was able to separate them with sensitivity of 83.5% and selectivity of 87.6%.

A point that these papers raise, is that good sample preparation is essential in order to get a good instrument response and thus good discrimination and classification[29]

2.7.1.2 Urinary Tract Infections (UTI)

The number of people suffering from UTI is continuously rising. It was estimated that 80% of UTI caused by Escherichia coli and the rest as a result of Enterocci, Klebsiella, Proteus, and Candida albicans [29]. Several studies have been done for diagnosing UTI using the eNose. Pavlou et al. [161] focused on using an eNose instrument with a polymer sensor array to distinguish patients with UTI and healthy controls by urinary VOCs. They did two experiments with 25 UTI and 45 control samples. In first experiment they used a neural network (NN) analysis, and they successfully able to separate samples to four groups based on their bacterial species. In a second experiment they used NN analysis method and they could identify 18 of 19 unknown UTI cases. A summary of other UTIs diagnosed with the eNose are presented in Table 2.8.

Table 2.8 Studies related the detection/identification of UTI

eNose	Bacterial Species	Incubation	Results	Reference
BH114-Blood-hound	Escherichia coli, Proteus spp., Staphylococcus spp.	4 h1/2 37 °C	100% prediction with GA-NN; 98% with back propagation NN	[161]
BH114-Blood-hound	Escherichia coli, Proteus spp., Staphylococcus spp.	5h 37 °C	100% of sensitivity, specificity, accuracy and predictability with fuzzy integral methodology	[186]
BH114-Blood-hound	Escherichia coli, Proteus spp., coagulase-Staphylococcus spp.,	5 h 37 °C	fuzzy integral methodology gives 100% of specificity, accuracy and predictability with fuzzy integral methodology	[201]
ChemPro 100i	Escherichia coli, Staphylococcus saprophyticus, Klebsiella, Enterococcus faecalis	no	LR gives 95% sensitivity, 97% specificity for classification of sterile from infected; LDA used for bacteria classification which gives 95% sensitivity,96% specificity	[202]

2.7.1.3 Cancer Diseases and eNose

There have been a number of studies using eNose's for urinary analysis of metabolic and gastro diseases. As an example, there were two separate pilot studies on using the eNose for prostate cancers diagnosis. The first group was using a commercial ChemPro® 100-eNose, they had 50 patients with prostate cancer and 24 with prostatic hyperplasia. They used leave-one-out cross-validation method for separation of samples and they achieved a sensitivity of 78%, a specificity of 67% and AUC 0.77 [197]. The second group had 14 patients with positive prostate cancer and 27 control samples. They used a Partial Least Square–Discriminant Analysis (PLS-DA) mathematical method and they achieved a 71.4% sensitivity for positive samples, which meant the eNose recognised 10 out of 14 with a specificity of 92.6%. As the core sensing technology is different between these instruments, it is difficult to compare them, but both show the promise of the approach.

In another study Arasaradnam et al. [167] used urinary VOCs with a FAIMS instrument to detect colorectal cancer (CRC) patients from healthy ones. They used 133 urine samples of which 83 had CRC and the remaining were healthy. By analysing the data with a Fisher Discriminant Analysis, they achieved a sensitivity of 88% and a specificity of 60%. The same group did another pilot study with 47 patients, 27 with Coeliac disease (CD), and 20 with diarrhoea-predominant IBS (D-IBS). They analysed the urinary VOCs with FAIMS, and they successfully distinguished between patients with CD and D-IBS by using a Sparse logistic regression method. They achieved a ROC (Receiver Operator Curve) with an area under the curve of 0.91 and sensitivity of 85%

[203]. There are many other studies about using urinary VOCs for diagnosing cancer, which have been summarised by Capelli et al [29]. In general, all different studies indicate promising results, where all of them were able to distinguish between patients with cancer from healthy volunteers. This shows that eNose instruments has potential for diagnosing cancers related to the gastro disorders.

2.7.1.4 Kidney Diseases

When the blood flow to the kidneys is reduced (due to any condition), then prerenal azotemia is produced. In the case of high azotemia levels in urea, creatinine increases in the blood. The build-up of these components results in very strong intense ammonia-like urine smell[10, 190]. Di Natale et al. [183] investigated using the eNose for detecting kidney disease. They used an eNose with a quartz-microbalance sensor array and a PCA method for processing the data. This study used urinary VOCs taken from children affected by kidney diseases and health children. The eNose was successful in separating samples containing blood from others.

2.7.1.5 Bowel Diseases

Resident bacteria in the large bowel, plus the existence of undigested food is at the centre of the several VOCs. Arasaradnam et al.[204] tried to monitor the VOC changes in bowel cleansing on patients using urinary VOCs. Samples were collected at different time periods; 48 h before procedure, time of procedure, one week after and two weeks after. In this study the WOLF (manufactured in-house Warwick) and FAIMS

have been used as eNose instrument. LDA and PCA have been used for WOLF data analysis and Fisher Discriminant Analysis (FDA) used for FAIMS. Both machines were able to separate complete versus partial bowel cleansing from others by using urinary VOCs.

One of the common gastroenterology diseases, is Inflammatory bowel disease (IBD), which causes abdominal pain, discomfort and altered bowel habits. Similar to other disease diagnosis, scientists are looking for a simple, reliable and non-invasive way to discriminate between Crohn's disease and ulcerative colitis (UC). Arasaradnam et al. [71], investigated using FAIMS (Owlstone Lonestar) and a commercial eNose Fox 4000 (AlphaMOS, Toulouse, France) to separate normal healthy from IBD patients. In this study they used urine samples, as a source of VOCs. Urine samples were used in this study were collected from patients with Crohn's, UC as disease group and healthy as the controls group. PCA and DFA was applied as a data analysing method for the FOX 4000 data set and FDA method was used for the FAIMS data set. Both machines showed a promising result for discriminating patients with IBD from the control group with accuracy above 75%.

One of the reason for having chronic diarrhoea is an excess of Bile acids. The additional Bile acid, which cannot be reabsorbed back into circulation, spills to the colon which cause diarrhoea. The current method of diagnosing bile acid diarrhoea (BAD) is imaging, which is expensive, therefor scientists trying to use eNose technology for diagnosing BAD as a more cost-effective method. In a study, Covington et al.[198] tested urine samples collected from patients with bile acid diarrhoea (23 samples), ulcerative

colitis (42 samples) and healthy control (45 sample) with an eNose system FOX4000 and FAIMS to differentiate between each group. LDA data analysis method was used on both machines and the results showed that there were differences between groups with reclassification accuracy of 83%.

Overall, this work shows that VOCs emitted from bodily fluids, such as urine, can be used for diagnosing gastrointestinal diseases. This means that eNose instruments have the potential to replace existing expensive diagnosis tools.

2.8 Conclusion

Recent advances in the manufacture of gas sensors, with different principles of operation, has led to the development of eNose instruments with higher sensitivity and selectivity. Near-market sensors have been reviewed in this chapter. A systematic review has been undertaken on the basics of eNoses and their application to the biomedical field. Different gas sensing technologies that have been used in eNose instruments, have also been reviewed. The principle of operation, advantages and disadvantages of each one has been explained in detail. There are several gas sensing technologies available that can be used in an eNose, but the most common at this time are MOX and polymer sensors. After that, the commercially available eNose instruments and their sensory systems were described.

The medical profession is becoming ever more interested in the use of gas-phase biomarkers for disease identification and monitoring. This is due in part to its rapid

analysis time and low-test cost, which makes it attractive for many different clinical arenas. This maps well onto the strengths of the electronic nose. However, reviewing the literature identifies specific weaknesses of current sensing technology and approaches. First, they mostly intolerant to two key environmental parameters, temperature and humidity. This is a particular weakness when dealing with biological waste material, including urine. Secondly, there is little focus on the challenges of sample storage and testing. This plays an important role as it can have effect on the diagnostic power of a sample, especially for urine samples. Next, the number of the samples in each study is often limited and is no more than 60 to 100 in total, making the statistical significance limited. In chapter 5, we will introduce an NDIR optical eNose instrument which we believe overcomes some of these issues.

Chapter

3 Urine Stability Study with eNose

3.1 Introduction

This chapter presents the experimental research using the commercially available Owlstone Lonestar FAIMS instrument. The experiment is based on using FAIMS with urinary volatile organic compounds (VOCs) from long range of storage times, to discover effect of sample storage on the amount VOCs releases from them.

As is discussed in the literature review, the medical profession is becoming ever more interested in the use of gas-phase biomarkers for disease identification and monitoring. Of the possible biological media available to "sniff", urine is becoming ever more important as it is easy to collect, can be provided without too much difficulty, has high patient compliance and is easy to store for batch testing. In many urinary based studies, it can be difficult to analyse chemical signals from samples at the point of

collection. The reasons for this are many, but usually due to a combination of the disease having low-prevalence combined with the logistical advantages (in terms of time, money and access to equipment) of batch processing. In this case freezing of the sample (normally at −80 °C) is undertaken. Thus, an important question that has concerned us, and probably others, is "what is the best before date for a urine sample?". Due to the way in which electronic noses analyse samples, it is very challenging to monitor the degradation of any specific biomarker. However, it should be possible to be guided on what a sensible storage period might be by understanding the general loss of chemical information (or by the way that the urine sample changes over time). Therefore, in this study we have attempted to understand the stability and degradation of urine samples, using the electronic nose as the measurement technology.

There have been a small number of studies using GCMS investigating sample age over 24 h in humans and in mice [205, 206]. Yet, these studies do not consider long-term storage and, more importantly for our studies, do not employ an electronic nose in their work. Therefore, we set out to understand the rate of urinary degradation at −80 °C using the electronic nose and from this infer when degradation of the sample becomes significant.

3.2 Samples Preparation

3.2.1 Patients

In diabetes mellitus, the deficiency of insulin alters the metabolism of carbohydrates, proteins and lipids, resulting in high glucose levels present in urine. Patients with type 2 diabetes (T2DM) were recruited from the metabolic clinic at University Hospital Coventry and Warwickshire (UHCW) NHS Trust between December 2009 and May 2014. In total, 48 samples from healthy controls obtained in less than 24 months and 87 diabetes samples were obtained over 53 months and tested as single batch of samples in May 2014 over the course of two weeks. The only criterion for inclusion was T2DM as defined by WHO criteria. Exclusion criteria included sepsis, concomitant diagnosis of inflammatory bowel disease, irritable bowel syndrome, coeliac disease or malignancy. Written informed consent was obtained from all individual participants patients included in the study. Patients were recruited as part of the FAMISHED study. Scientific and ethical approval was acquired from the local Research and Development Office as well as Warwickshire Ethical committee ref: 09/H1211/38. Demographic details are shown in Table 3.1.

Table 3.1 There were a total of 87 diabetic patients; with incomplete data on 15 patients hence this table demonstrates demographics on the remaining 72 patients. OHA—oral hypoglycaemic agents; HbA1c—glycated haemoglobin. HbA1C in normal subjects is 20–42 mmol/mo

Demographic Data		Diabetes Medication	Frequency
Male (%)	44 (61)	OHA	39
Female (%)	28 (39)	Insulin	7
Mean age	56	OHA + Insulin	18
Median age	59	Nil	8
Mean BMI	39	HbA1c	(mmol/mol)
Median BMI	39	Mean HbA1c	67
		Median Hb A1c	57

3.2.2 Urine Collection, Storage and Transfer Patients

Urine samples from patients with T2DM at UHCW NHS Trust were collected at clinic and stored at −80 °C within two hours of collection. They were transferred to the School of Engineering, University of Warwick in a box of dry ice. The samples were then defrosted in a laboratory fridge at 3 °C overnight prior to analysis.

3.3 Commercial Machines

3.3.1 FAIMS

In this study, a commercial FAIMS instrument was employed, specifically a Lonestar (Owlstone, UK). The principle operation if FAIMS has been explained in literature review section.

3.4 Analysis Methodology

3.4.1 FAIMS

5 mL of urine were aliquoted from each sample into a 10 mL glass vial and placed into an ATLAS sample system (Owlstone, UK) attached to the front of the FAIMS, (Lonestar, Owlstone, UK). The ATLAS is a dynamic headspace sampler system that controls the sample temperature, sample agitation and the flow rate over the sample. The ATLAS headspace sampler is contained of four separate components, the Sampling Module Assembly, the Pneumatic Control Box, the Heater Control Box and the Split Flow Box (SFB)[207] .

This setup is commonly used for samples of this type by our group [168, 198]. This heated the sample to 40 ± 0.1 °C. Each sample was tested three times sequentially, with each run having a flow rate over the sample of 200 mL/min of clean dry air. Further make-up air was added to create a total flow rate of 2 L/min. The FAIMS was scanned from 0 to 99% dispersion field in 51 steps, −6 V to +6 V compensation voltage in 512 steps and both positive and negative ions were detected to create a test file composed of 52,224 data points. Fig. 3.1 shows the experimental setup, with Figure 3.2 showing a typical output for a diabetic urine sample (positive ions only). The output of FAIMS is a three-dimensional matrix which is based on the molecules that pass through the electric field between two plates and received at the detector (red molecules in figure 3.2). The electric field is a dispersion field (DF) which varies from 0 to 100 percent in

51 steps and is proportional to the ion's mobility. The molecules which are attached to the plates and lose their charge cannot reach the detector (blue and purple molecules in figure 32). To overcome this issue and receive more molecules in the detector, another voltage is applied to the plate. This voltage is called compensation voltage and is applied in 512 steps. This voltage will repel or attract ions based on their charge. Figure 3.2 shows the ions received in the detector based on dispersion field and compensation voltage.

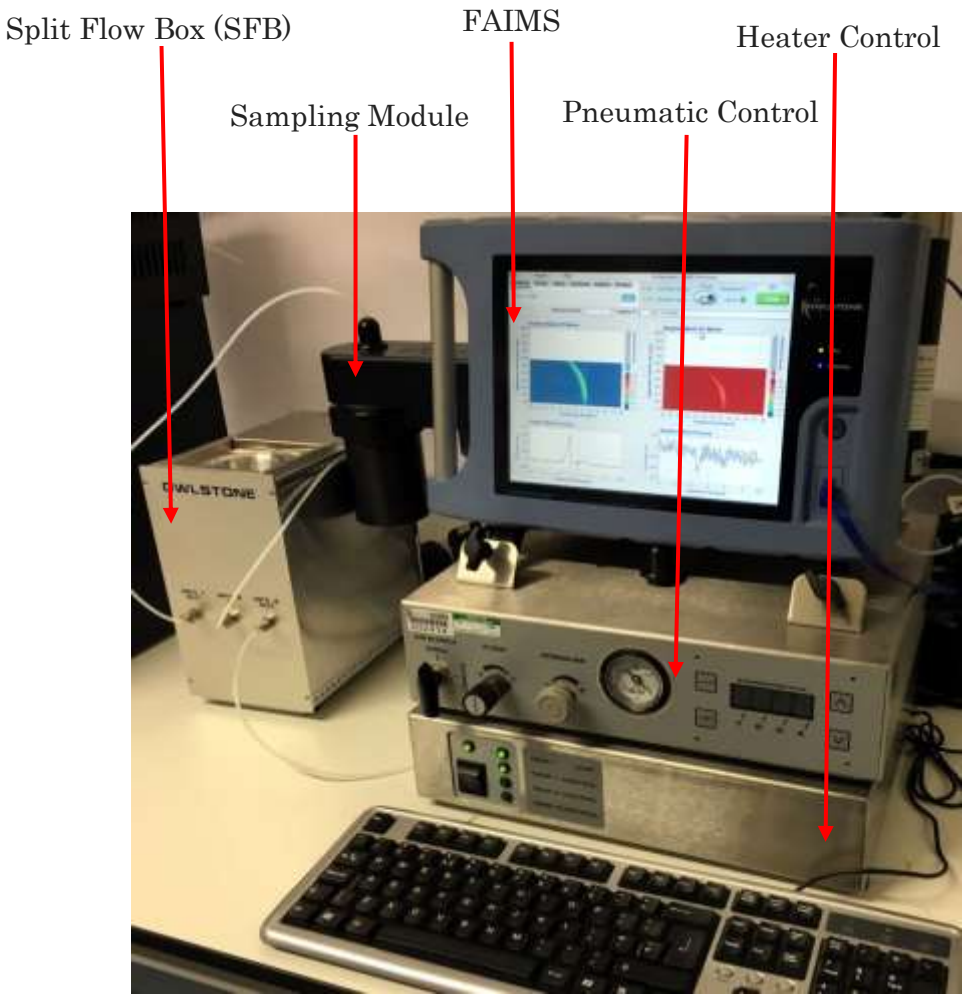

Fig. 3.1 FAIMS experimental setup with Lonestar and ATLAS sampling system

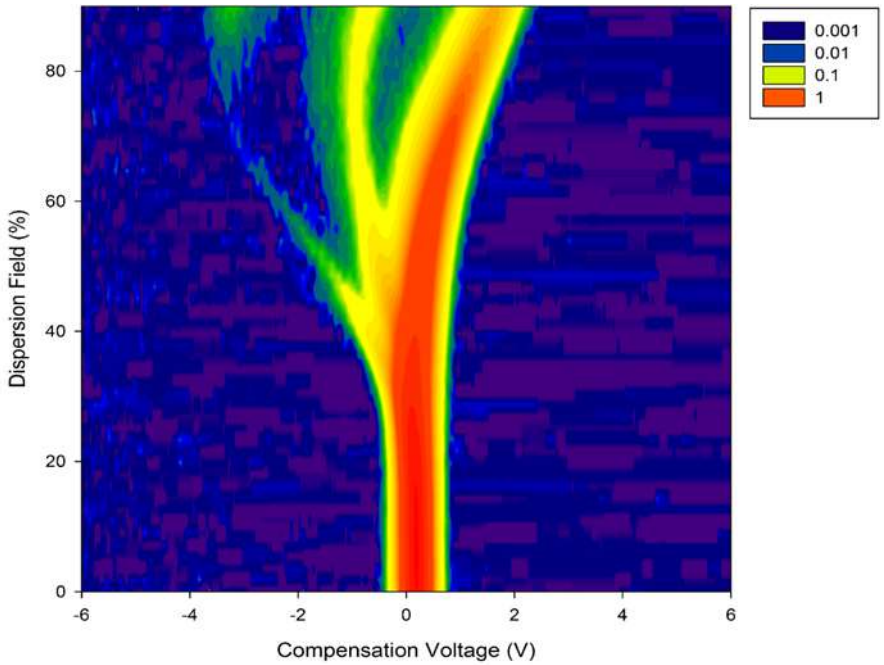

Fig. 3.2 Typical FAIMS output to a diabetic urine sample

3.5 Results

Since the urine samples stability is unknown, the initial analysis considered was the total chemical concentration (a mixture of gases and volatile organic compounds). In FAIMS this is easily achieved by summing up all of the values at a zero-dispersion field (hence no separation), which provides a measure of the total ion count. Fig. 3.3 demonstrates the changes in urinary gas/volatile concentration between 2009 and 2014, using this data. The graph shows that the total amount of chemicals released decreases with sample age with more modern samples having a higher output. This trend is confirmed in both the positive and negative electric fields of the FAIMS instrument depicted by the red and green dots, respectively. We have also averaged the total output of positive and negative ions to emphasis the changes over time, as shown in Table 3.2.

It is worth noting that as the samples get much older (greater than 3 years), the output increases once more, with an associated increase in variance between the samples.

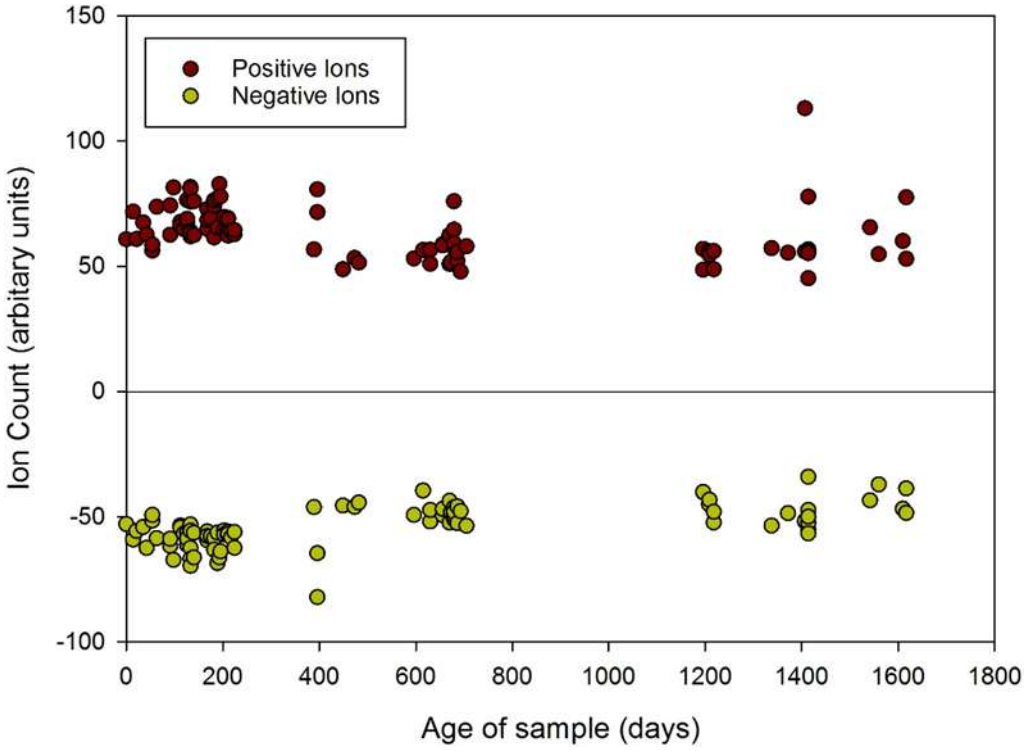

Fig. 3.3 Change in total number of urinary volatile organic compounds over time (from December 2009 to May 2014)

Table 3.2 Changes in output signal for both positive and negative ions as a function of time. Percentage for year one taken as 100%

Positive Ions (Arbitrary Units)						
Year	2014	2013	2012	2011	2010	2009
Age (days)	0–147	148–503	504–859	860–1215	1216–1572	1572–1617
Average	68.2	67.0	57.0	53.4	62.3	63.4
s.d.	7.4	8.6	6.5	3.8	17.7	12.6
%	100.0	98.2	83.6	78.3	91.3	93.0
Negative Ions (Arbitrary Units)						
Year	2014	2013	2012	2011	2010	2009
Age (days)	0–147	148–503	504–859	860–1215	1216–1572	1572–1617
Average	−58.4	−58.2	−48.5	−44.9	−48.6	−44.7
s.d.	5.3	7.8	3.5	4.7	7.0	5.2
%	100.0	99.7	83.0	76.9	83.2	76.5
Threshold Values (Positive Ions only)						
Year	2014	2013	2012	2011	2010	2009
Age (days)	0–147	148–503	504–859	860–1215	1216–1572	1572–1617
Average	54.3	55.5	53.2	54.3	52.8	52.3
s.d.	2.3	2.2	2.2	1.8	2.1	1.5
%	100.0	102.2	98.0	100	97.2	96.3

In addition to measuring the change in overall gas/volatile concentration, we also investigated the chemical diversity of the samples. We define chemical diversity as a measure of the amount of different chemicals in the sample, independent of concentration. As FAIMS separates chemicals based on mobility, it is possible to measure the diversity of chemicals at a specific dispersion field, though we are unable to separate chemicals with the same differential mobility. In our case, we took a 50% dispersion field (selected as a compromise between chemical separation and measuring as many chemical as possible), then used a threshold value of 0.01 to remove the

background noise. This result shown in Fig. 3.4. Again, this result has been averaged into each year and is shown in Table 3.2.

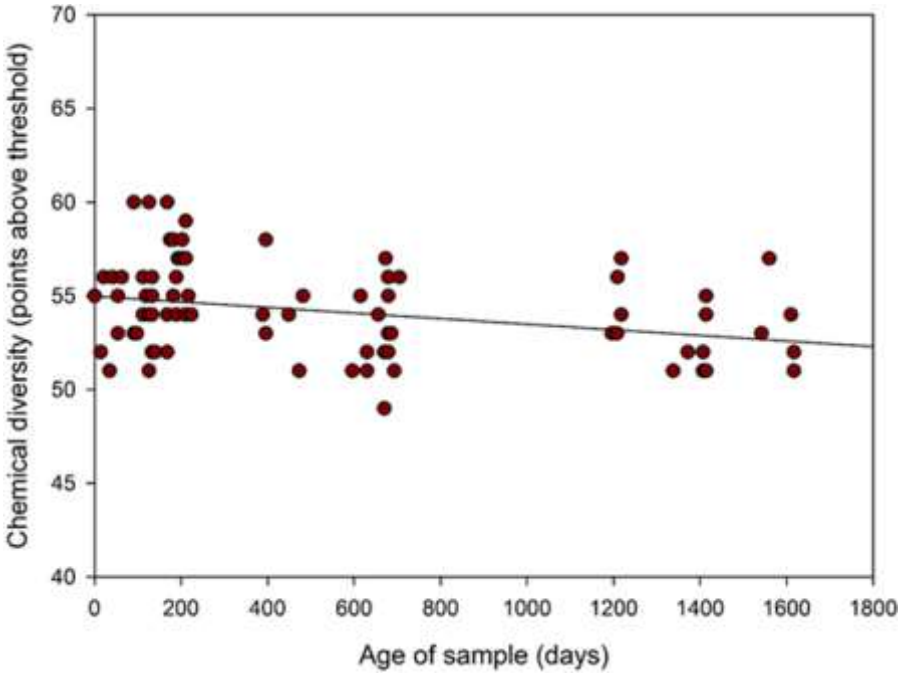

Fig. 3.4 Chemical diversity of urinary volatile organic compounds over time (from December 2009 to May 2014), with linear fit to emphasis output change

Of note, there is less variation in the total number of emissions in the more recent samples with greater uniformity and stability of concentrations together with tighter clustering of the total number of chemicals released. This is particularly evident for the urine samples obtained from October 2013 to May 2014, which demonstrates that the chemical information is stable for at least 9 months, as shown in Fig. 3.5 and Table 3.3. In the latter table, the data for 12 months is included and after a 9-month period there data suggests a fall-off in chemical output. Some care should be taken due to the

variance in measurements, but there is a clear reduction in chemical output after 9 months.

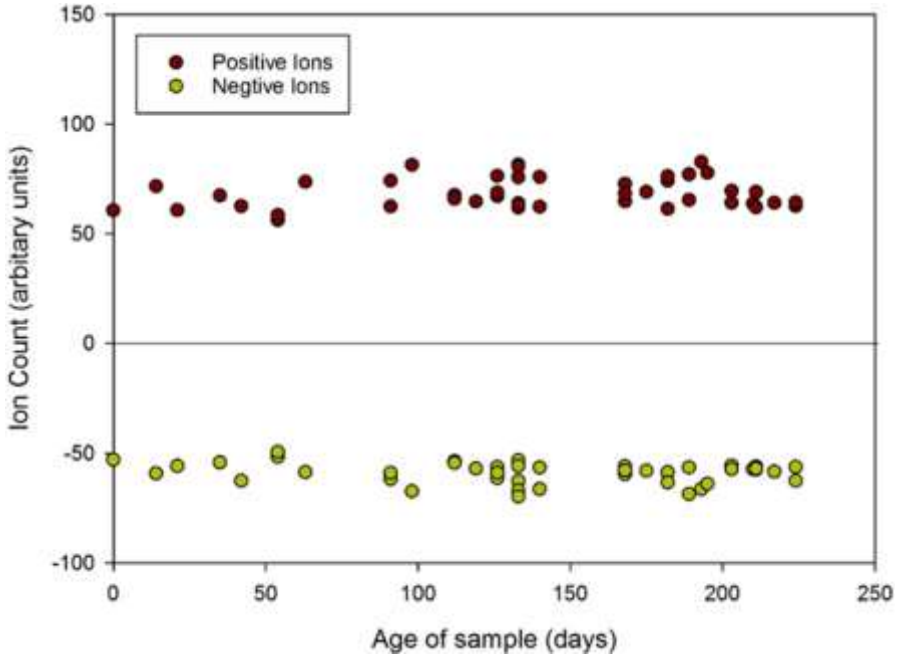

Fig. 3.5 Change in total number of urinary VOCs over time (from May 2014 to September 2014)

Table 3.3 Total positive ion counts for samples collected in 2014 in 3 monthly periods

Year	May 2014–March 2014	February 2014–December 2013	November 2013–September 2013	August 2013–June 2013	May 2013–March 2013
Age (days)	0–88	89–178	179–269	270–356	357–445
Average	64.0	70.0	69.0	No data	64.4
s.d.	6.3	6.8	6.7	No data	12.1

3.6 Discussion

In this chapter, we set out to understand how the gases and vapours emanating from a stored urine sample are affected by storage time, using the electronic nose. In these experiments diabetes samples were used, which were collected over an extended period of time. In most cases samples would be tested well before this four-and-a-half-year period, but it is common to store blood and other samples for many years for future researchers. Our study suggests that this is not feasible when dealing with urine samples for gas analysis. It is likely that the loss of chemical signal would be associated with a specific disease, however here we only considered one disease—diabetes and we did not track biomarkers as the sample ages. Furthermore, it is very unlikely that individual groups would undertake this type of study for each disease, making this an interesting result and could guide other researchers. It is also likely that other biological samples (such as blood and stool) would also degrade at −80 °C and further work is needed to understand this process.

The loss of gases and volatiles from a stored urine sample is not totally unforeseen. The results indicate that we are losing chemical information—both the amount of signal available and the diversity. The latter is not unexpected as when chemical concentration reduces, some chemicals will then fall below the detection limit of the instrument. When the samples get very old, their emissions become very erratic, suggestion some secondary breakdown has occurred in some samples, significantly increasing the total emissions.

The reason for this is loss of signal is not totally clear, however it is well known that all gases and vapours will emanate from a sample over time as equilibrium is reached between the urine and the airspace in the storage container. This process can be reduced at −80 °C, but is not halted, especially for low molecular weight gases dissolved in the sample. In addition, we may be observing water in the urine evaporating as it ages with the subsequent release of water-soluble volatiles. For the very old samples, we may be seeing bacterial activity that could be resulting in a higher chemical output, as described in [8]. Finally, in our case, the samples are stored in standard plastic sterilin bottles, commonly used by the medical profession. It may be possible that the plastic is absorbing volatiles over time. This requires further investigation but was beyond the scope of this study.

From our experiments, we can tentatively propose a urine sample best before date of 12 months, though ideally samples should be tested within 9. Analysis of the results shows that there is no significant loss in chemicals over this 9-month period but appears to increase relatively rapidly after this. However, care should still be taken to ensure that when samples are collected from different groups (disease and control) then samples should be collected at similar times and not be separated by a significant period. We have found (unpublished results) that even fresh samples vs. 6-month-old samples could result in separation (using pattern recognition techniques) based on age instead of disease.

Of final note, for samples taken over the first 9 months, the variation in chemical output and the differences in chemical diversity only changes by around 10% across the

samples. The diabetic patients were under no dietary controls and urines were collected as spot samples. Though the samples were from a single disease group, it is interesting that the differences in gender, age and diet only produced a relatively small change in volatile output.

3.7 Conclusion

Gas phase biomarkers are becoming of ever increasing interest to researchers. One instrument showing promise is the electronic nose—an instrument that attempts to mimic the biological olfactory system by analysing samples as a whole. Urine is an important sample type, due to its ease of collection and clinical utility. However, when undertaking this type of research, the question of long-term stability in storage becomes important, especially for diseases with low prevalence. Although in this study samples were taken and analysed from those with diabetes and we did not track any specific biomarker (which is difficult with the electronic nose), it is biologically plausible that these results could be used to infer for diabetes and other medical conditions a possible storage time. Our results suggest that even at −80 °C, changes of total chemical concentrations are noticeable before 200 days and continue over time. Extrapolating our results would suggest that storage at −20 °C would result in more rapid loss of chemicals but remains uncertain at which time point the stored sample loses its diagnostic value.

Chapter

4 Discrimination of Diabetes from Control Samples Using eNose Technology

4.1 Introduction

This chapter presents the experimental research results of using two commercial eNose instruments, the Owlstone Lonestar FAIMS and AlphaMOS FOX4000 with urinary volatile organic compounds to diagnose the urine samples collected from diabetic patients and healthy controls.

Diabetes affects 8.3% of all adults (387 million people) in the world, with 43% being underdiagnosed, resulting in 4.9 million deaths per year (mostly in low and middle-countries) [208]. Treatment can be as simple as life-style changes but requires correct diagnosis. Diabetes is a standout amongst the most widely recognized chronic disease caused by metabolic failure to function in a normal way in breaking down carbohydrate. Diabetes happens either when the pancreas does not create enough

insulin or when the body can't utilize the insulin it produces. The level of glucose in the blood shows if the person is suffering from diabetes or not. Blood based methods are currently used but are invasive. Another technique for diagnosing diabetes quickly is measuring glucose level in urine. In healthy control people the level of glucose in urine is very low; however, diabetic people have high level of sugar in their urine, which cause their urine to smell sweet or fruity. Hence, this increases chance of using eNose technology for diagnosing diabetes from urine odour. Although using urinary VOCs to detect diabetes seems reasonable and possible, there hasn't been an appropriate and comprehensive study on this area. Siyang et al. and Sabeel et al. tried to diagnosing diabetes with eight commercial chemical gas sensors and Cyranose 320 respectively with PCA data analysing method but unfortunately, they didn't provide the sensitivity or specificity of their experiments, but it did suggest that using eNose for diagnosing diabetes from urinary VOCs is possible. Ping et al. discovered that ethanol, methyl nitrate, acetone and complex volatile organic compounds (VOCs) exist in diabetic human patient breath [209]. However, breath analysis has a high degree of variability and requires fasting before the sample is taken.

4.2 Study Overview

Our approach was to undertake a pilot study to investigate if urinary VOCs (volatile organic compounds) could be used as a non-invasive means to identify patients with type 2 diabetes Mellitus (T2DM). These samples were collected over a four-and-a-half-year period and stored at −80 °C and then analysed using by Owlstone Lonestar

FAIMS and FOX4000, as two types of electronic nose. From previous study, which was explained in chapter 3, it was discovered that samples over 12 months old will not emit enough VOCs, so this chapter will focus more on analysing samples less than 12 months old for diagnosing diabetes samples from healthy control ones.

4.3 Patients

138 urine samples were collected at the University Hospital Coventry & Warwickshire, UK. Of these 71 samples came from patients with type 2 diabetes, with a further 67 samples from healthy controls. Samples were collected in clinic and were frozen at -80 ^{o}C within two hours. Scientific and ethical approval was obtained from the Warwickshire Research & Development Department and Warwickshire Ethics Committee 09/H1211/38. Written informed consent was obtained from all patients who participated in the study. For analysis, samples were thawed to 4 ^{o}C in a laboratory fridge for 24 hours prior to testing (to minimize chemical loss), then 3 ml of urine sample was aliquoted into 10 ml glass vials. Demographic details of patients are indicated in Table 4.1.

Table 4.1 Demographic information of used urinary samples (incomplete data for 2 diabetic patients)

Demographic Data	Diabetes	Control
Male (%)	27 (39.1)	43 (64.2)
Female (%)	42 (60.9)	24 (35.8)
Median age (year)	57	53.5
Mean alcohol (units/week)	1.8	1.09
Median alcohol (units/week)	0	1
Median BMI	39.7	26.1

4.4 Commercial Machines

4.4.1 FAIMS

Similar to the previous chapter, a commercial FAIMS instrument was employed in this study, specifically a Lonestar (Owlstone, UK). The principle operation of FAIMS has been describe in literature review.

4.4.2 FOX 4000

The second instrument used in this study, was a commercial electronic nose (FOX 4000, Alpha M.O.S, France) combined with a HS100 autosampler. Fox 4000 consists of injection system, sensor chambers with sensor array, mass flow controller and acquisition board with microcontroller. The eNose contains 18 metal oxide gas sensors, which are placed in three chambers and were calibrated regularly in line with manufacturers recommended procedures to ensure stability. These three chambers are called T, P and LY. All the sensor's names and their application are indicated in Table 4.2.

The basic operation principle of electronic nose is based on sensor's electronic resistance changes in presence of volatile compounds. The output response of eNose can be calculated by equation 4.1 [210].

$$R = (R_0 - R_T)/R_0 \qquad (4.1)$$

Where R is response of sensor, R_0 is initial resistance of metal oxide sensor at time zero and R_T is sensor's conductance value.

Table 4.2 α-FOX4000 eNose sensor arrays & their applications

Sensor No.	References	Description
S1	LY2/LG	Oxidizing gas
S2	LY2/G	Ammonia, carbon monoxide
S3	LY2/AA	Ethanol
S4	LY2/GH	Ammonia/ Organic amines
S5	LY2/gCTL	Hydrogen sulfide
S6	LY2/gCT	Propane/Butane
S7	T30/1	Organic solvents
S8	P10/1	Hydrocarbons
S9	P10/2	Methane
S10	P40/1	Fluorine
S11	T70/2	Aromatic compounds
S12	PA/2	Ethanol, Ammonia/Organic amines
S13	P30/1	Polar compounds(Ethanol)
S14	P40/2	Heteratom/Chloride/Aldehydes
S15	P30/2	Alcohol
S16	T40/2	Aldehydes
S17	T40/1	Chlorinated compounds
S18	TA/2	Air quality

4.5 Analysis Methodology

4.5.1 FAIMS

5 mL of urine were aliquoted from each sample into a 10 mL glass vial and placed into an ATLAS sample system (Owlstone, UK) attached to the front of the FAIMS, (Lonestar, Owlstone, UK). The ATLAS is a dynamic headspace sampler system that controls the sample temperature, sample agitation and the flow rate over the sample. This setup is commonly used for samples of this type by our group [168, 198]. This

heated the sample to 40 ± 0.1 °C. Each sample was tested three times sequentially, with each run having a flow rate over the sample of 200 mL/min of clean dry air. Further make-up air was added to create a total flow rate of 2 L/min. The FAIMS was scanned from 0 to 99% dispersion field in 51 steps, −6 V to +6 V compensation voltage in 512 steps and both positive and negative ions were detected to create a test file composed of 52,224 data points.

4.5.2 FOX 4000

The 3ml samples were agitated and heated to 40 °C for 10 minutes before 2.5 ml of the sample headspace was injected into the electronic nose (flow rate over the sensors was 200 ml/min of zero air, data was recorded for 180 seconds at a sample rate of 1 Hz). The summary of the FOX 4000 analytical conditions are indicated in Table 4.3.

Table 4.3 Summary of experimental setup

Volume of sample in the vial	3ml
Total volume of vial	10ml
Acquisition time	180s
Flow	200ml/min
Injection speed	500ul/s
Incubation temperature	40 °C
Syringe flushing time	120s

Fig. 4.1 shows the FOX 4000 experimental setup and Fig. 4.2 indicates typical response of FOX 4000 with 18 sensors to diabetic urine sample's volatile compounds. Each curve signifies one sensor's response. Concentration and nature of sensed molecules plus type of metal oxide sensors used [211].

The data from the FOX 4000 are generated by sampling each of the 18 metal oxide sensors over 180 Seconds. These readings are concatenated into a single vector representing a single sample, and thus the raw data are of dimension 2376.

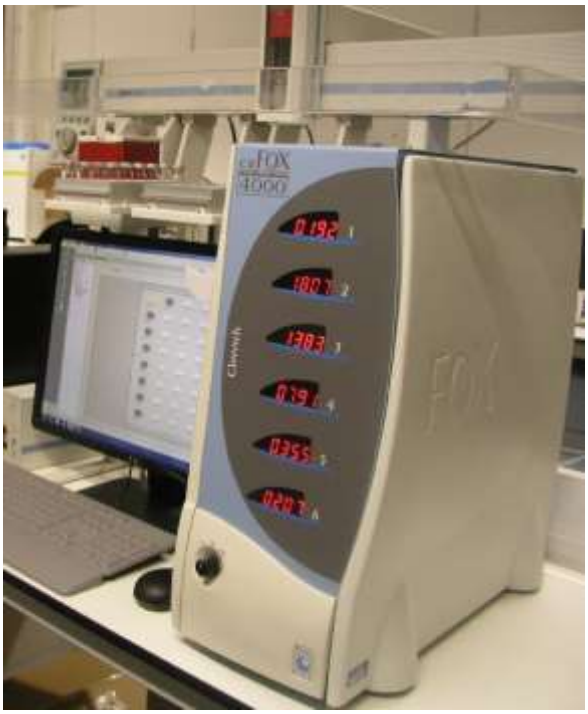

Fig. 4.1 αFOX 4000 experimental setup

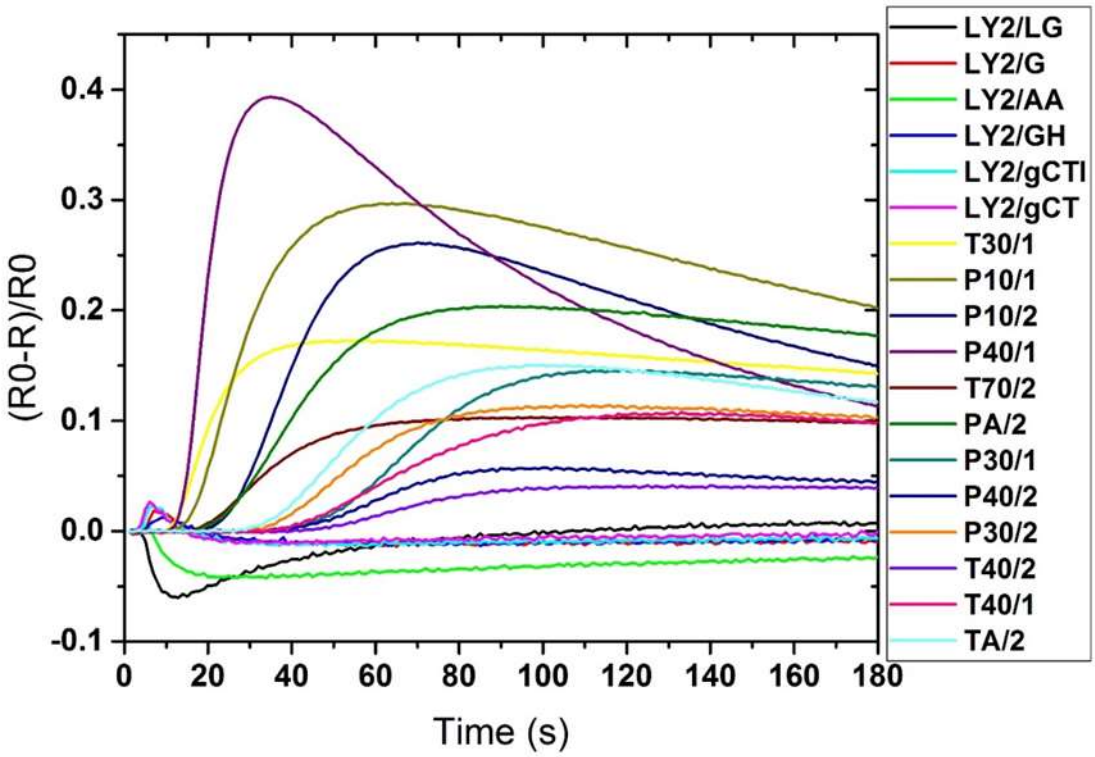

Fig. 4.2 Typical response of αFOX 4000 with 18 sensors to diabetic urine sample's volatile compounds

4.6 Results

4.6.1 FAIMS

Each FAIMS data set consists of 52224 data points that are stored in a 512 x 102 matrix. The first step of data processing was performing pre-processing step to the data by applying 2D wavelet transform (using Daubechies D4 wavelets) to each data set. This step aimed to decompose the signal and extract subtle chemical signal within wider range of signal. 2D wavelet transform will concentrate the chemical information into several levels which consist of a small number of wavelet coefficients. These

coefficients would then be the input for a 10-fold cross-validation, using 90% of the data as a training set, and the remaining 10% as a test set. Within each fold, supervised features selection was performed using Wilcoxon rank sum test by calculating the p-values for every pair of features in the training set. Principal Component Analysis (PCA) was performed to see distribution of data in the scatter plot. Ten most statistically important features, which had the lowest P-values were then used to predict the result of the test set. Four different classifiers were used for prediction, specifically Sparse Logistic Regression, Random Forest, Gaussian Process, and Support Vector Machines. Finally, the performance of classifier algorithms and their diagnostic capabilities were calculated and displayed in a graphical plot called Receiver Operator Curve (ROC). ROC provides information about Area Under Curve (AUC), sensitivity, specificity, Positive Predictive Value (PPV), Negative Predictive Value (NPV), and P-values.

As it was explained in previous chapter (chapter 3), sample age is affecting the vapour emission from the sample. Fig. 4.3 shows that using PCA method on the whole group of samples from zero to four years is not sufficient to distinguish between diabetic samples from control ones. However, by separating samples with their age and applying PCA method, the results of the PCA shows better separation between diabetes and control groups on newer samples. Fig. 4.4 indicates the PCA analysis on samples older than 3 years, the variation of samples is too much although there are not enough samples in this period. Since there are enough number of samples between 1 and 2 years old, the PCA analysis is statistically more reliable compare to the sample older

than 3 years. It is clear from Fig. 4.5, that PCA does not show enough separation between diabetic from control group for samples between 1 and 2 years. The best separation is related to the samples age less than 1 year as expected, where the separation is clear between two different groups, as shown in Fig. 4.6. Only three samples have cross selectivity between diabetes and control groups. The result of analysis of data with receiver operating characteristic (ROC) classification method are summarised in Table 4.4 Summary of the ROC analysis details for samples with less than 1 year oldTable 4.4 and illustrated in Fig. 4.7.

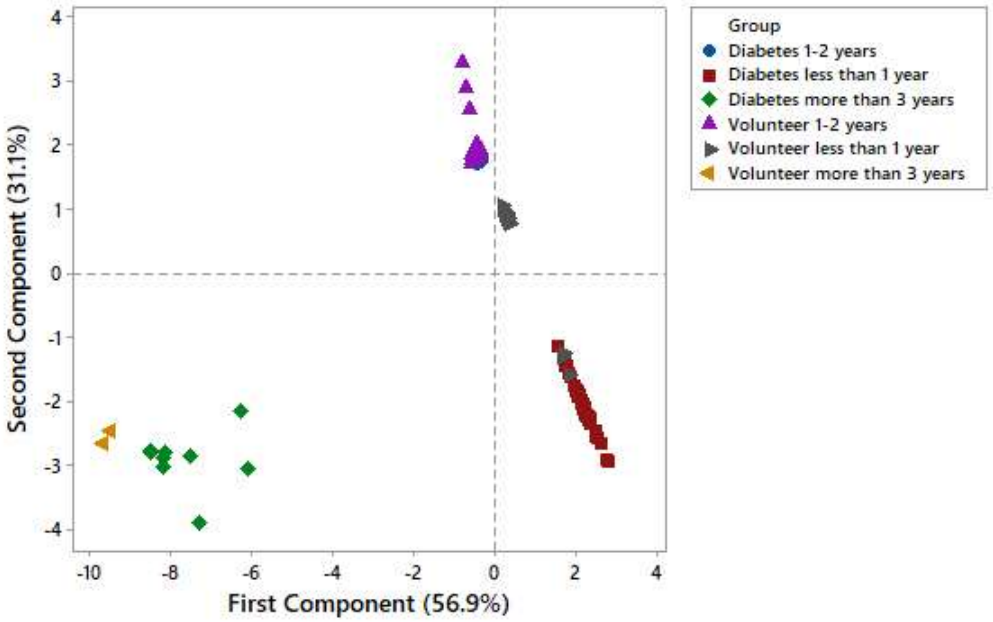

Fig. 4.3 PCA analysis on samples between 0 and 4 years

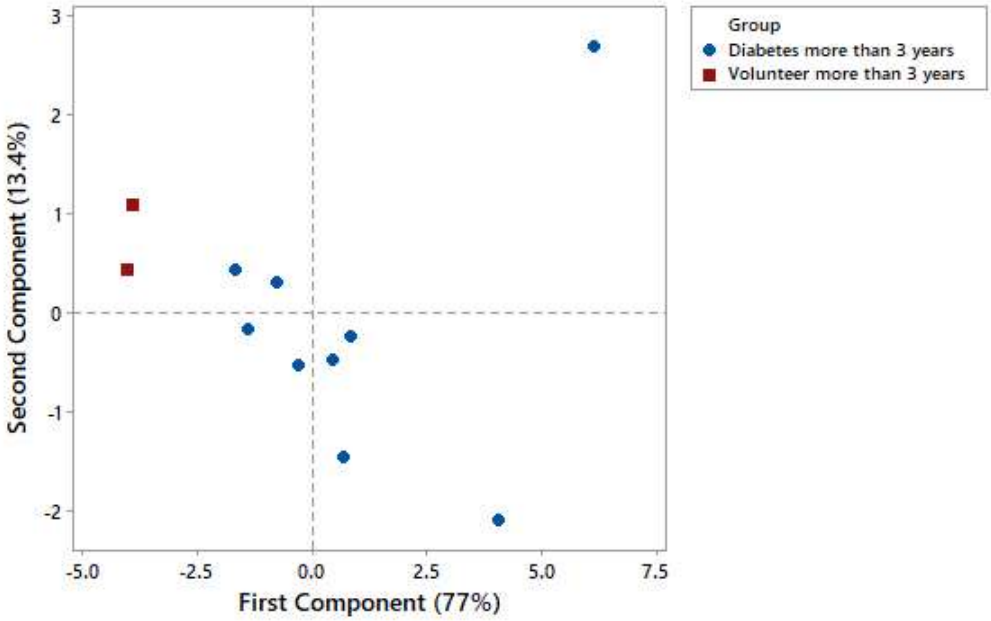

Fig. 4.4 PCA analysis for sample more than 3 years old

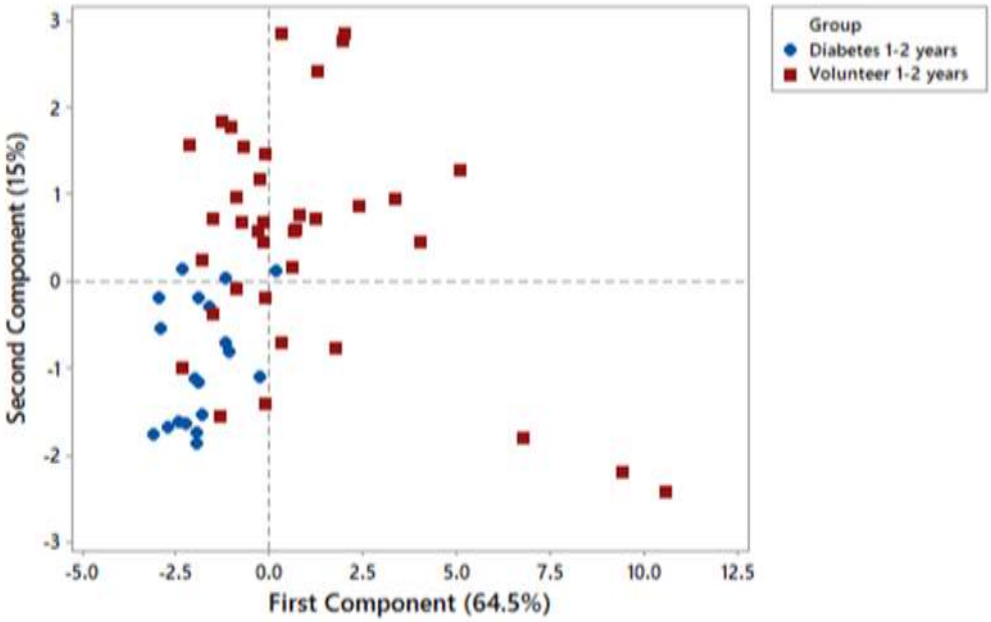

Fig. 4.5 PCA analysis for samples between 1 and 2 years old

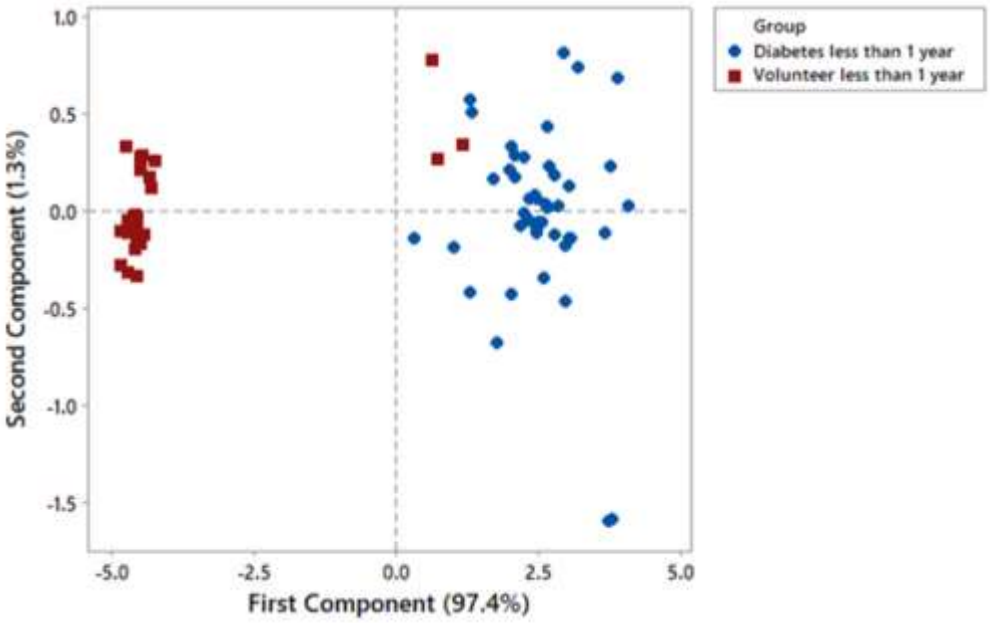

Fig. 4.6 PCA analysis for samples less than 1 years old

The ROC analysis was processed for samples less than 12-month-old with four different analysis methods. Gaussian process appears to be the best method since it has the highest area under curve and also from medical side it is important to have low negative predictive value (NPV) which this method has it among the others. the area under the curve in ROC curve shows how good is the separation. The max value for area under the curve in ROC curve is 1. AUC values for all methods, which have been used for data with less than a year, is more than 0.9, which is considered as a high value.

Table 4.4 Summary of the ROC analysis details for samples with less than 1 year old

Methods	AUC	Sensitivity	Specificity	PPV	NPV	P-value
Sparse Logistic Regression	0.91 (0.8 - 1)	1 (0.92 - 1)	0.89 (0.72 - 0.98)	0.94	1	$9.438*10^{-11}$
Random Forest	0.93 (0.85 - 1)	1 (0.92 - 1)	0.89 (0.72 - 0.98)	1	1	$3.466*10^{-11}$
Gaussian Process	0.96 (0.91 - 1)	0.98 (0.88 - 1)	0.89 (0.72 - 0.98)	0.94	0.96	$4.384*10^{-15}$
Support Vector Machine	0.93 (0.85 - 1)	1 (0.92 - 1)	0.89 (0.72 - 0.98)	0.94	1	$3.363*10^{-12}$

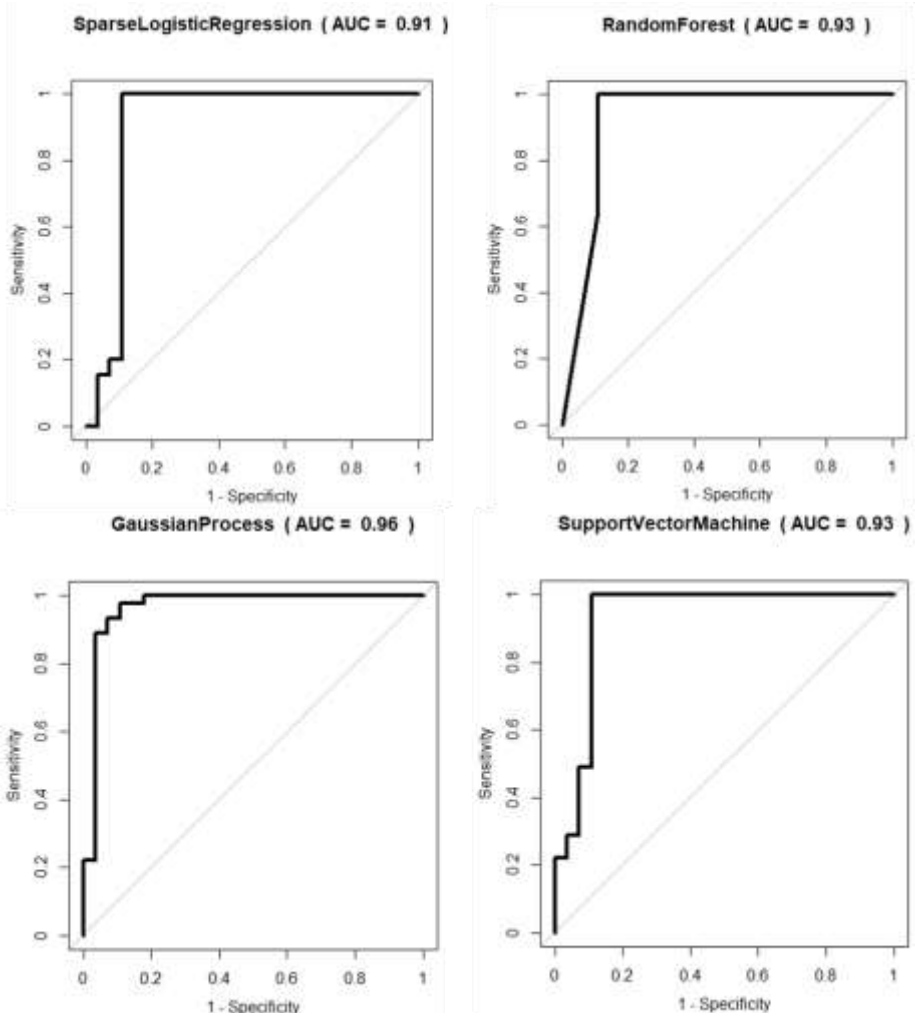

Fig. 4.7 Receiver operating characteristic (ROC) analysis of samples age less than 1 year

4.6.2 FOX 4000

Fig. 4.8 shows a radar plot of the maximum change in resistance divided by the initial sensor resistance in clean air (averaged across all sensor responses per disease group), illustrating that no single sensor can separate control and disease samples.

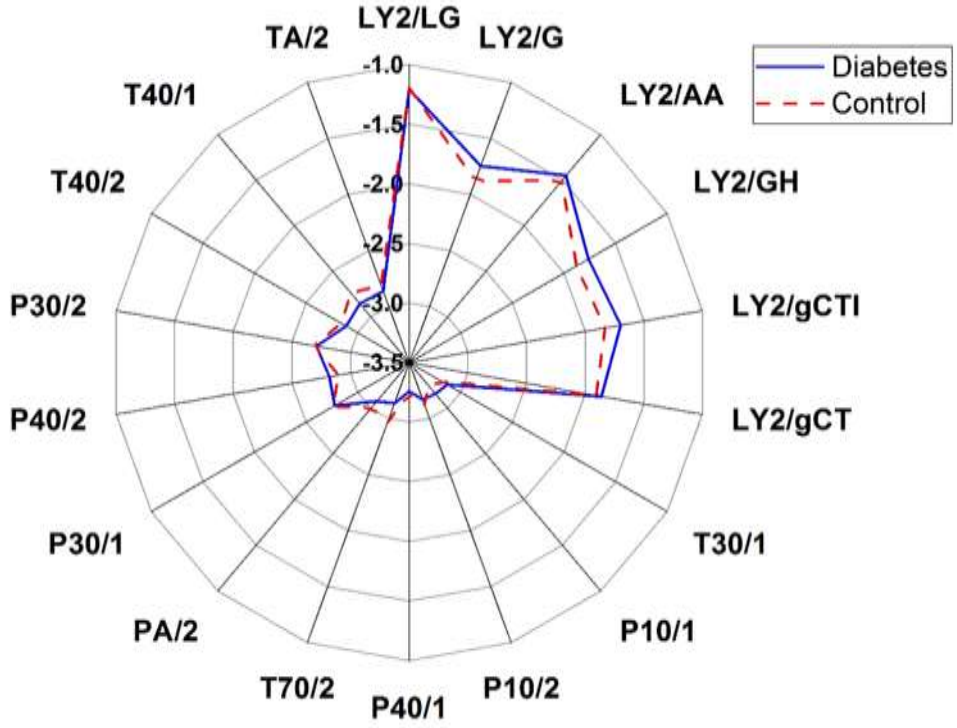

Fig. 4.8 Averaged of maximum change of sensor resistance in clean air

PCA analysis was used for classification of the features that were extracted by dividing the maximum resistance by the baseline resistance. Plotting only the first and second PCA components shows the disease classification has been affected by urine samples storage age. Fig. 4.9 illustrates the diabetes and control samples collected in 4 years where the classification is not separated appropriately. Fig. 4.10 shows the

classification for diabetes and control samples collected and tested in less than 18 months. The results show that newer samples tightly clustered and sufficiently separated from the disease class in comparison to the group with older samples.

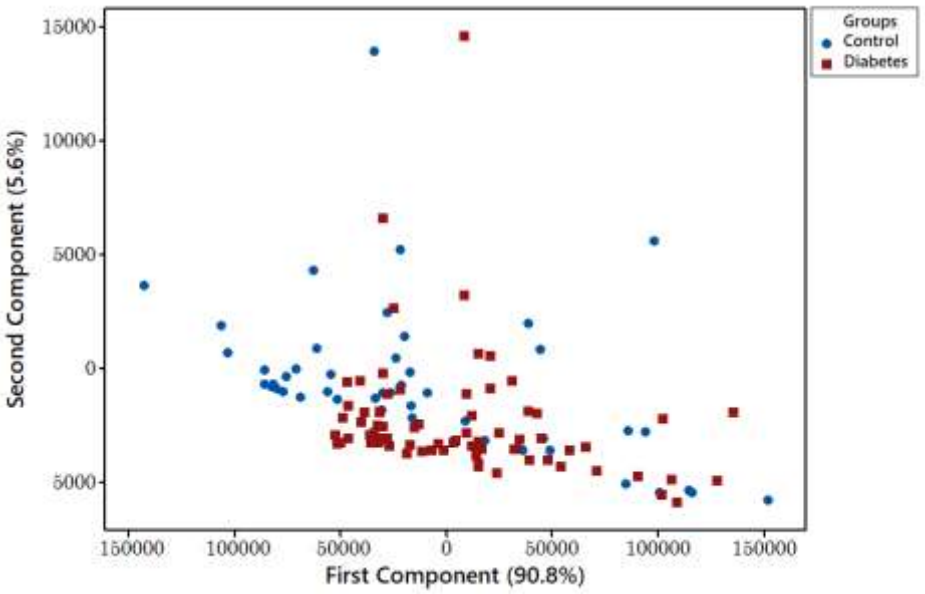

Fig. 4.9 PCA components 1 and 2 shows 4 years old disease and control samples separation

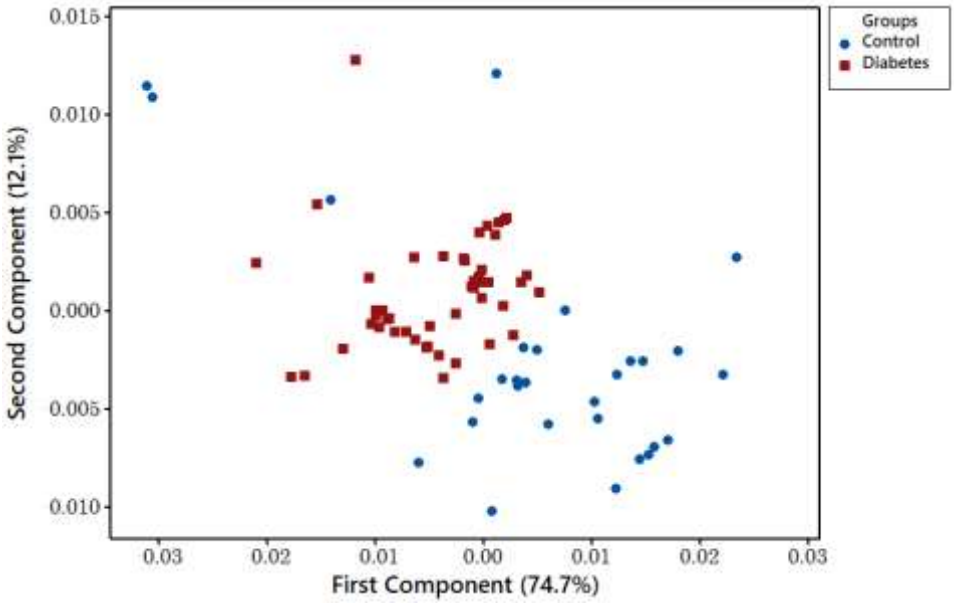

Fig. 4.10 PCA components 1 and 2 shows 18 months old disease and control samples separation

Fig. 4.11 shows the linear discrimination analysis (LDA) result for samples with four years old. As can be seen, there is no clear separation between groups. Fig. 4.12 shows LDA method's result on newer samples with less than 18 months. This shows clear separation between both groups.

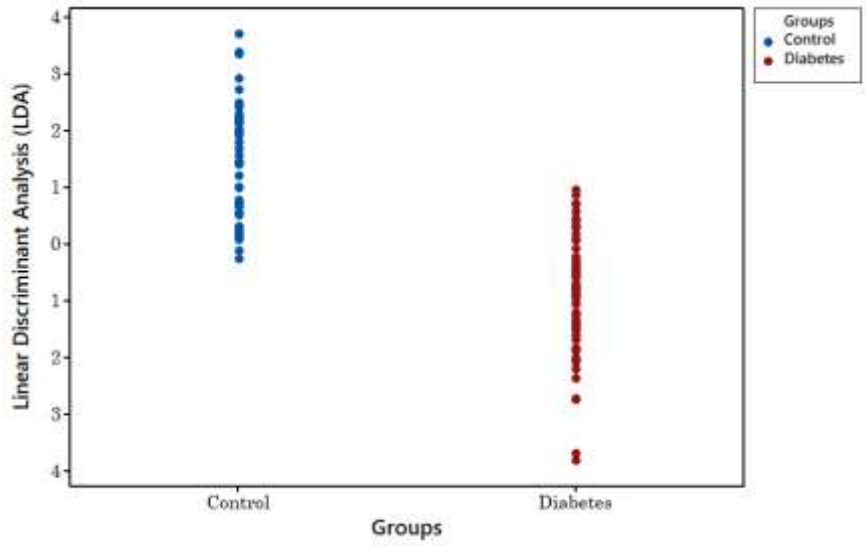

Fig. 4.11 LDA classification of 4 years old disease and control samples

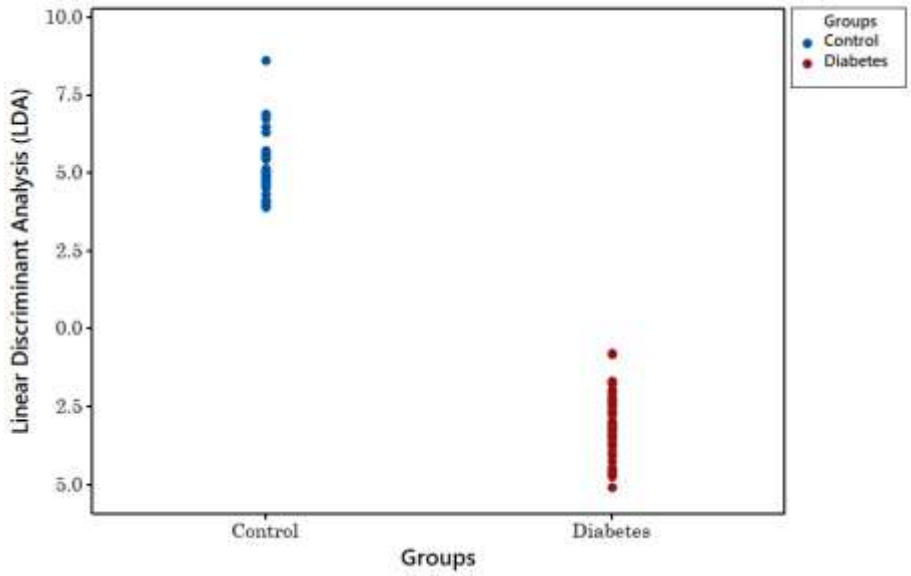

Fig. 4.12 LDA classification of 18 months old disease and control samples

To analyse this set of data, maximum variances of sensors resistance were chosen as features. Then the four classifiers shown in Table 4.5 were analysed using the Boruta package [212]. Four different methods have been used to ensure validity of the results, Table 4.5 summaries the result of these methods for samples within 4 years and Table 4.6 summarises the result for samples within less than 18 months.

Table 4.5 ROC with Boruta package analysis for data with 4years old

Methods	AUC	Sensitivity	Specificity	PPV	NPV	P-value
Sparse Logistic Regression	0.91(0.85-0.96)	0.84 (0.74 – 0.91)	0.88 (0.75 - 0.95)	0.91	0.78	1.278e-14
Random Forest	0.88 (0.82 – 0.94)	0.63 (0.51 – 0.74)	0.96 (0.86 - 0.99)	0.96	0.62	4.496e-13
Gaussian Process	0.83 (0.76 – 0.91)	0.8 (0.69 – 0.88)	0.85 (0.72 - 0.94)	0.9	0.73	2.264e-10
Support Vector Machine	0.76 (0.67 – 0.86)	0.88(0.78 -0.94)	0.62 (0.47 - 0.76)	0.79	0.77	5.697e-07

Table 4.6 ROC with Boruta package analysis for data with less than 18month

Methods	AUC	Sensitivity	Specificity	PPV	NPV	P-value
Sparse Logistic Regression	0.99(0.97-1)	0.98 (0.89 – 1)	1 (0.91 - 1)	1	0.97	2.279e-15
Random Forest	0.98 (0.95 – 1)	0.98 (0.89 – 1)	0.87 (0.72 - 0.96)	0.91	0.97	1.306e-14
Gaussian Process	0.94 (0.89 - 0.99)	1 (0.93 – 1)	0.79 (0.63-0.9)	0.86	1	1.166e-12
Support Vector Machine	0.91(0.84 - 0.99)	0.98(0.89 -1)	0.89(0.75 - 0.97)	0.92	0.97	1.635e-11

From Table 4.5 & 4.6, it is clear that Sparse Logistic Regression worked more efficiently than the other methods since it has a greater area under curve value. Fig. 4.13 and Fig. 4.14 indicate the ROC curve analysis of 128 samples of VOCs differentiating between diabetes and control samples for two different sample age groups.

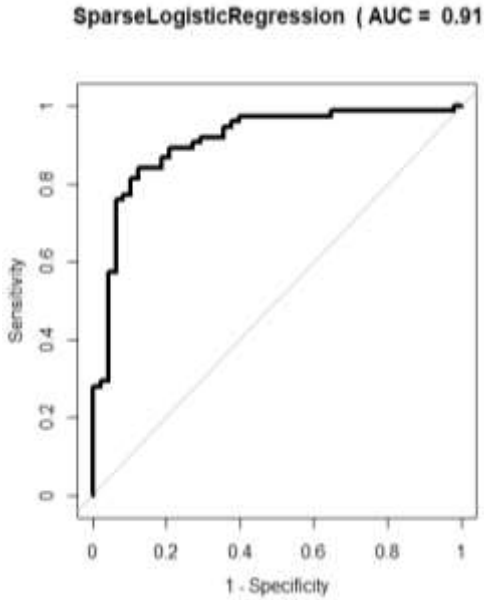

Fig. 4.13 ROC with Boruta package analysis for data from samples up to 4

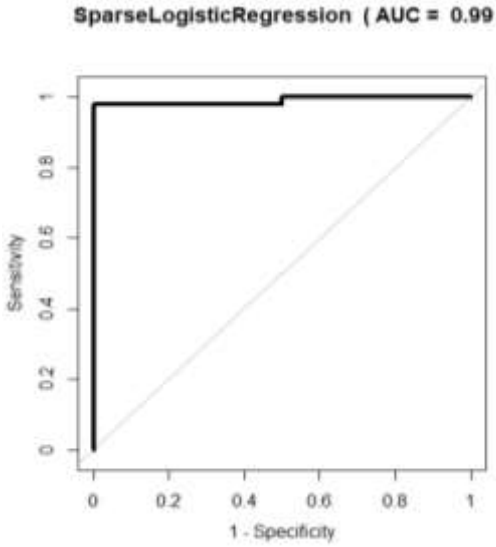

Fig. 4.14 ROC with Boruta package analysis for data from samples less than 18 months old

4.7 Discussion

This chapter has introduced Diabetes is a very major global health concern, affecting 1 in 12 of the population. The power of FAIMS and FOX 4000 eNose to distinguish healthy from diabetic patients is considerable. Using an electronic nose, along with statistical and machine learning techniques, have shown that we can accurately classify diabetic patients from healthy controls using only the aromas emanating from a urine sample. High prediction accuracy was achieved, by combining PCA with a sparse logistic regression and gaussian process classifier. No single sensor was found to be able to distinguish healthy and disease patients, yet combining all sensors allows a high degree of predictive accuracy. It offers hope in developing a low-cost, point of care, rapid diagnostic tool that potentially be an alternative non-invasive means to diagnose and (in the future) monitor the progression of diabetes.

The secondary result of this chapter shows the proof of the vapours emanating from a stored urine sample are affected by storage time using the FOX 4000 and FAIMS as electronic nose's. In most cases samples would be tested well before this four-and-a-half-year period. Our study suggests that this is not feasible when dealing with urine samples for gas analysis.

4.8 Conclusions

Diabetes affects a large proportion of the world population and results in millions of deaths every year. Currently more than 40% of individuals with type 2 diabetes are undiagnosed. Here an Alpha M.O.S FOX-4000 and FAIMS electronic nose were used to analyse urinary aromas from subjects with type 2 diabetes and healthy controls. Performing PCA and applying a classification algorithm, a high predictive accuracy was achieved. This study provides evidence that it may be possible to use urinary gas phase bio-markers to diagnose and monitor diabetes.

.

Chapter

5 Development & Construction of Gas Test Rig

This chapter describes the development and construction of gas test rig. It describes the aim of building the test rig, its specification and limitations in detail.

5.1 Requirements and Aims

As mentioned in literature review, at the heart of the eNose is the gas sensor array. For most gas sensors, the lowest concentration of a target inorganic gas is usually defined in their datasheet. However, the response of these sensors to volatiles organic compounds are often not tested by sensors manufacturers (or not reported). Since we aimed to develop an eNose (chapter 6) system with tuneable optical sensors, it is necessary to find out their sensitivity to different gases in-house before using them for measuring VOCs produced from urine.

Gas sensors have a different level of selectivity and sensitivity according to their construction and their sensing properties. As discussed earlier, if they are used for a

biomedical application, they may need sensitivity in part per million (ppm) to part per billion (ppb) levels [213]. Therefore, it is important to be able to characterise sensors to ensure that they have the appropriate properties for a given requirement. To facilitate the improvement and characterisation of the selectivity and specificity of optical sensors a gas/vapour test rig was designed and fabricated in-house at the University of Warwick. This rig allows the testing of sensors to different concentrations of gas mixtures, with varying humidity over a long period of time from minutes to hours. This can be used to replicate the chemical environment produced by human/biological samples.

5.2 Gas Rig Specification

The gas rig was designed based on parameters that are needed to characterise gas sensors. The gas rig system contains four different sections: a Humidity generator to be able to control the humidity between zero to 100%, a gas mixture to be able to mix different gases, VOC generator and gas analyser to be used as a test bench. Fig. 5.1, gives an overview of the approach to develop the gas rig.

The gas rig is able to automatically run and alter gas concentration and humidity values without constant monitoring, allowing minute-to-hour period repeatability within 5 ml/min over a range of 10 ml/min to 500 ml/min for gas concentration in gas mixture and 10 ml/min to 350 ml/min for humidity. It allows the gas mixture to be connected to the gas cylinder. Different concentration of cylinder can be bought depending on the concentration requirements.

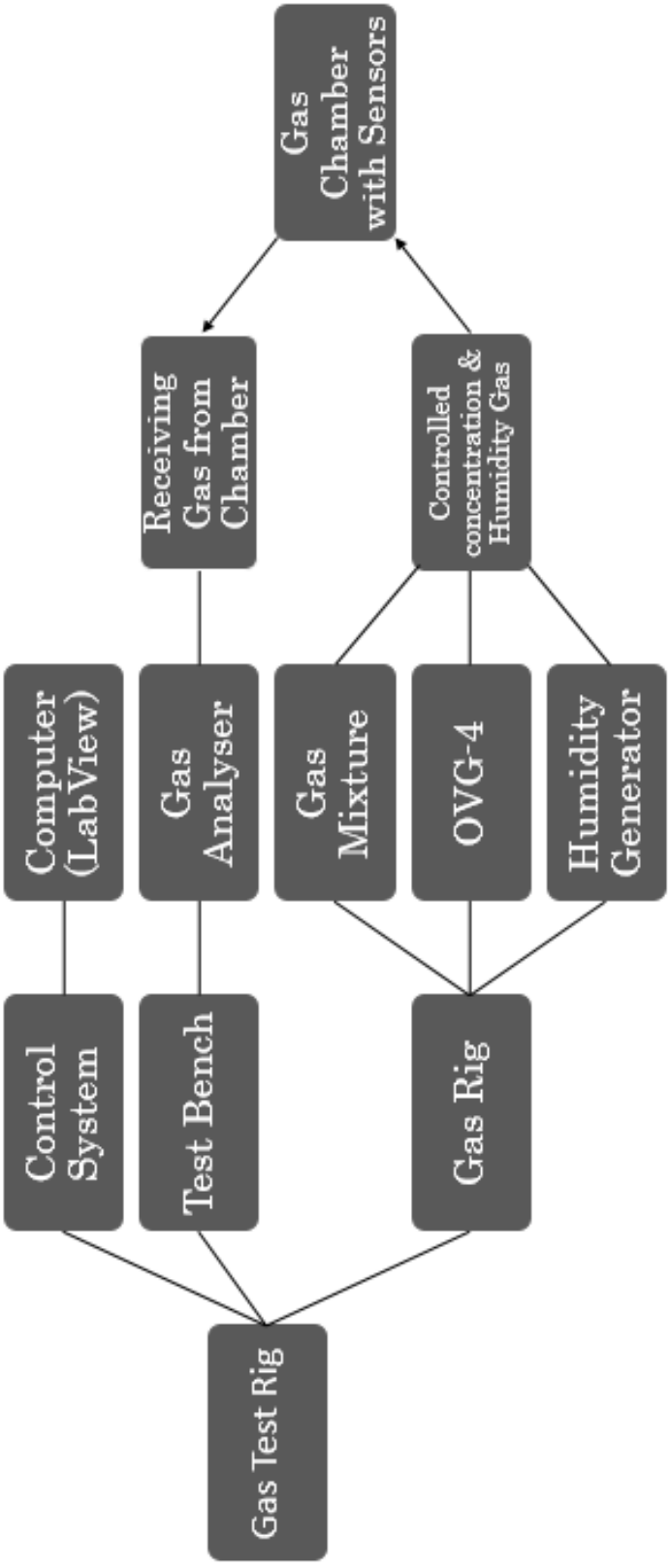

Fig. 5.1 Hierarchy flowchart of the gas rig

5.3 VOC Generator

A commercially available VOC generator – OVG-4/GEN-SYS, was purchased from Owlstone (UK) was used to produce accurate and repeatable volatile organic compound (VOC). The OVG-4 system uses permeation tubes [214]. Utilising the properties of permeation tubes provide controllable concentrations of calibration analytes. A permeation tube is a small cylinder, which contains specific chemicals with a concentration range between part per trillion (ppt) and part per million (ppm)[214]. The tube is then incubated in the internal permeation oven where the tube temperature changes in 0.1°C steps over a range of 30 to 100°C. The internal mass flow controllers provide a calibrated flow of air or nitrogen through the permeation oven, which will produce a constant VOC concentration. This concentration of the VOC can be calculated using equation 5.1[215] .

$$i = \frac{PR}{F_{SA}} \qquad (5.1)$$

Where i = Concentration / ng ml^{-1}, PR = Permeation rate / ng min^{-1}, F_{SA} = Sample flow / ml min^{-1}.

5.4 Gas Mixer

The purpose of gas mixer unit is to allow the user to mix two different gases. The users can control the gas flow rate of the two gases. If one of the chosen gases is zero air, then the gas mixer can be used as a dilutor. By considering the flowrate of zero air and the target gas, the user can calculate the concentration of the output gas, mixed at

the outlet of the gas mixer box. Since this system might be used for dangerous gases such as CO, the system includes both mechanical and electrical safety valves. These valves allow the gas lines to be closed off in case of a mass flow controller (MFC) failure. The gas mixture system is a part of the gas test rig that is controlled by LabVIEW (National Instruments, USA) software. Fig. 5.2 shows the pathway the gases take before being mixed. If a gas is needed, its corresponding electronic valve opens. The gas flow rate is controlled by the corresponding MFC.

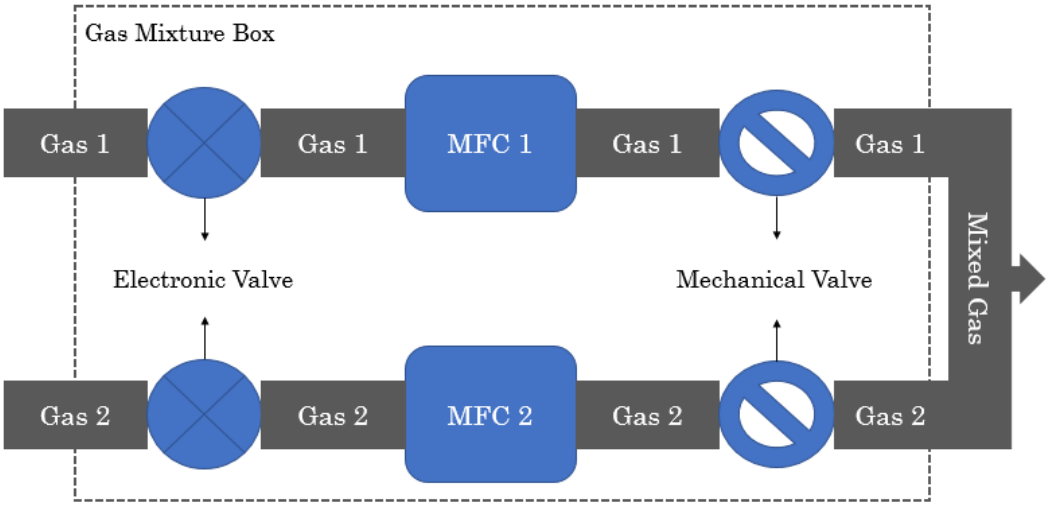

Fig. 5.2 Gas mixer flowchart

5.4.1 Mechanical Parts

- **Mass Flow Controller (MFC)**

Two UFC-1100A (Unit Instruments Inc., USA) mass flow controllers (MFC) were used to control the flow before mixing. The UFC-1100A is a high-performance mass flow controller with a maximum pressure of 500 PSI and (in this case) a maximum flow rate

of 500 ml/min. 1/8" tubing was connected to both inlet and outlet connection of the MFC by Swagelok compression fittings. The user controls the MFC flow rate by applying a voltage to a control pin. This voltage varies between 0 to 5 V, which is linearly related to the MFC's lowest and highest flowrate. The actual flow rate can be read from a varying voltage between 0 to 5 V on a feedback pin.

- **Electronic Valve**

For safety and to ensure there is no leak in case the MFC is not totally closed, electronic valves ETO-2-12 (Clippard, USA) were used on each line. This valve is common throughout the gas control systems. These ETO-2-12 valves have a fast ON/OFF time, taking between 5 to 10 milliseconds. The power consumption of these valves is 670 mW. Their operating voltage is 12 V. All fittings used to these valves are stainless steel Swagelok, male Connector, 1/8 in. BSP to a 10-32 male NPT thread.

- **Mechanical Valve & Enclosure**

For extra safety an extra stainless steel mechanical valve (Swagelok, USA) was added to the output of the unit. This requires the user to open and close the valve manually.

5.4.2 Mechanical Design

A physical model of the gas mixture system was designed in SolidWorks (Dassault Systèmes, France) software version 2015, (Fig. 5.3) to ensure that all parts,

components, structural supports and fasteners could be fitted inside the 19-inch rackmount enclosures (Schroff, France).

Fig. 5.3 CAD model of gas mixer

5.4.3 Electronic Design

The Owlstone GEN-SYS casing provides a 24 V supply to each unit plugged into the system. The electronic control board was designed to maintain the voltages required for two MFCs and two electronic valves. It also produces +/-15 V for the MFCs and 12 V for the electronic valves from main 24 V provided by the Owlstone GEN-SYS. The electronic control board also contained a National Instrument Data Acquisition board (NI-DAQ) (USB-6001 OEM). This allowed the control of MFC flow rates and valves via the LabVIEW program. The NI-DAQ is a data acquisition board with 8 analogue inputs (14-bit resolution ADCs), two analogue outputs (DACs) and 13 digital I/O lines. Two ADCs are used for reading the returning voltages from MFCs. Two analogue outputs

(DACs) were used to set the voltages on the MFCs proportional to the flow rate and 2 digital I/O lines are used to turn the electronic valves on and off. A two layers PCB was designed using Autodesk EAGLE software and is shown in Fig. 5.4.

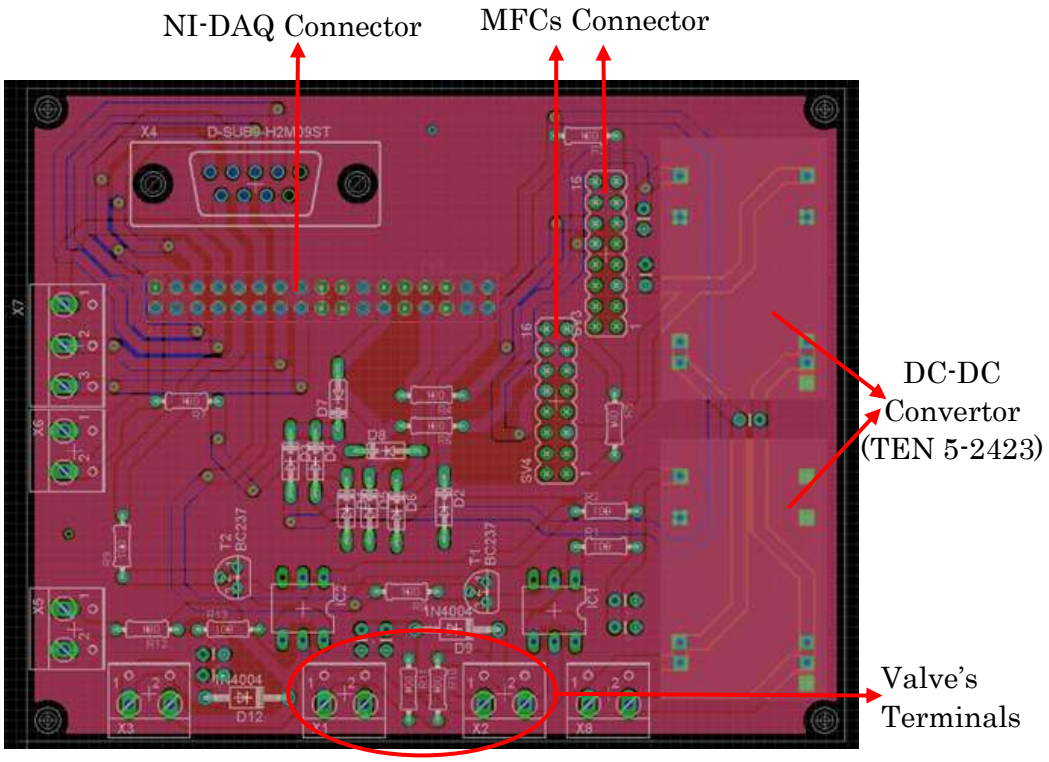

Fig. 5.4 Gas mixer 2 layers PCB circuit design

5.4.4 Assembly of the Gas Mixer

The back face of the 19-inch rackmount enclosure, contains a single hole on the top left corner for attaching the XLR socket, used to provide the unit with 24 V supply power, and two 8 mm holes for the 1/8" Swagelok bulkhead fittings down the right side for inlet gases. The front panel of enclosures has a liquid crystal display on top to display the flowrate values, rocker switch to turn the gas mixture unit on and off, 1/8"

Swagelok bulkhead fittings for outlets, two mechanical valves to let the gases come out, and two LEDs, which show whether electronic valves are on or off. The interface PCB was placed under the MFCs to save space. Fig. 5.5 shows the gas mixer system.

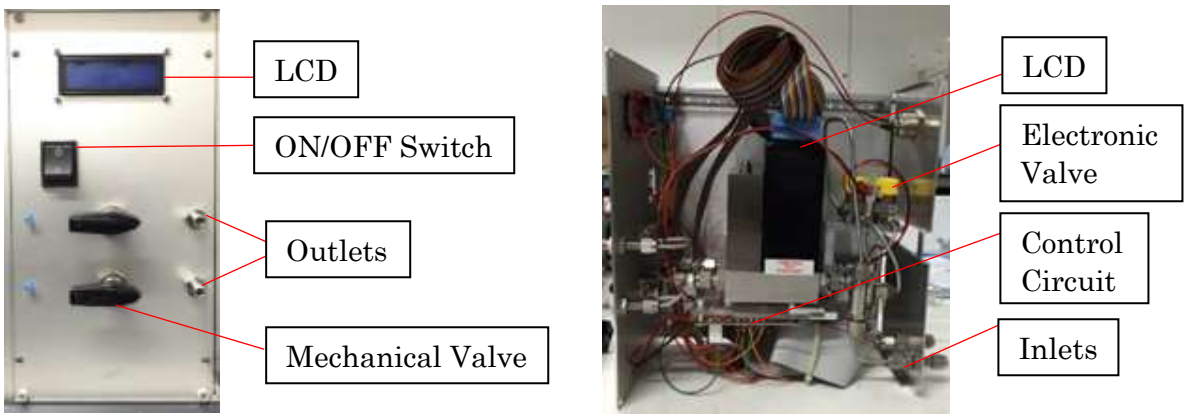

Fig. 5.5 Gas mixer system (a) front view (b) side view

5.5 Humidity Generator

The majority of gas sensors are intolerant to wide changes in humidity. Humidity effects the sensitivity of the sensor and its baseline value. Often, the sensors' response is reduced, for the same gas concentration, when the humidity is increased[88]. Since the majority of biological samples have a high humidity level, it is important that the gas test system is able to implement humidity control. The aim of the humidity generator system is to provide a single airflow at a controlled humidity level. The concept of the humidity generator is to pass zero-air through the bubbler filled with a volume of water to humidifying the air. The humidity generator has an inlet for zero-air that goes to the external bubbler. The flowchart of the humidity generator system

is shown in Fig. 5.6. The system has three electronic valves (same as used in 5.2.1) and two flow paths controlled by two MFCs. One of the MFCs, controls the flow rate that passes zero air through to an external outlet, through the bubbler and then back in to the humidity generator through another inlet (controlling humid line). The other MFC controls the flow rate of the zero-air gas line to decrease the humidity in the output of the system, by mixing the 'humid air line' with the dry zero airline. The mixture is measured with a commercial temperature and humidity sensor SHT75 (Sensirion) and pressure sensor MPXM2053GS (NXP) to allow closed control loop of the system. The measured value of humidity from the sensor is sent to the main control software. If the reading value matches the set value, the third valve will be turned on and the humid air will be available on the outlet port.

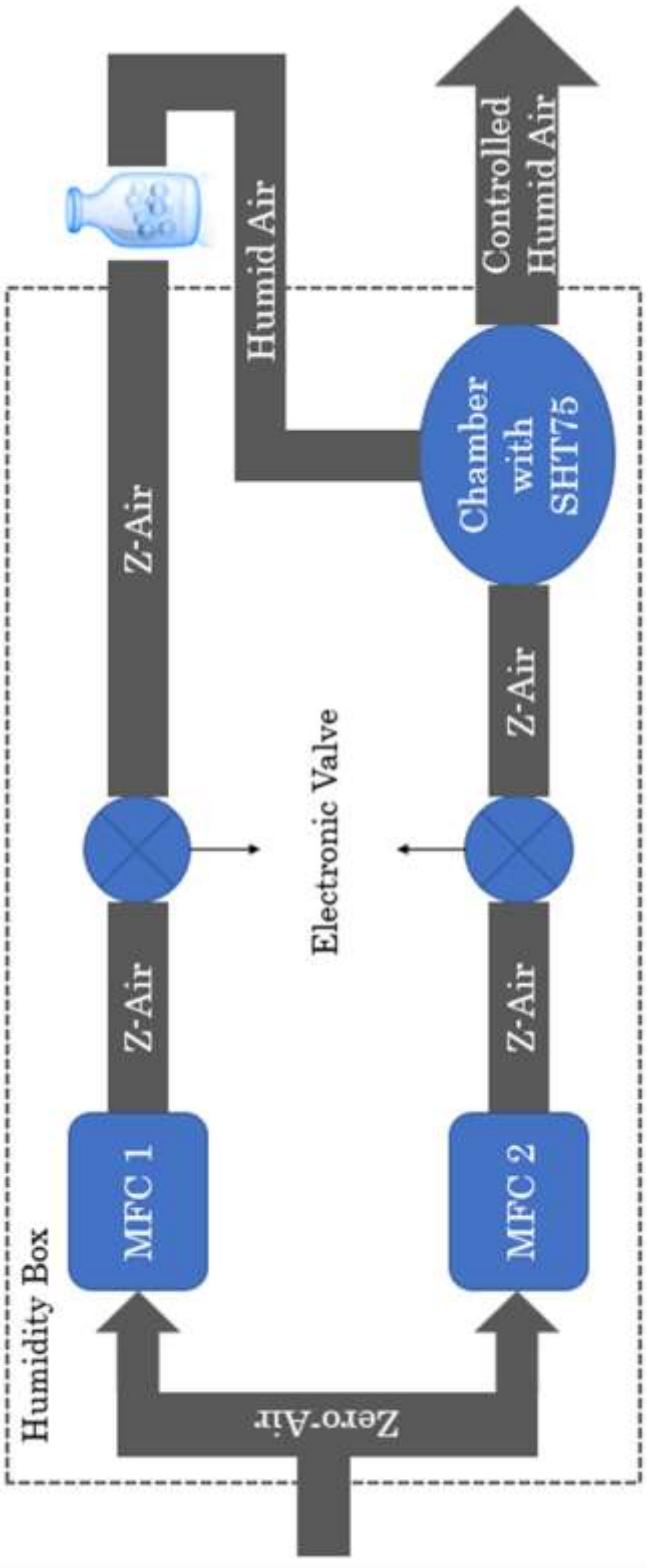

Fig. 5.6 Humidity generator system flowchart

5.5.1 Mechanical Parts

Most of the mechanical parts used for building the humidity generator are the same as the gas mixture box (section 5.2.1). The only difference is the model of MFCs. In this case two 5850TR MFCs were used. 5850TR MFCs has the same pin layout, tubing and fitting connectors as UFC-1100A. The difference is the max flow rate. In these MFCs the maximum flow rate is 350 ml/min.

5.5.2 Electronic Circuitry

As explained in part 5.2.3 the Owlstone GEN-SYS provides 24 V for the whole system. The circuit for humidity generator is more complex than gas mixture system. Here a 4D screen is used to display humidity, temperature and absolute humidity value on the screen as well as sending data to the main gas rig system running the LabVIEW program through a DAQ board (6008 OEM). The 4D screen chosen for this project was (uLCD-32PTU-AR). The uLCD-32PTU-AR screen is a 1.7" screen, which is compatible with Arduino. Arduino is an open-source platform that has both a physical programming circuit board and a software environment to write the code and upload it through computer on the microcontroller.Requirement and specifications to design and develop control electronic board to run the system were:

- For MFC:
    - Converting 24 V to +15 V, -15 V

- Providing DAQ line to control the flow
- Using a ADC line to read the feedback value from MFC to make sure the set value is the same as feedback line

- For electronic valve:
  - Converting 24 V to 12 V
  - Providing a digital pin to turn valve on and off
  - Connecting LEDs to the valve pins so if the valve is on the related LED will be on and vice versa

- DAQ (6008 OEM):
  - The data acquisition board is required to connect all the transferring lines such as digital and analogue lines from board to main gas rig control system and it is powered by USB cable from computer

- Temperature and humidity sensor (SHT75):
  - Two SHT75 sensors are used in the system, one for sending value to main control system on the computer and the other was used to send the data to the screen by Arduino-UNO
  - Providing 3.3 V to run the sensor
  - Providing SDA & SCL communication line for transferring data

- Pressure sensor MPXM2053GS:
    - Providing 10 V to turn on the circuit
    - The output of the sensor is an analogue voltage, which is required to connect to ADC line on both DAQ & Arduino-UNO
- uLCD-32PTU-AR Screen:
    - This is a LCD screen which is compatible with Arduino and needs 5 V to turn on and RX, TX communication line to send the data for display through Arduino
- Arduino-UNO:
    - To turn on the Arduino 7 V to 12 V is required
    - Arduino works separately from DAQ. It gets data from SHT75 and pressure sensor and displays it on screen
    - Arduino also provides 3.3 V for running SHT75 sensors

To have a stable voltage, a TEN 40-2423 converter was used. The TEN 40-2423 convertor, converts 24 V to three different voltages, +15 V, -15 V and 5 V. To achieve other voltage values different regulators were used on the board. There are voltage generators that convert the main 24 V DC to +15 V, -15 V, 12 V and 10 V.

Fig. 5.7indicates the electronic schematic design for humidity generator. Each section, on Fig. 5.7, is labelled with a number. Part 1, shows the power connectors coming from voltage generator circuit with desired voltages. Part 2 is related to connector for DAQ (6008 OEM), which is responsible for controlling the flow through MFCs, turning on/off the valves and receiving data from temperature and humidity circuit in order to control the humidity. Part 3 contains the connectors for the pressure sensor and two humidity and temperature sensors, where one temperature and humidity sensor was connected to NI-DAQ, and the other one, along with a pressure sensor, are connected to the Arduino microprocessor board to display results on screen. Parts 4 and 5 are associated with the MFCs connectors and signal communication between the DAQ and MFCs. Part 6, shows the circuit related to turning on/off the electronic valves. The control signals come from a NI-DAQ. Part 7, is related to the Arduino Uno connector, which is controls the screen on the humidity generator. Pressure sensor and temperature and humidity sensor's output goes to the Arduino Uno board to display the relative humidity, temperature and absolute humidity values on the screen. Fig. 5.8 shows the layout of the two layers of the PCB. For designing the PCB layout, Altium (Altium Limited, Australia, 2016) was used.

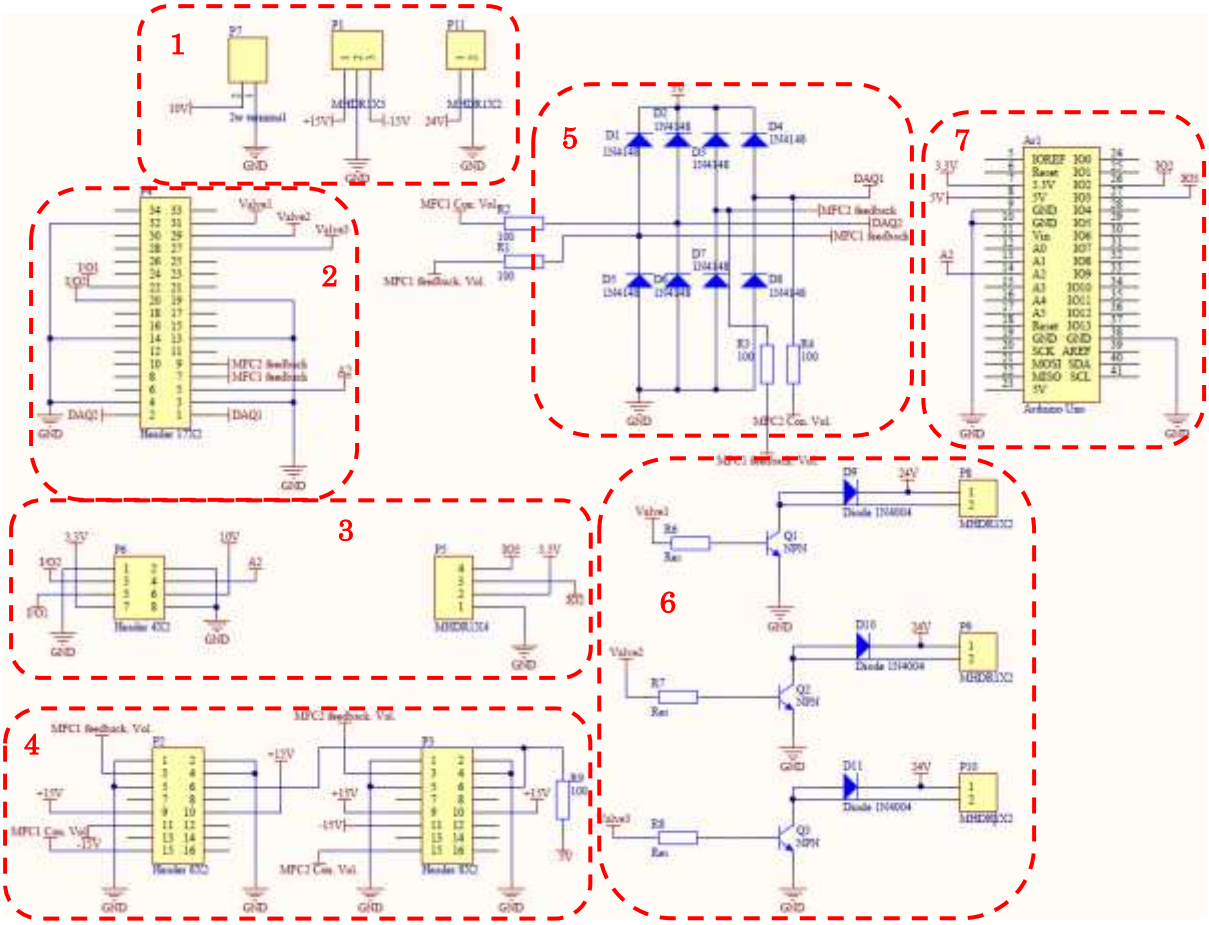

Fig. 5.7 Schematic design of electronic circuit for humidity generator instrument

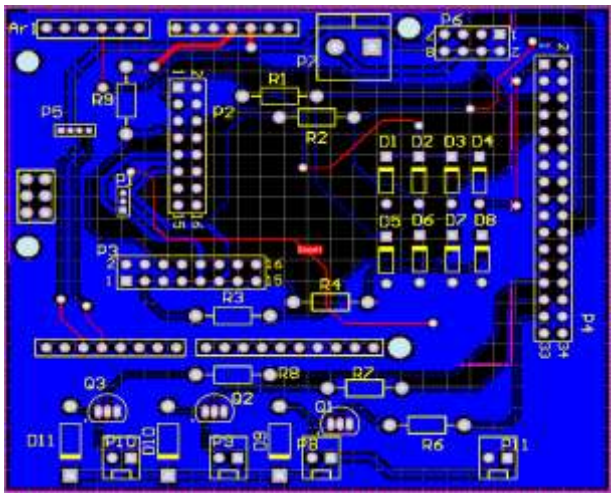

Fig. 5.8 Two layers PCB layout of the humidity generator

5.5.3 Arduino Programming & LCD Screen

To display the temperature, humidity, and absolute humidity on the screen of the humidity unit, the sensor outputs were processed using an Arduino Uno and the result was displayed on the 4D Systems screen. The SHT75 sensor requires two lines to communicate with Arduino, these lines are 'Data' and 'Clock'. The data line gives the temperature in degrees centigrade and the relative humidity as a percentage.

There are 4 types of different pressure measurement, absolute pressure, atmospheric pressure, differential pressure, and gauge pressure [216]. Atmospheric pressure is the average pressure at sea level, which is nominally 101.325 kPa. Absolute pressure is referred to the vacuum of free space, which is zero [216]. Gauge pressure is relative to atmospheric pressure and can be either positive and negative. The differential pressure shows the pressure difference between any two points. Fig. 5.9 shows different pressure measurement type in graphical way.

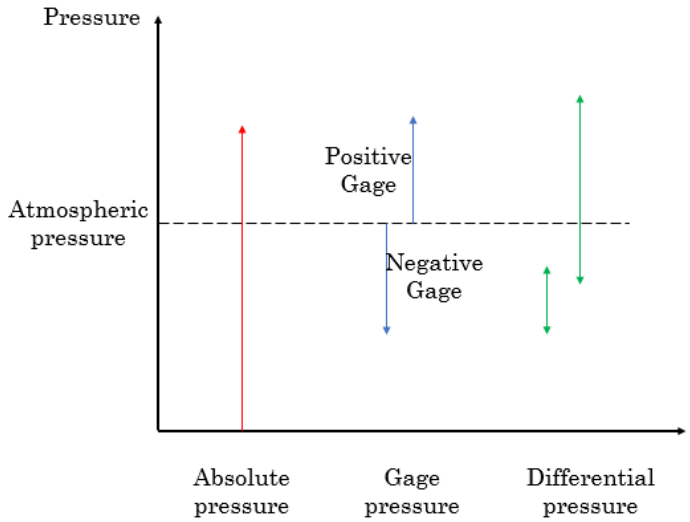

Fig. 5.9 Different pressure measurement types

For this project a gauge sensor was used, because of its compact size, which helped in decreasing the humidity generator manufacturing time. The sensor output is an analogue signal, which goes to the 10-bit resolution Arduino UNO ADC. The output voltage can be converted to kilopascal using equation 5.2 [217];

$$KPa = \frac{sensor\ reading\ in\ voltage - 1}{0.02} + 60 \qquad (5.2)$$

Using the pressure sensor (MPXM2053GS) output, it is possible to calculate a more precise absolute humidity value, in part per million (ppm) [218]:

$$PPM_V = \frac{P_W}{P_{tot} - P_w} * 10^6 \qquad (5.3)$$

Where P_w and P_{tot} are the water vapour pressure and total pressure respectively. P_{tot} value is measured by pressure sensor and P_w value is based on the output from the temperature and humidity sensor (SHT75), which gives the relative humidity value in percentage. The relative humidity (RH) is at all temperatures and pressures defined as the ratio of the water vapour pressure (P_w) to the saturation water vapour pressure (P_{ws}) at the gas temperature [218]:

$$RH = \frac{P_W}{P_{Ws}} * 100\% \qquad P_W = \frac{RH * P_{Ws}}{100} \qquad (5.4)$$

The saturation water vapour pressure (P_{ws}) can be calculated from the equation below:

$$P_{Ws} = A * 10^{(\frac{m*T}{T+Tn})} \qquad (5.5)$$

Where A, m and T_n are constant, and T is temperature in (°C). At temperatures ranging from -20°C …+50°C, A = 6.116441, m = 7.591386, T_n = 24.7263. Pressure sensor's accuracy is around 1 to 2% different from the actual pressure[218].

To programme the screen, 4D workshop IDE software (version 4.5.0.8) was used. This software was specially developed for 4D screen in Australia. It is possible to code the screen by four different methods; Designer, ViSi, ViSi Genie, and Serial. ViSi Genie was used in this project, which had an advanced environment and thus doesn't need any coding. The user can decide what objects to use, lay the display out and the code will be written for it automatically, which helps to have a rapid development.

5.5.4 Assembly of Humidity Generator

The back face of the 19-inch rackmount enclosures contains a single hole on the top left corner for attaching the XLR socket, used to provide the unit with 24 V supply power, and two 8 mm holes, for the 1/8" Swagelok bulkhead fittings, down the right side for inlet for the zero air. The front panel has a 4D system display, rocker switch to turn the unit on and off, three 1/8" Swagelok bulkhead fittings for outlets, and three LEDs that show the state of the electronic valves. When the valve is on it will let air pass and the corresponding LED will be turned on. Fig. 5.10 shows how all electronic and mechanical parts are fitted together in a 19-inch rackmount enclosure that will be fitted in the final gas rig. Fig. 5.11 is a final system in operation.

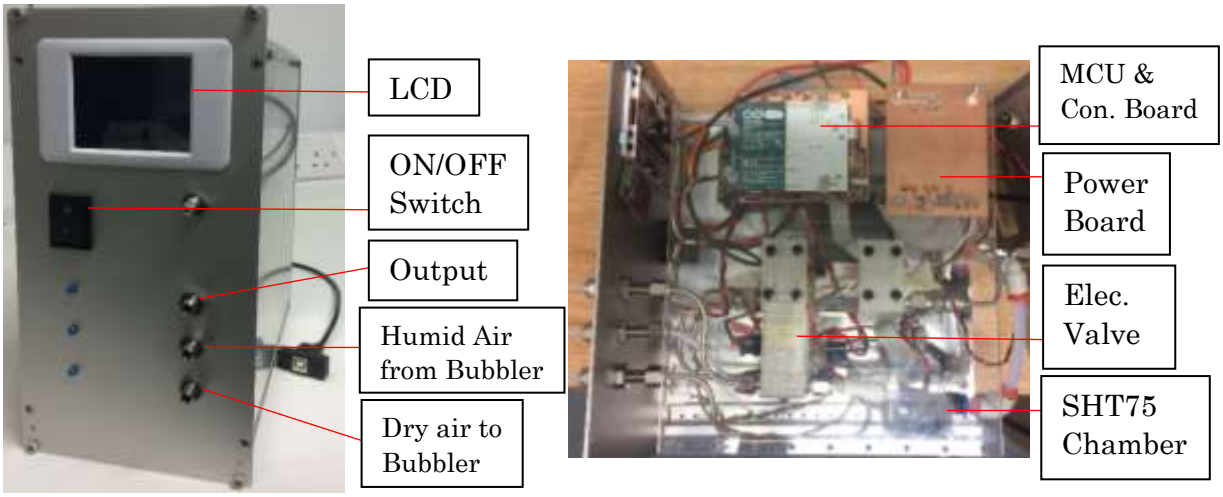

Fig. 5.10 Humidity generator system; (a) front panel, (b) side view

Fig. 5.11 Humidity generator system during a test, connected to bubbler

5.6 Gas Rig Setup

As discussed earlier, after the gas mixture unit and humidity generator unit were developed and tested, they were fitted into the Owlstone GEN-SYS outer case. Fig. 5.12 shows the completed gas rig system.

Fig. 5.12 Main gas rig; (a) gas mixture, (b) OVG-4, (c) humidity generator

5.7 Gas Analyzer

An important addition to the gas rig test system, was the gas analyser. Its purpose was to measure the output of the rig (after any test chamber) to ensure that what gas composition was requested is actually what was delivered. The gas analyser contains an array of commercial sensors that are sensitive to different gases.

5.7.1 Sensors

This system includes 8 different sensors. The first sensor is a mass flow meter (UFM1100) (MFM), which is used to measure the total flow from the gas rig. The second and third sensors are a Clairair infrared methane gas sensor and Alphasense NDIR CO_2 sensor respectively. The fourth sensor was SHT 75 sensor to measure temperature and humidity. The fifth, sixth, seventh and eighth sensors were Alphasense A4 4-Electrode gas sensors which includes NO_2, CO, H_2S and PID respectively (for total VOC measurement).

- **Mass Flow Meter (MFM)**

The MFM has the same topology as the MFC, which was described in section 5.2.1. The only difference is that the MFM does not have a control pin for the user to control the flow rate. The MFM only has a feedback pin that is modulated between 0 to 5 V – depending on the flow rate through it. When the reading voltage is zero then the flow rate is zero ml/min and when it is on five volts, the flow rate is 500 ml/min. The MFM requires +15 V, -15 V supply. The inlet and outlet fittings used to connect the MFM to the system are ¼ inch Swagelok connectors.

- **Methane Gas Sensor (Prime1)**

To detect methane and hydrocarbons a high-resolution infrared gas sensor (Prime 1, Clairair) was purchased. This sensor was used because of its resolution (0.01% volume for 0 - 10% volume and 0.1% volume for 10 - 100% volume, with a sensing range

of 0-100% LEL Methane, 0-100% LEL Hydrocarbons or 0-100% volume Methane). The technology used in this sensor is MEMS technology and it uses the non-dispersive infrared method to detect the presence of hydrocarbon gases [219]. To use this sensor an OEM 4-20 mA transmitter produced by Clairair was used (Cirrius X). [220].

- **Alphasense NDIR CO_2 Sensor**

Carbon dioxide was measured using an AlphaSense IRC-AT Carbon dioxide sensor, again based on an NDIR measurement approach. This sensor can detect 0 to 100% CO_2 in control processes [221]. To use this sensor a RC-TX NDIR CO_2 transmitter board was used, which has an output signal of 4-20 mA.

- **Temperature & Humidity Sensor (SHT75)**

The temperature and humidity sensor used in gas analyser is the same as humidity system discussed in section (5.3.2).

- **Alphasense A4 4-Electrode gas sensors (NO_2, CO, H_2S and PID)**

For detecting specific gases, three electrochemical and one PID sensor was purchased from Alphasense, along with a commercial interface board. The electrochemical sensors were for NO_2, CO and H_2S (common test gases), supplemented with a photoionization detector (PID) for VOCs. The unit gives an analogue voltage, which can be related to gas concentration[222].

5.7.2 Electronic Circuitry

An electronic interface circuit was developed to provide the appropriate control and measurement signals to all of the different sensors. The electronic circuit should be able to transfer data from the sensors to the main processor on the computer. Since the main control program was written in LabVIEW, a DAQ (6001 OEM) board from National instrument was used as part of the interface. The design specifications were:

- For MFM:
    - Converting 24 V to +15 V, -15 V
    - Reading the flowrate value from MFM by using a ADC line on the data acquisition board
- For Methane gas sensor:
    - The operating voltage between 8 V and 36 V
    - The OEM board output is current (4-20 mA). This will be converted to a voltage and connected to an input analogue pin on the DAQ
- For Alphasense NDIR CO_2 Sensor:
    - The NDIR transmitter board has an input voltage range of between 5 V and 24 V

- The NDIR transmitter board output is the current (4-20 mA). This needs to be converted to voltage and connected to an input analogue pin on DAQ

- Temperature and humidity sensor (SHT75):
  - Sends the value to the main control system on the computer through the DAQ, using the SDA & SCL communication lines for transferring data
  - Providing 3.3V to run the sensor

- For Alphasense A4 air quality gas sensors:
  - Analogue Front End (AFE) board requires 3.3 V to 6.4 V.
  - The electrochemical sensors have two output pins called Working electrode and Auxiliary electrode, both outputs are analogue, which are connected to ADC pins on the DAQ
  - PID sensor requires a separate supply voltage between 3.6 V and 10 V. Also, it has only one analogue output that requires one analogue input pin on DAQ.

- For DAQ (6001 OEM):

- According to large number of analogue signal coming from sensors, two 6001 OEM DAQ were used.

The electronic circuit was designed to meet all these requirements. To have a constant and steady voltage for the MFM, (TEN 5-2423) Tracopower DC-DC convertor was used, which converts 24 V to +15 V and -15 V. The (TEN 8-2411) Tracopower, Isolated Board Mount DC/DC converter was used to convert 24 V to 5 V. In this project, a 2 layers electronic control board was designed in Autodesk EAGLE software, as shown in Fig. 5.13.

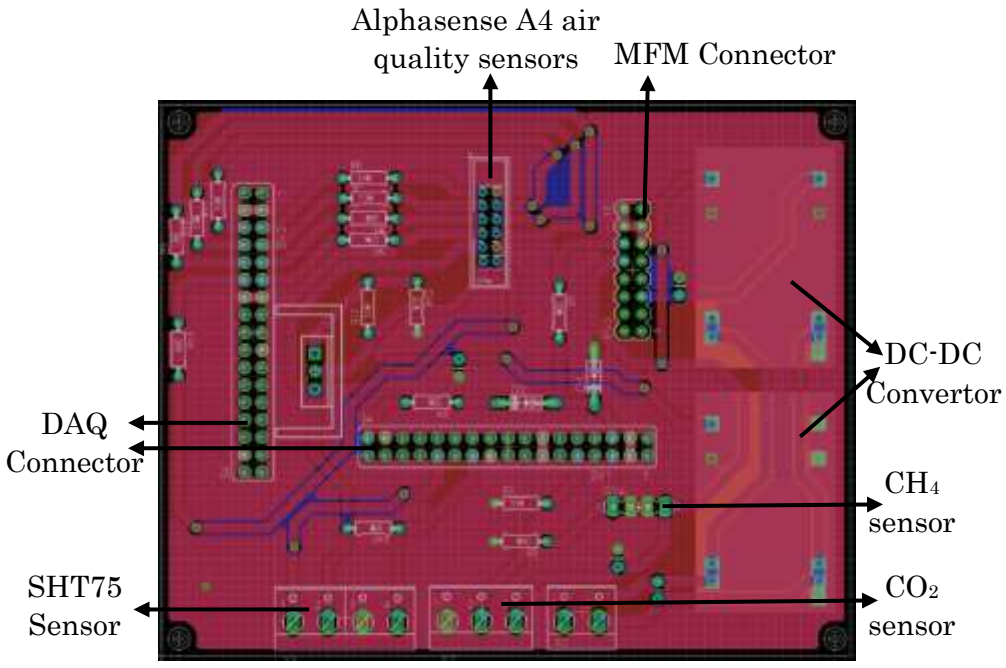

Fig. 5.13 Gas analyser two layers control board

5.7.3 Assembly of Gas Analyser

One of the requirements for the gas analyser was to have the sensors fitted in a compact way to save space around the rig. Fig. 5.14(a, b) illustrate the compact gas analyser instrument inducing 8 sensors. Fig. 5.14(c) shows the front panel of gas analyser with two ¼" Swagelok fittings as inlet and outlet. The back panel of the gas analyser is shown in Fig. 5.14(d). The back panel has a ON/OFF button, 12 V adaptor socket to turn the whole system on and two USB B sockets to connect two DAQs to the computer.

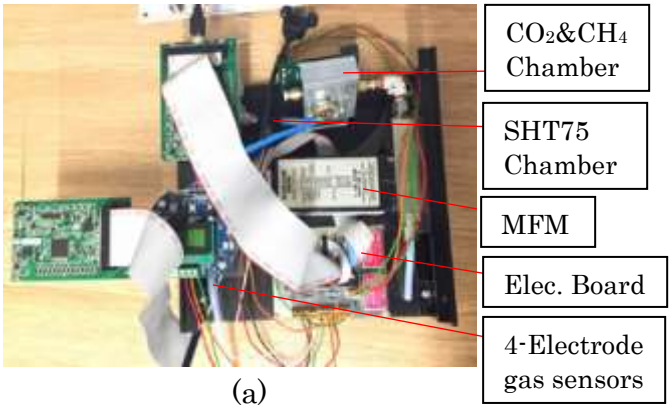

(a)

(b)

(c)

(d)

Fig. 5.14 Gas analyser system; (a) opened box from top view, (b) top view of closed box, (c) front panel, (d) back panel

5.8 Controlling the Gas Rig System

As mentioned before, data from all parts of the gas rig, including the gas analyser shown in Fig. 5.15, are sent to the software through different NI-DAQs controlled by LabVIEW. The LabVIEW program was chosen as a main control system based on the project's initial plan and it was programmed before developing the whole test rig. The user interface system between the units in the test rig was developed using LabVIEW software by Dr James Covington. The fully integrated software lets the operator to either manually control the actuation of the gas mixer and humidity generation parts or define different gas concentrations and humidity levels. Then values will be automatically sent to the separate parts under test at accurately measured time periods. The gauges for flow rates, temperature and humidity of the units and sensors outputs from gas analyser are shown on the front screen shown in Fig. 5.16. The back-end of the LabVIEW software can run each part of the rig individually.

Fig. 5.15 Gas rig system with gas analyser on top of it

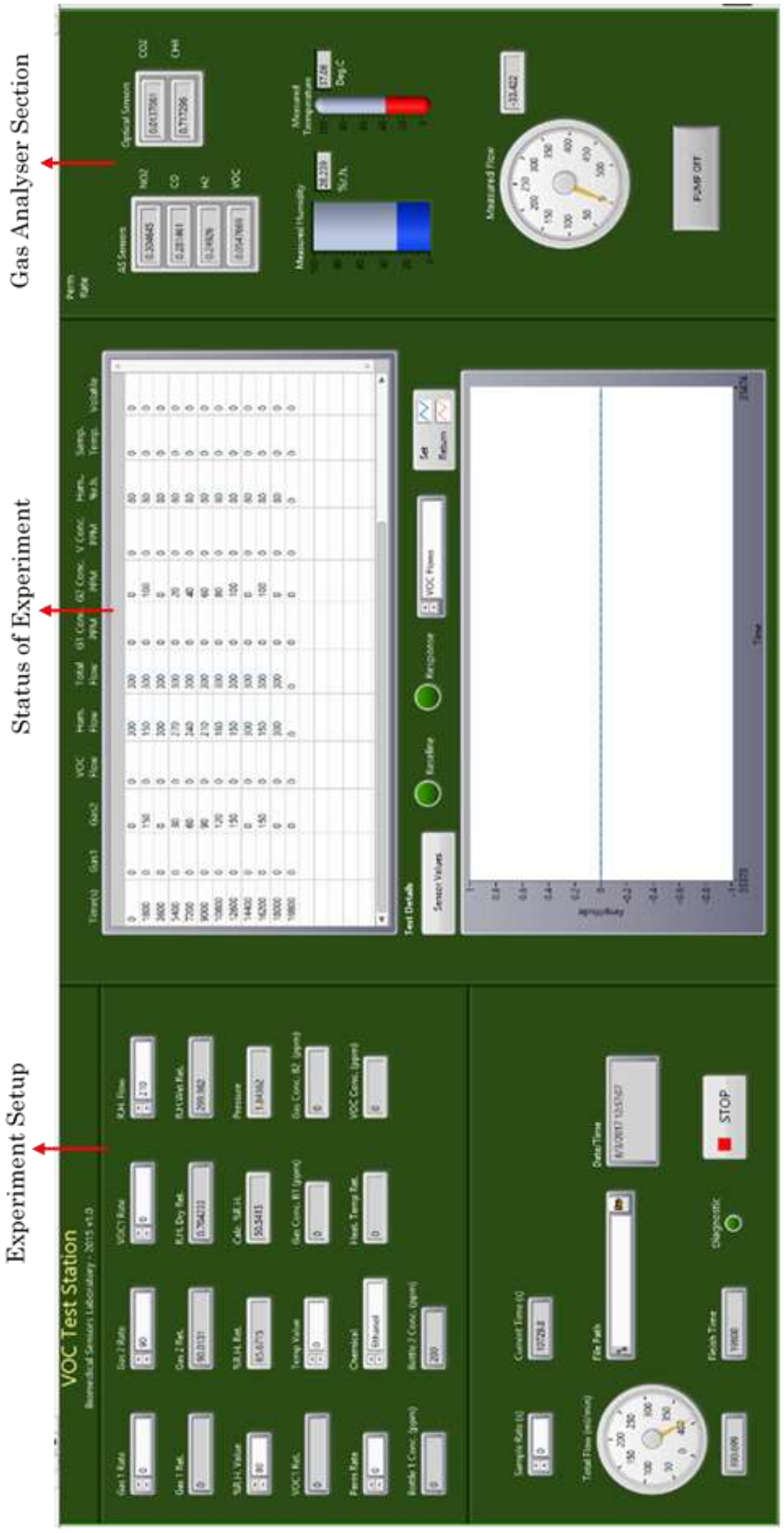

Fig. 5.16 LabVIEW user interface screen

5.9 Test Setup

In the LabVIEW user interface, the operator has the flexibility to change variables to set up an automatic test. On the screen, there are Gas 1 and 2 flow rate section, where user can choose the starting and ending point with step size, so the program can automatically alter the flow rate. In addition, there are return values for each gas flow rate to show if the setup value is close to an outlet value or not. The user can enter the target gas's cylinder's concentration, and the program can calculate the outlet gas concentration after mixing two different gases. There is a section related to percentage of relative humidity where user can choose the initial and final relative humidity values with the number of exposures in a certain period of time and LabView will change the humidity percentage automatically. The software is divided to two parts, first part is related to setting up the parameters for gas test and second part is related to the gas analyser reading.

5.10 Test Results

To test the reliability and repeatability of the gas rig a number of experiments were designed and undertaken. Fig. 5.17 indicates the difference between the expected flow rate, which was setup by the user and the actual measured flow rate at the outlet of the gas mixture. The total flow rate of the gas mixture was set to 400 ml/min. The experiment was designed in a way that the increase of the flow rate of one gas results in a decrease of the other. The aim was to find out if there is any fluctuation on the outlet of gas mixture. From Fig. 5.17, it shows that the measured flow rate at both

MFCs are mapped on the flow rate, which was setup by user. At the beginning one of the MFCs flow rate was zero, then it was increase by steps of 10 ml/min up to 100 ml/min and after that it was increased by 50 ml/min up to 400 ml/min every 5 mins. The other MFC has the opposite trend and its flow rate was dropping.

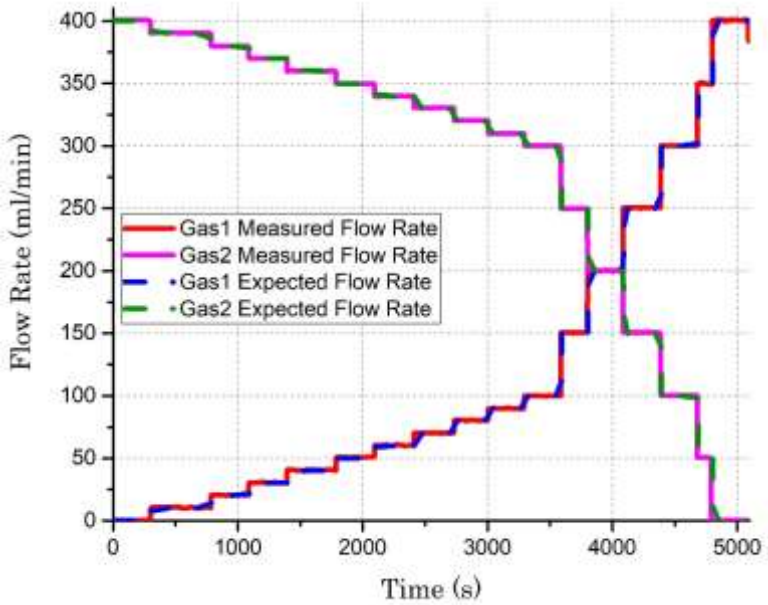

Fig. 5.17 Reliability test of flow rate of gas mixture unit

Experiments were designed to find out the accuracy of the humidity generator. To discover the accuracy of the humidity generator, humidity was set to zero and increased by 5% up to 100% relative humidity every 10 mins. Fig. 5.18 shows that in the beginning it took a few minutes to reach the lowest humidity, which was almost zero percent. The other point that is observed from the figure is that it takes more than 10 mins for humidity to settle down, since it has a big overshoot in the beginning of each increment. The most important part of Fig. 5.18 is that actual humidity can go over 65%. This can

be improved by changing the MFCs from max 350 ml/min to 1 l/min or the bubbler can be changed to a bigger bottle with a high amount of water.

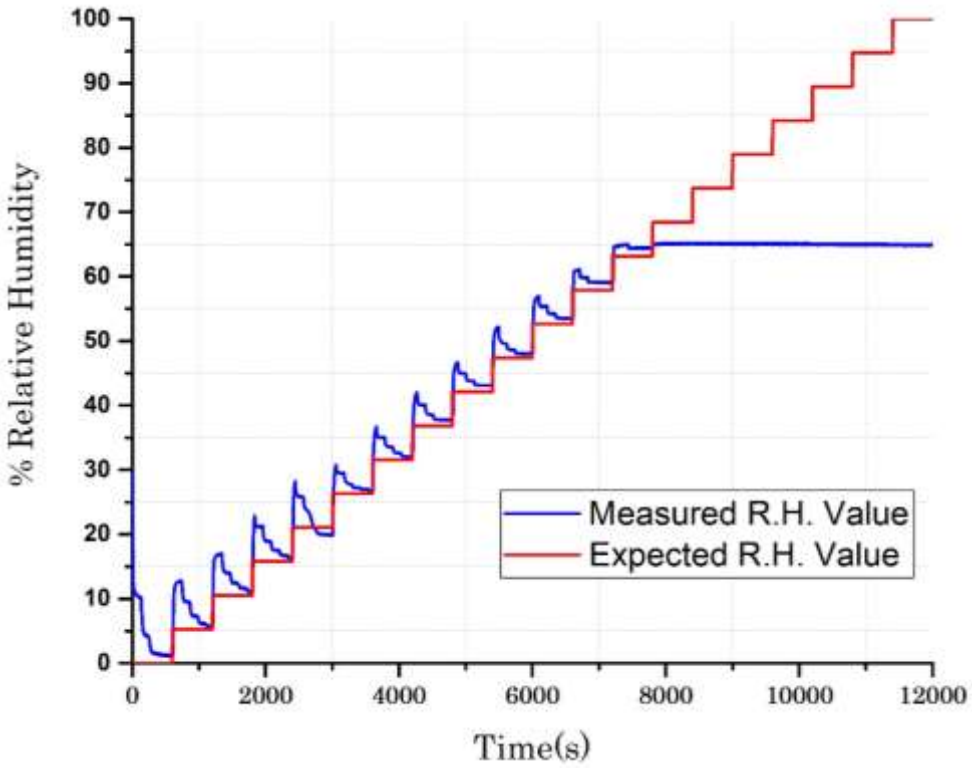

Fig. 5.18 Expected relative humidity vs measured relative humidity at humidity generator unit

5.11 Portable Gas Mixer

Initially the gas rig was used in a controlled laboratory environment, this was further developed to allow use in a variety of different environments. The modifications also allowed for an increase in capacity of the gas mixing unit (to add additional gases). A portable gas mixing system was designed and constructed due to the high demand of

using gas dilutor for testing different gas sensor systems. Since this dilutor is portable it is only designed for non-hazardous gases.

The desirable modifications of this gas mixer was that it would be a portable unit. This gas mixture unit will be used for non-dangerous gases. Therefore, electronic or mechanical valves, which would normally be used as safety precautions, were not used in this system. There are two UFM-1100A MFCs with a maximum flow rate of 250 ml/min were used in this project (which were available in the lab). The flow rates of gases are controlled with the 4D system touch screen, run by an Arduino Uno.

5.11.1 Electronic Circuitry

The MFCs required a steady and stable +15 V, -15 V. Since the control line on the MFCs required 0 to 5 V, the MCP4725 12-Bit digital to analogue convertor (DAC) Adafruit breakout was purchased. The system also needs 12 V and 5 V to power the Arduino Uno and MCP4725 respectively. The input voltage of this box is 240 V DC where it is changed to +15 V, -15 V,12 V and 5 V through a rectifier circuit. For the initial build of the unit, easily available components were used to ensure the system could be reliably rebuilt and that all components were available.

5.11.2 Coding the Gas Mixer

The gas system's maximum operation period is predefined as 30 mins with a minimum and maximum flow rate of the 10 ml/min and 250 ml/min respectively. The

MFCs control voltage has a linear relation with the amount of gas that flows through them, the Map function was used in coding the system that maps the 0 to 5 voltage value to the 0 to 250 ml/min flow rate.

5.11.3 Assembly

The back face contains a single hole on the bottom left corner for attaching the XLR socket used to provide the unit with 240 VAC supply power, rocker switch to turn the unit on and off and two holes for the 1/4" Swagelok bulkhead fittings in the middle for inlet gases. The front panel has 4D system touchscreen LCD on the right hand side, bulkhead fittings for outlets and four LEDs corresponding to +15 V, -15 V, 12 V and 5V. Fig. 5.19 and Fig. 5.20 show the top view and front view of the portable gas mixture.

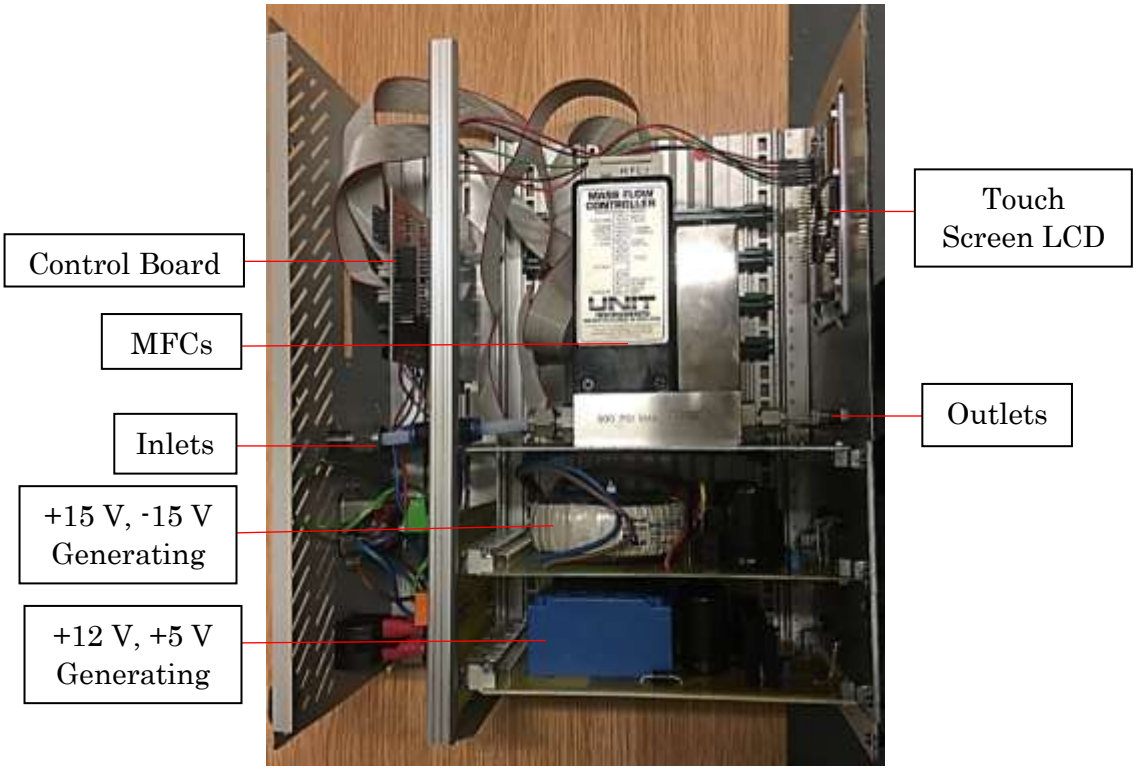

Fig. 5.19 Portable gas mixer top view

Fig. 5.20 Front view of the gas mixer

5.12 Conclusion

This chapter focused on development and construction of gas test rig. This test rig was designed and built for evaluating and testing the sensitivity and selectivity of the gas sensors that were used in an optical eNose (chapter 6). The test rig includes humidity generator, gas mixture, VOC generator, and gas analyser sections. These parts enable the user to change the factors that can affect the eNose sensory array automatically. Gas mixture can be used to mix the flow rate of two gases and dilute them. The humidity generator is able to make relative humidity up to 65% and the gas analyser setup at the other end of the sensory chamber is used as a test bench.

Chapter

6 Development & Construction of NDIR Optical eNose Instrument

6.1 Introduction

This chapter reports on the development of a Non-Dispersive Infrared Sensor (NDIR) optical electronic nose, which is intended to be targeted towards healthcare applications – investigating gas phase biomarkers that emanate from biological samples (be it urine, stool, breath, sweat or blood). The electronic nose (eNose) uses an array of four different tuneable infra-red detectors to analyse the gas/volatile content of a sample under test to create an olfactory optical map of a complex odour and, by using some form of pattern recognition technique, is easily able to discriminate samples with different olfactory maps.

The majority of previously reported eNose instruments rely on metal-oxide (MOX) or conducting polymer (CP) resistive sensors, though others exist. However, MOX and CP sensors can suffer from drift, poor repeatability, cross selectivity and being sensitive to humidity. For this reason, we are investigating and developing an optical based eNose, using a non-dispersive infrared detection approach to overcome the current disadvantages of eNose instruments. Certain gas sensors, particularly those based on optical spectroscopy, have enabled the detection of individual gas species, such as methane (or similar hydrocarbons) with low cross-sensitivity to other gases. Gas sensors based on optical absorption offer fast responses, minimal drift and high gas specificity, with zero cross response to other gases.

The NDIR optical eNose instrument has the facility to scan a range of wavelengths from 3.1 μm to 10.5 μm with a step size of 20 nm (this is according to the sensors wavelength range). The use of a tuneable filter, instead of expensive lasers, reduces the overall cost of the system. In this case, any fixed frequency measurements can be considered as "virtual sensors". Since every gas has its own infrared absorption frequency [223], this eNose can be used for identifying each gas in the sample vapour as well as identifying complex odour as a whole without identification of each individual chemical[65].

The ideal instrument would be capable of real time measurement of gas phase molecules in human waste, such as urine and exhaled air at concentrations in the sub-ppm range with a bench-top size and minimal or no maintenance.

6.2 Overview of Optical eNose

Fig. 6.1 shows the side overview of NDIR optical eNose. This system has four gas cells which includes different detector and emitters with a heater around each gas cell to prevent any contamination. This system can be controlled by a tablet or PC and the results are displayed on the screen.

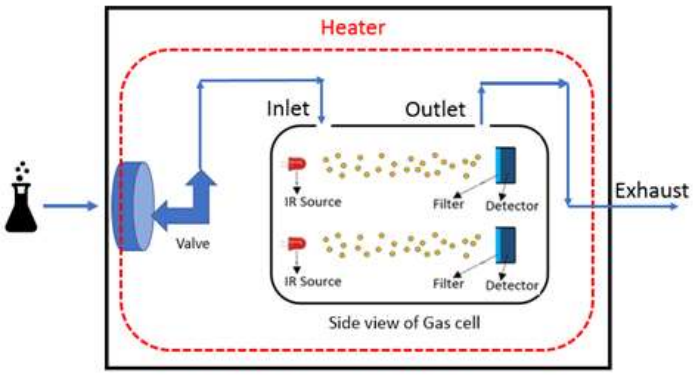

Fig. 6.1 Overview of NDIR optical eNose

6.3 Optical eNose Development

The principle detection method used here is similar to conventional NDIR and is based on the molecular absorption of IR and a subsequent fall in detected signal. This can be partially related to molecular groups as different chemical structures absorb specific IR frequencies. The number of photons absorbed is directly proportional to the power of the photon beam from the emitter and thus the amount of the gas/vapour detected. NDIR gas sensing is one of the most widely used optical gas detection

techniques, and there is a wide range of cell designs in commercial manufacture. Gas sensors based on optical absorption offer fast responses, minimal drift and high gas specificity, with zero cross response to other gases as long as their design is carefully considered. The optical eNose contains 7 main parts. The first three parts are related to optical sensing section, sensors (detectors), emitter, and gas chamber. The fourth part is the heater. Then the rest is related to controlling section, which includes electronic, mechanical and software parts.

6.4 Sensor Technology

The sensor technology used in this optical eNose was variable colour detectors or also known as tuneable detectors. This is a novel technology that was developed at InfraTec R&D lab (Germany)[224]. This technology allows users to be able to scan a range of wavelengths by simply adjusting control voltage across the filter instead of the conventional method where filters are fixed to a specific frequency of interest. The filter changes by applying the voltage. This voltage is computer controlled, which is explained in the software design section (section 6.11). The filtering technique used in these sensors is Fabry-Pérot interferometry (FPI detectors). The advantages of FPI filters are[224]:

- Able to identify unknown compounds
- Able to identify known compounds by overlapping their infrared wavelength absorption footprints with the existing library[223]

- Measurement flexibility in detecting substances
- Analysing multi-components with chemometric methodology
- Miniaturized, inexpensive and robust

6.4.1 FPI Operation Principle

FPI detectors contain two parallel and flat reflecting plates. These plates work as a half wave generator, which produce successive interference of a continuous transmittance peaks, Fig. 6.2 [224]. Central wavelength (CWL) position changes by changing the peak position. This can be achieved by increasing or decreasing the distance between these two plates. There is a bandpass filter in series with Fabry-Perot filter (FPF) which gives an exceptional narrowband filtering, Fig. 6.3 [224].

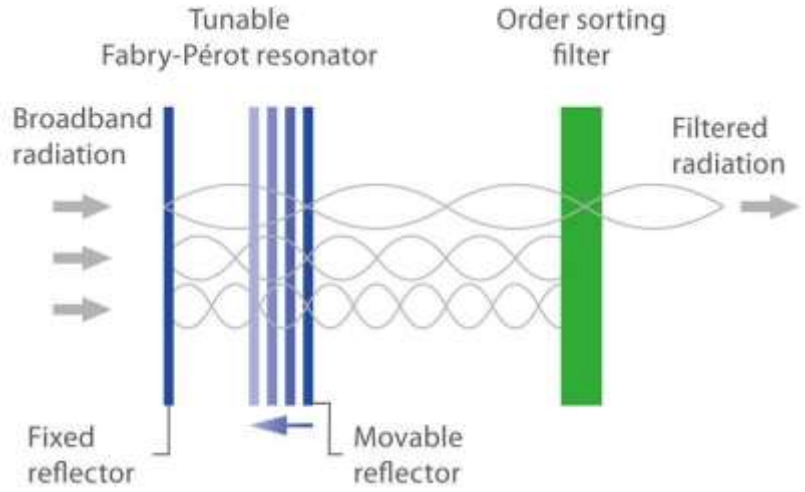

Fig. 6.2 Operation principle of FPF filter [224]

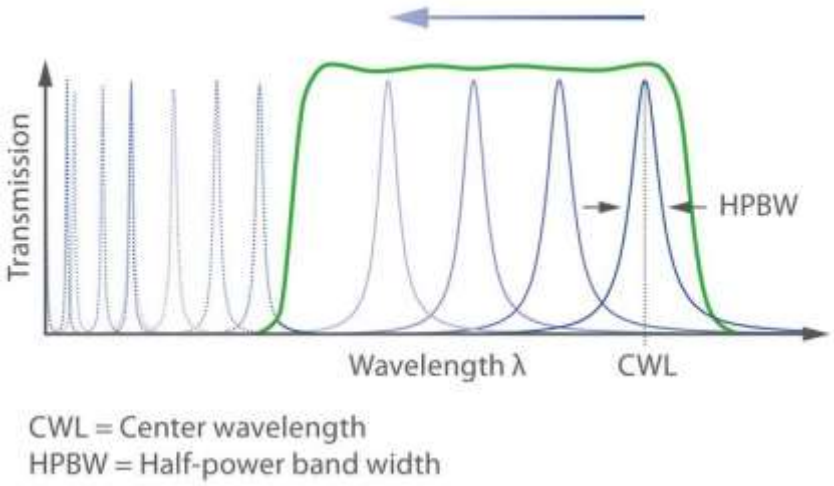

Fig. 6.3 Changing the CWL principle and bandpass filter [224]

Fig. 6.4 shows the Fabry-Perot Interferometer (FPI) filter design principle, with its two thick parallel reflectors. One of them is fixed and the other one can move vertically up and down. The distance between two reflectors d, is called the optical gap. This optical distance can be changed by applying different voltages. This gap results in lots of multiple beam interference. The filter will only allow radiation to pass that satisfies the resonant conditions. The resonant condition can be changed by the user and this leads to the change of the transmitted radiation wavelength [224, 225]. The wavelength changes (λm) can be calculated with equation 6.1.

$$\lambda_m = {}^{2\,n\,d\cos(\beta)}\,/_{m} \qquad (6.1)$$

Where n is gap reflective index, β is angle of incidence, m is order of interference, and d is an optical gap.

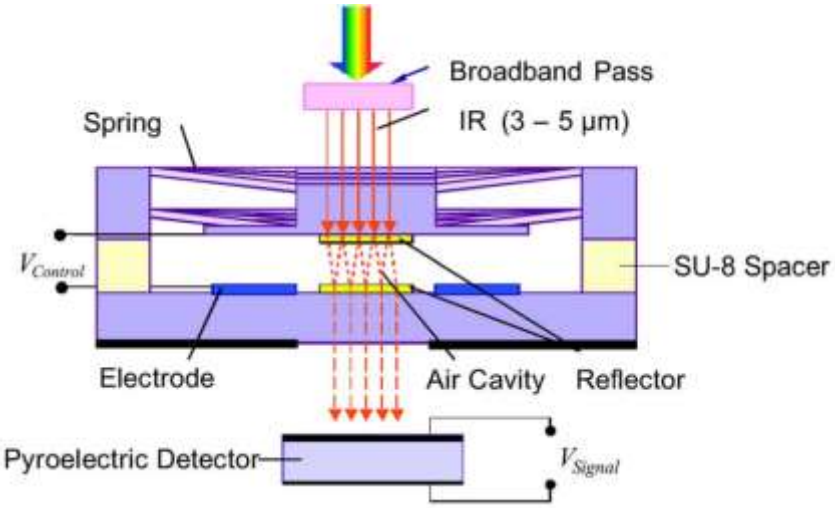

Fig. 6.4 Principle of FPI filter [225]

6.4.2 FPI Operation Principle

At the centre of the optical eNose is an array of four optical tuneable detectors, covering the mid and long wave infrared range (IR – 3.1 to 10.5 µm) [225]. The tuneable filter sensors used are listed in Table 6.1.

Table 6.1 List of sensors which has been used in an optical eNose

Manufacturer	Type	Optical wavelength(um)
InfraTec	LFP-3144C-337	3.1 to 4.4
InfraTec	LFP-3850C-337	3.8 to 5.0
InfraTec	LFP-8850C-337	5.5 to 8.0
InfraTec	LFP-80105C-337	8.0 to 10.5

The first sensor LFP-3144C-337, which needs a maximum voltage of 30V for controlling the central wavelength. This value increases to 45V for the LFP-3850C-337, to 60V for the LFP-8850C-337, and 90V for the LFP-80105C-337 sensor.

6.5 NDIR Source

Using the right NDIR source is important because the emitter should be able to emit mid and long wave infrared ranges to cover the optical sensor wavelengths. The other specifications, which are important in choosing the emitter, are: being low power, long life time, high emissivity, and small size.

To achieve these requirements EMIRS200 emitters manufactured by Axetris Company was used. EMIRS200 infrared source are designed with micro-machined technology. The principle of operation of this emitter is based on black body radiation characteristics. In this emitter, "a resistive heating element is deposited onto a thin dielectric membrane which is suspended on a micro-machined silicon structure"[226]. EMIRS200 are packaged in compact cans with protective cap and broadband filters such as Sapphire, CaF_2, BaF_2 or Germanium[226]. Fig. 6.5 indicates the effect of each filter on the transmission of the IR beam. Since sensor array covers the mid and long wave infrared range (IR – 3.1 to 10.5 μm), the best option in this case is BaF_2 filter.

The advantages of Axetris EMIRS200 IR source with BaF_2 filter are: high emissivity of 95%, have fast electrical modulation of 50% at 50Hz, low power

consumption of 450mW, long lifetime > 10 years, and large black body radiation of 2 to 14 µm.

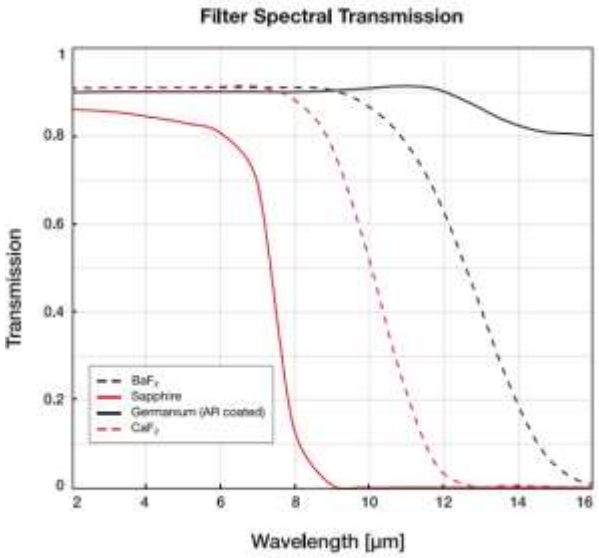

Fig. 6.5 NDIR transmission trend with different filters [226]

6.6 Gas Chamber

Gas chamber can be designed in two different ways. The first one is called high resolution, Fig. 6.6.a and the other one is high signal to noise ratio (SNR),Fig. 6.6.b.

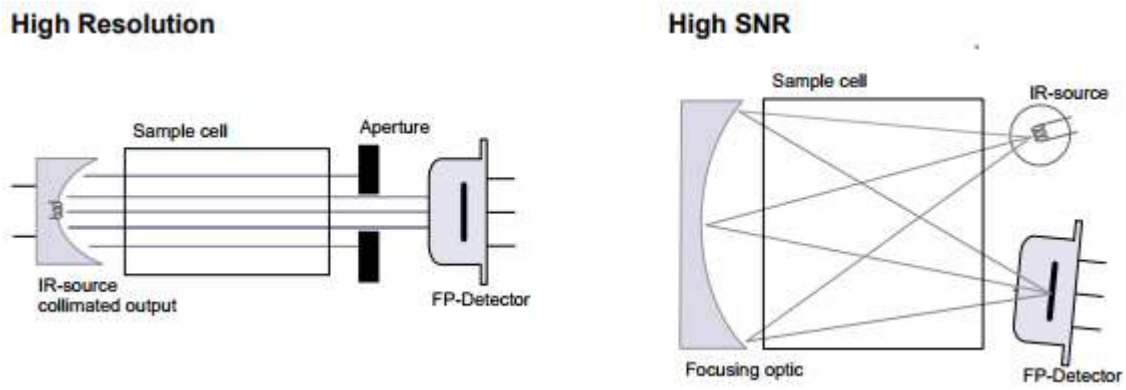

(a) (b)

Fig. 6.6 Different chamber design for optical path for optical eNose. (a) high resolution, (b) high SNR

Since we were interested in really low concentration of different gases or VOCs, high resolution method was chosen. According to literature review, the length of gas chamber in high resolution method is very important in sensitivity of the optical sensors. According to Beer-Lambert law [121], increasing the optical path will increase the sensitivity, but this decreases the signal to noise ratio from emitter to detector and the number of photon absorbed is directly proportional to the power of the photon beam from the emitter and the amount of detectable gas. Hence, a different chamber was designed to find the best chamber length Fig. 6.7. Experiments with a curved gas chamber showed that NDIR beams cannot reach to the detector. Then a 1m straight length chamber was designed and manufactured with a movable emitter inside to find

the best distance for optical path. Different light paths of 10cm, 20cm, 30cm, 40cm and 50cm were tested. The results from these experiments demonstrated that the sensor response for same concentration of gas in the 30cm chamber shows the highest differential voltage in presence of the gas compared to the other chamber lengths, Fig. 6.8. The voltage drop in the presence of 1000ppm CO2 for 10cm chamber is 55.4 mV, 20cm is 77.9 mV, 30cm is 103.3 mV, 40cm is 58 mV and for 50cm chamber is 47.1 mV.

After choosing the right length, two different chambers were designed and manufactured as shown in Fig. 6.9.

Fig. 6.7 Different optical path design, 1m and 30 cm straight optical path, 30 cm curved optical path

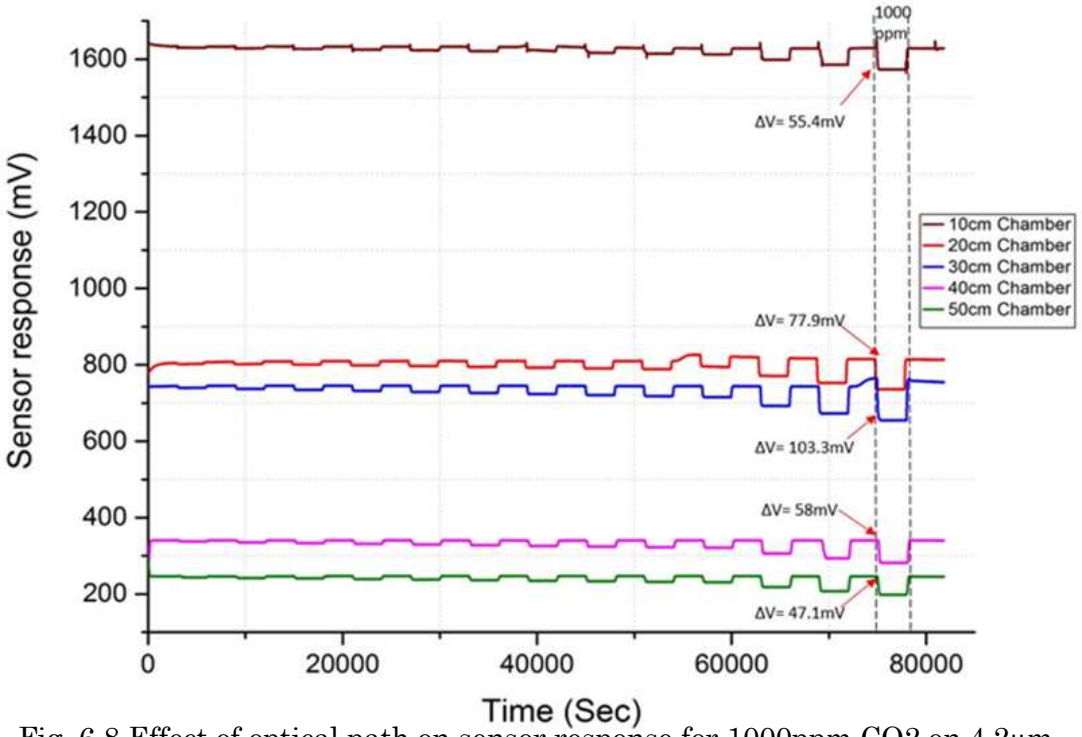

Fig. 6.8 Effect of optical path on sensor response for 1000ppm CO2 on 4.2µm

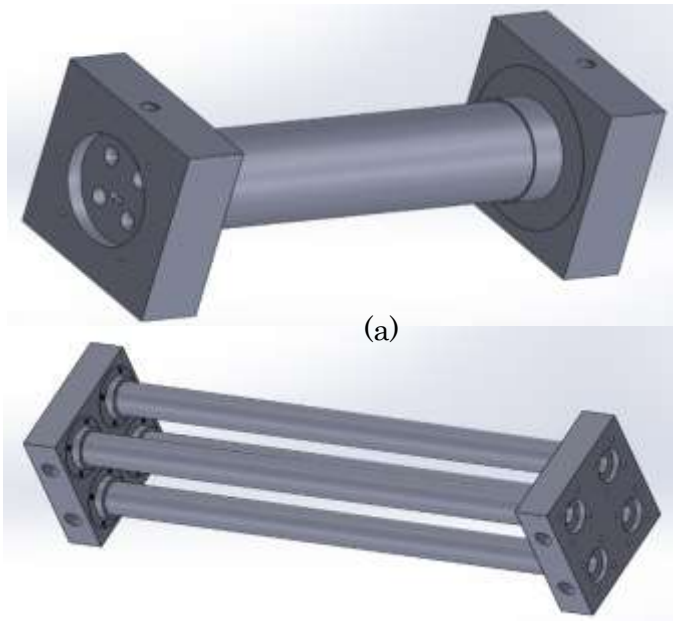

(a)

(b)

Fig. 6.9 Two different chambers design for optical path, (a) all four sensors in one chamber with four different emitters, (b) four different chambers for each optical sensor

Fig. 6.9.a was designed in a way that all four optical sensors are aligned to the four emitters– all fitted into a single chamber with wide diameter and 30 cm long. The chamber is made from stainless steel and was wrapped with nichrome wire and heat insulator. Within the chamber a SHT75 (Sensirion) temperature and humidity sensor was fitted to provide feedback for the environmental control of the chamber. However, in practice this design wasn't successful, because of the wide diameter of the gas chamber emitter, beams were lost, so there wasn't sufficient signal at the detector. Thus, an alternative design was created.

Fig. 6.9.b shows the final gas chamber design where all sensors and detectors are aligned in different 30 cm long stainless-steel tube with smaller diameters. Since stainless-steel has a shiny surface, infrared light reflects more in a small diameter. This optical eNose is designed for medical applications so the chamber was made from stainless-steel to also avoid any contaminations.

Fig. 6.10 shows the fabricated stainless-steel gas chamber which was used for finding the effect of chamber diameter on sensitivity of optical detector.

(a)

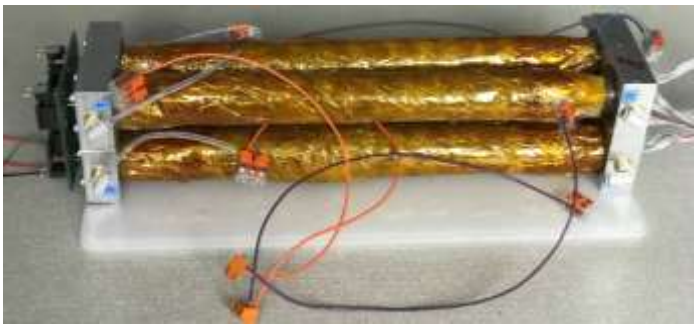

(b)

Fig. 6.10 Manufactured and tested chambers where (a) all four sensors are in one chamber with four different emitters, (b) four different chambers for each optical sensor

6.7 Chamber Heater

As stated earlier, this eNose will be used for detection of VOCs emitted from human waste for medical application, so it shouldn't contain any contamination. Normally the stainless-steel will be colder than the sample temperature, thus there is the potential for condensation on the inside of the instrument, which will cause instrument contamination. To prevent this issue, the stainless-steel chamber was wrapped with nichrome wire and a heat insulator. Nichrome wire is a resistive heating

element, which is made from nickel, chromium or iron. The nichrome wire's heat dissipation has a direct relation to the amount of voltage and current applied to it. The nichrome wire used for heating the chambers is covered with an insulator to prevent any short circuit. To secure the nichrome wire on the stainless-steel chamber, Kapton tape was used, which is an additional heat insulation.

The temperature inside the chambers is controlled by proportional, integral and differential (PID) algorithm. The temperature value can be chosen by user through windows interface and is called setpoint (SP). There is a feedback value that comes from inside the chambers and shows the current value per second. This is called process variable (PV). The PID control loop manages to keep PV and SP equal. To turn the heater on there is an electronically switch, which lets the current pass through the nichrome wire. This is the 'control voltage' (CV) and it helps the system to reach SP from PV. The PID control system equation is shown below:

$$CV = MV_{(t)} = K_P e(t) + K_i \int_0^t e(\tau)d\tau + K_d \frac{d}{dt} e(t) \qquad (6.2)$$

Where e(t) is the difference between the SP and PV. The K_P, K_i and K_d are the proportional, integral and differential constants respectively. K_P defines how far PV is from SP. K_i and K_d, state how long PV has been off from SP and how fast PV is moving toward SP. So, these constant values should be chosen carefully. For example, if K_d is too big then it'll cause an overshoot. Sensor's maximum operating temperature is the limit of the temperature inside the gas chamber. The specification for this part is to achieve the SP temperature value between 10 mins and 15 mins. The maximum temperature of inside the chamber shouldn't exceed 65 °C to prevent sensor damage.

So, to give a margin of safety, the temperature inside the chamber, was set to a maximum of 55°C. To find the best values for K_P, K_i and K_d, a program was written in Arduino IDE and Processing 3.2.3 to simulate these values and estimate the best approximation, with the quickest in time and less overshoot in temperature. After testing many combinations for K_P, K_i and K_d, the values of 150, 50 and 60 were chosen for K_P, K_i and K_d respectively. Fig. 6.11 and Fig. 6.12 show two examples of how the required temperature was reached. In both examples the error is less than 3°C. However, the temperature inside the chamber shouldn't rise too much, as high temperatures inside the gas chamber affects the NDIR emitter's beams. The power requirement for each chamber heater was 33.6 W with 24V applied voltage.

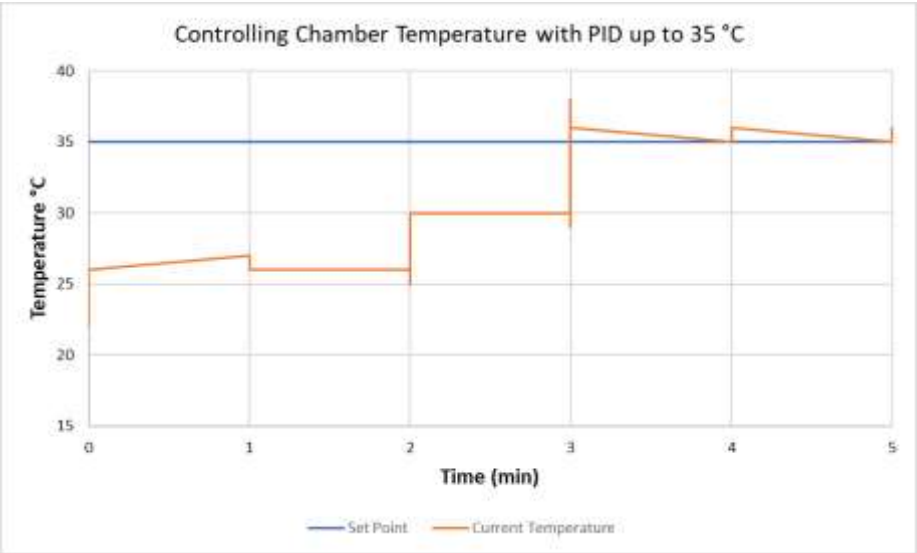

Fig. 6.11 Chamber temperature increases to reach 35°C as a set point

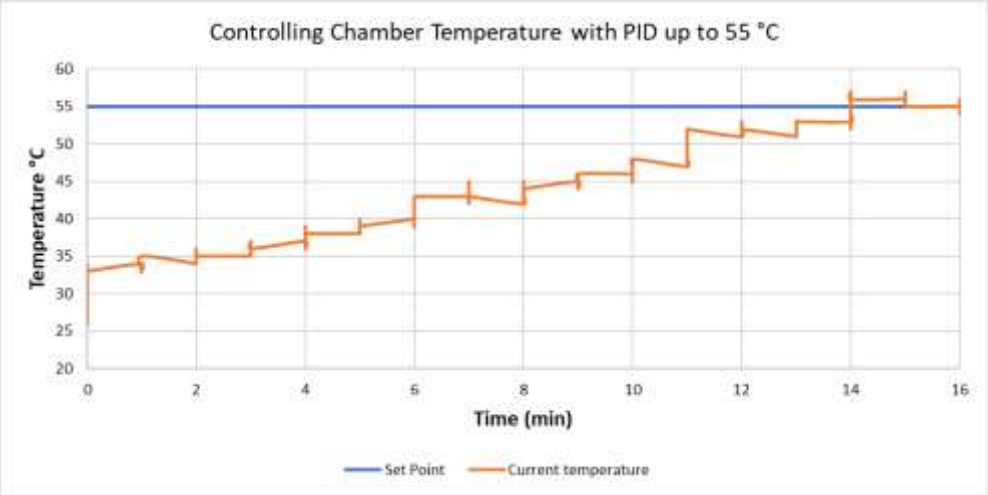

Fig. 6.12 Chamber temperature increases to reach 55°C as a set point

6.8 Microcontroller

The Teensy 3.6, USB microcontroller development board (PJRC, USA) was used in this project as the main microcontroller. Teensy 3.6 works as a bridge between sensor boards and the windows program and includes a 32 bit 180 MHz ARM Cortex-M4 processor[227].

Teensy 3.6 is chosen because it is faster than other available boards. It has 3.3V UART communication voltage level, which is required for communicating with the sensor boards. In addition, teensy 3.6 provides enough UART communication line for communicating with the 4 separate sensor boards.

6.9 Electronic Design

Electronic requirement for this optical eNose can be divided to four major parts: sensors electronic driver board, emitters driver board, heater board, and control system electronic board. These are discussed below.

6.9.1 Sensors Electronic Driver Board

An electronic board was designed to run all 4 sensor boards and start the communication with the sensors. According to the sensor's datasheets, the sensor boards require different supply voltage specifically, 3.3 V, ±5 V, 12 V and 30V to 90 V with less than 100 mA current. The first sensor LFP-3144C-337 needs a maximum voltage of 30V for controlling central wavelength. This value is increased to 45V for LFP-3850C-337, to 60V for LFP-8850C-337, and to 90V for LFP-80105C-337 sensor. The sensor's electronic driver board was designed to work with 24 V, then generating the required lower voltages and negative voltage by using linear voltage regulators. The voltage regulators used in this circuits were LM2937IMP, L78L05ABD, LD1117S33TR, and L79L05ABD to generate 12 V, 5 V, 3 V, and -5 V respectively. The most important and critical part was to convert 12 V to 90 V. Since 90 V is considered as a high voltage, it is important to switch on the high voltage last and turn it off first. Therefore, two circuits were implemented to ensure this. The first switch used a delay based on a simple RC-combination, Fig. 6.13.

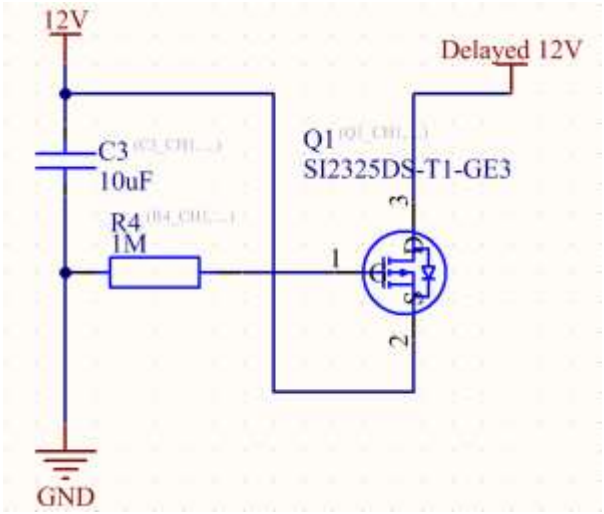

Fig. 6.13 Protecting circuit with delaying 12 V

The switch off protection makes sure that in the case of disconnecting the +12 V, the 90V voltage (VDDH) is also disconnected, Fig. 6.14.

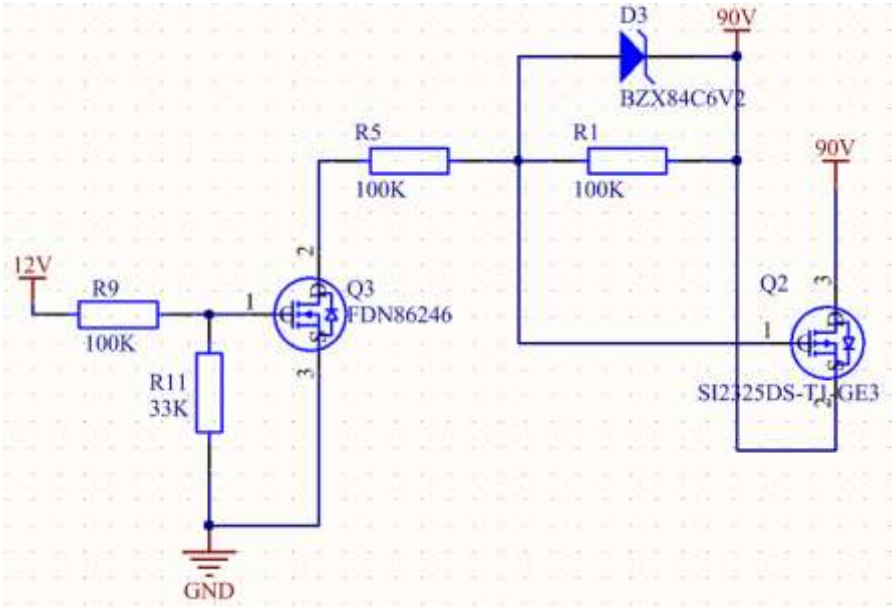

Fig. 6.14 Protection circuit to turn of 90 V first

To generate the 90 V from 12 V, a step-up converter in combination with a transformer was used. A LT1372HVCS8 high frequency switching regulator was used with a flyback transformer to increase the voltage. By changing the value of C1 and R2, the switching frequency changes and by varying the value of R3 and R7 the output voltage can be changed Fig. 6.15. Each sensor board has a universal asynchronous receiver-transmitter (UART) communication line with 3.3 V. The sensors electronic driver board was designed in a way that it has four UART communication lines, one for each sensor with 3.3 V.

Fig. 6.16 illustrates the 3D version of PCB design and Fig. 6.17 shows the final version of 2 layers PCB after manufacturing and assembling. Each section is related to one of the optical sensors. It contains 4 headers for each sensor and one main connection, which transmits and receives all the information to microcontroller (MCU).

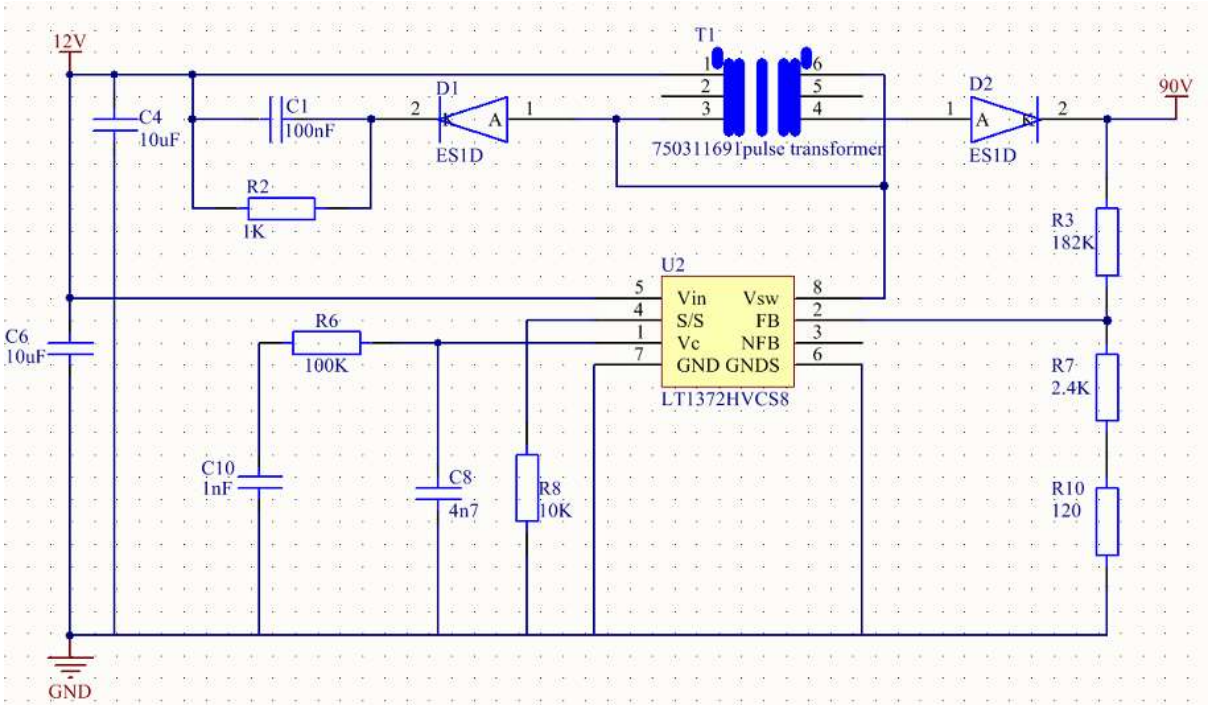

Fig. 6.15 Boosting circuit to change 12 V to 90 V

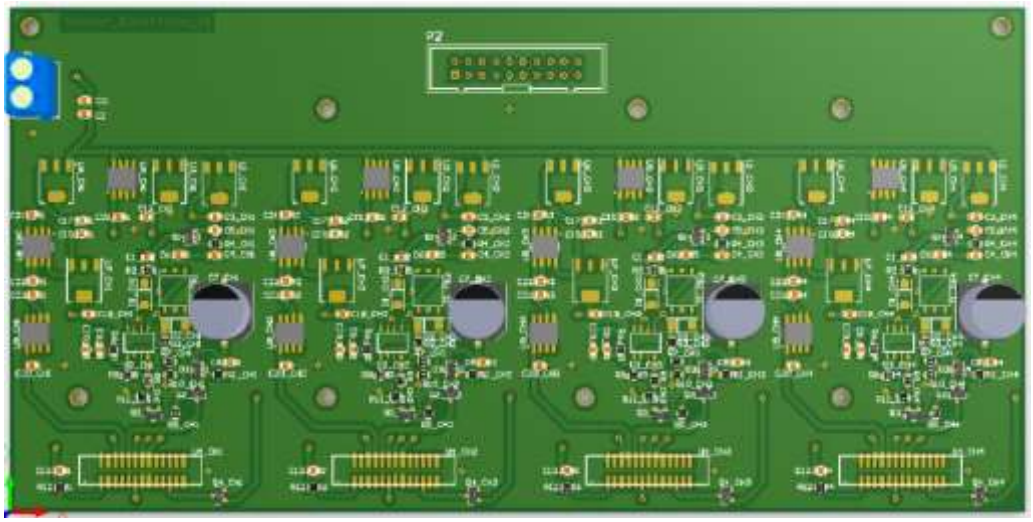

Fig. 6.16 3D of the PCB layout of sensors electronic driving board

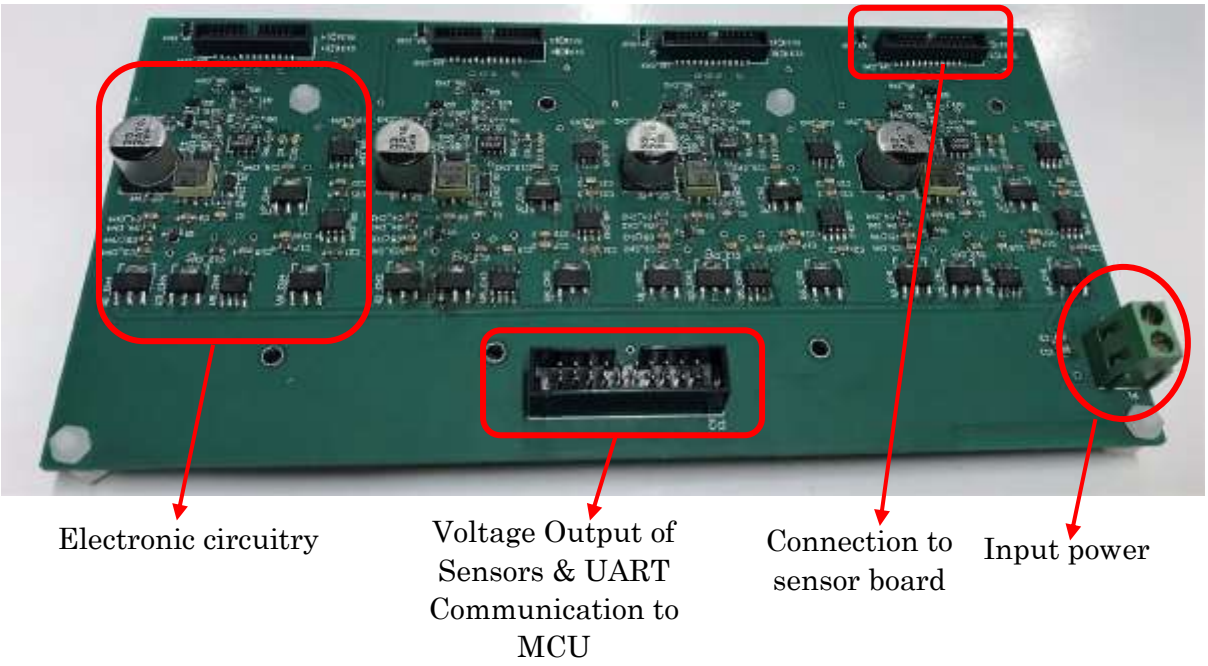

Fig. 6.17 Manufactured PCB board for controlling 4 sensor boards

6.9.2 Emitters Electronic Driver Board

According to the Axetris EMIRS200 IR source datasheet, these emitters can be driven in three ways: voltage regulated, current regulated, and power regulated. In this case, a power regulated circuit was designed for driving emitters. The power regulated design can compensate the inherent variation in source parameters. Power regulated mode is more efficient for DC voltages with low frequency pulses. There are two circuit designs for power regulated, constant power mode, and power-controlled mode. Power controlled mode design was used in this part, which is more efficient and avoids reducing the lifetime of the emitters.

Fig. 6.18 shows the power regulation circuitry for running the emitters. There is a power and current monitor chip (MAX4211), which gives an output voltage for feedback purposes and is proportional to the power at IR-Source. Fig. 6.19 shows the manufactured board, which runs all the emitters. Teensy 3.2 MCU was used for generating square wave pulses to turn the emitter on and off, with the frequency of 10Hz (according to datasheet this is the optimal frequency to run the emitter). The advantage of using Teensy 3.2 is that the switching frequency can be changed when needed by computer control.

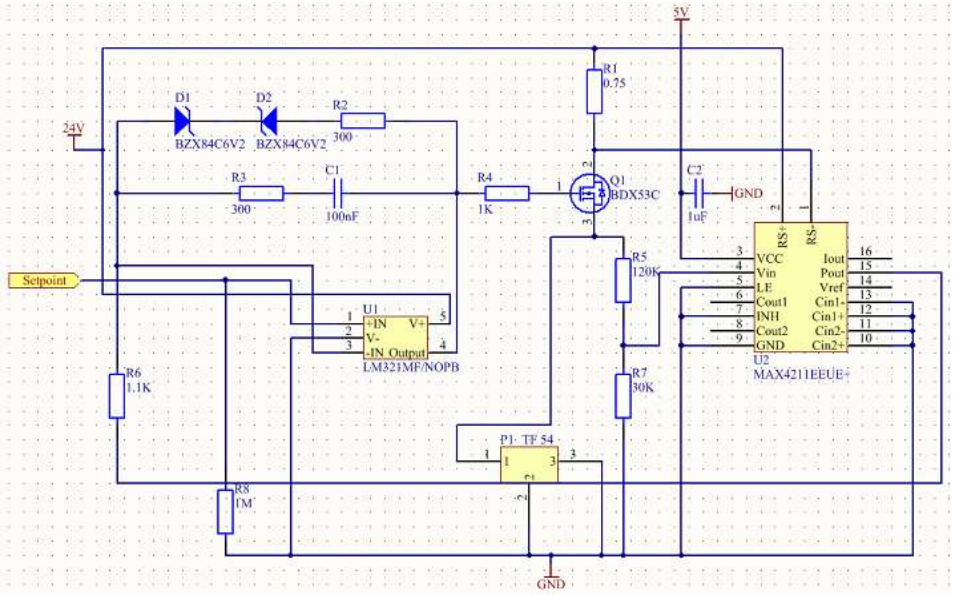

Fig. 6.18 Power regulated circuit for running emitters

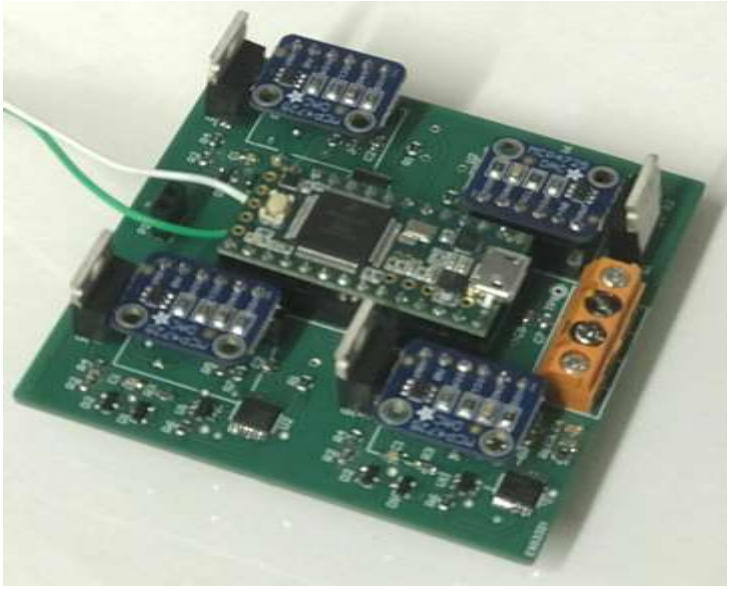

Fig. 6.19 Power control circuitry for running 4 emitters

6.9.3 Heating System Driver Board

The heating system (on the chambers) uses a simple electronic circuit, which switches the voltage on/off across the nichrome wire shown in Fig. 6.20. It is switched on/off when the temperature drops too low. A control signal is a digital signal, which turns on the MOSFET to let current go through the nichrome wire, when temperature reading is less than the set temperature and it turns the MOSFET off when the reading temperature is equal or higher than the set temperature.

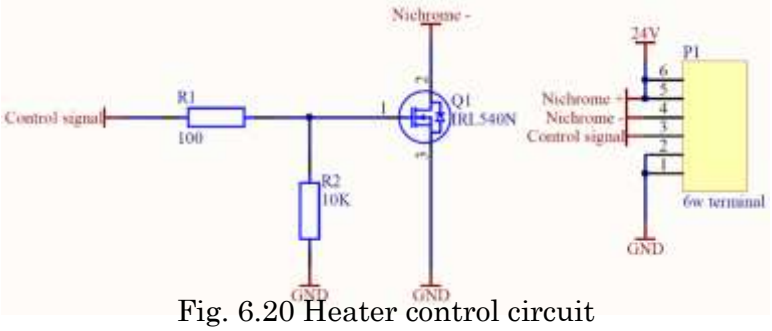

Fig. 6.20 Heater control circuit

6.9.4 Voltage Control Board

The system is designed to work with two different 24V DC input power adaptors. Two input power adaptors were used to separate the heater input power from the main circuitry. This is because of the high current flow on the heater side. The voltage control board provides the desired voltage for each part of the system. The advantages of having this circuit is that, if one part of the system has an issue it won't affect the rest of the instrument. Fig. 6.21 shows the breakout of the power system in optical eNose.

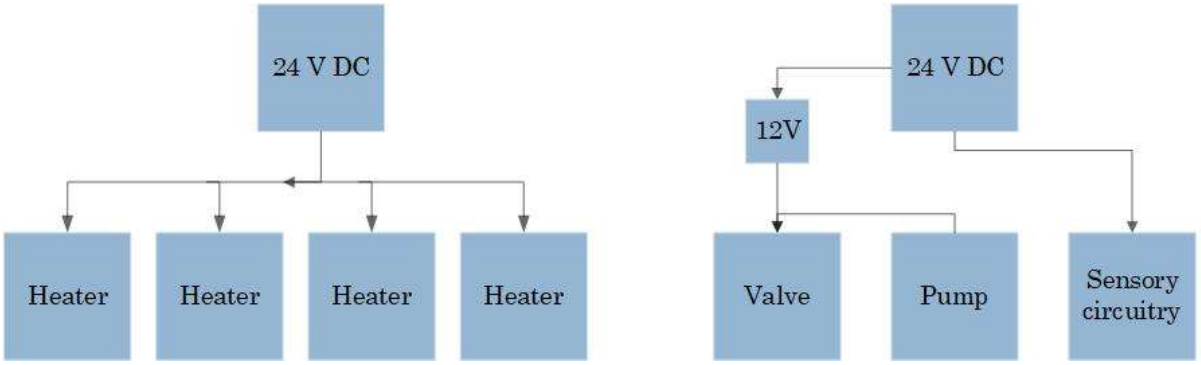

Fig. 6.21 Power division of optical eNose

6.10 Pneumatic System

The optical eNose airflow system is reconfigurable. The flow path of the instrument is shown in detail in Fig. 6.22. The air flow can pass through the sensor's chambers in series by turning on the pump at the end of the loop or it can pass through parallel sensor's chambers. Each design has its own advantages and disadvantages. In the series version, since pump is flushing at the end of the cycle, it is not possible to

determine where the sample's VOCs is, this process can happen quickly, which may not give enough time for sensors to detect the sample. But the advantage is that all sensors will receive the total amount of VOCs. In the parallel version there is enough time for each sensor to detect the VOCs of sample, but the issue is the amount of VOCs is divided between each chamber and due to slight pressure differences, the amount can be dissimilar for each chamber. After the sample passes through all chambers it goes to exhaust (outlet).

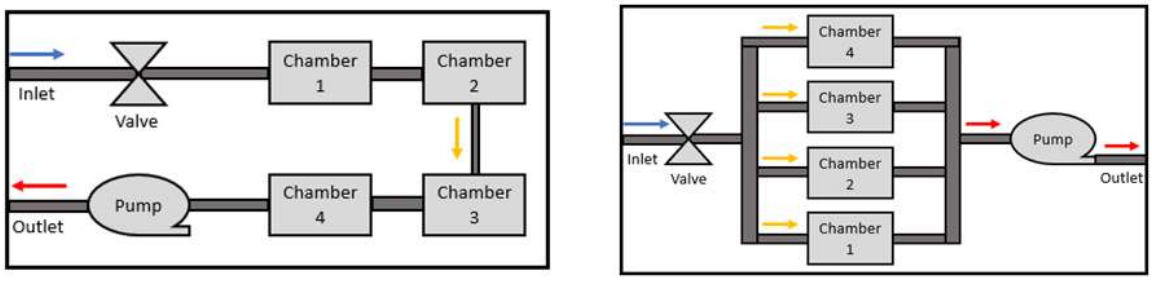

(a) (b)

Fig. 6.22 Airflow layout in optical eNose, (a) chambers series, (b) chambers parallel

6.11 Software Design

Currently, the tuneable optical sensors are used in isolation. This software is not suitable for the optical eNose because four optical sensors are used simultaneously. Consequently, a novel communication protocol was developed that was able to interface with all four sensors simultaneously. The protocol consists of three major aspects:

- Sensors
- Teensy 3.6

- Universal Windows Application (UWA)

During a test, sensor parameters are continuously streamed between the sensor and the laptop. The flow path of this stream is shown in Figure 18. The optical sensors provide on-demand parameters including temperature, wavelength, detector response etc. The Teensy 3.6 was used to pull these parameters from the optical sensors via four UART communication lines. The parameters are processed and transferred to the UWP app to be visualised by the user and saved for further analysis. The following sections describe the optical sensor software interface, Teensy 3.6 C++ library and UWP software. The overview of the communication of the instrument is shown in Fig. 6.23.

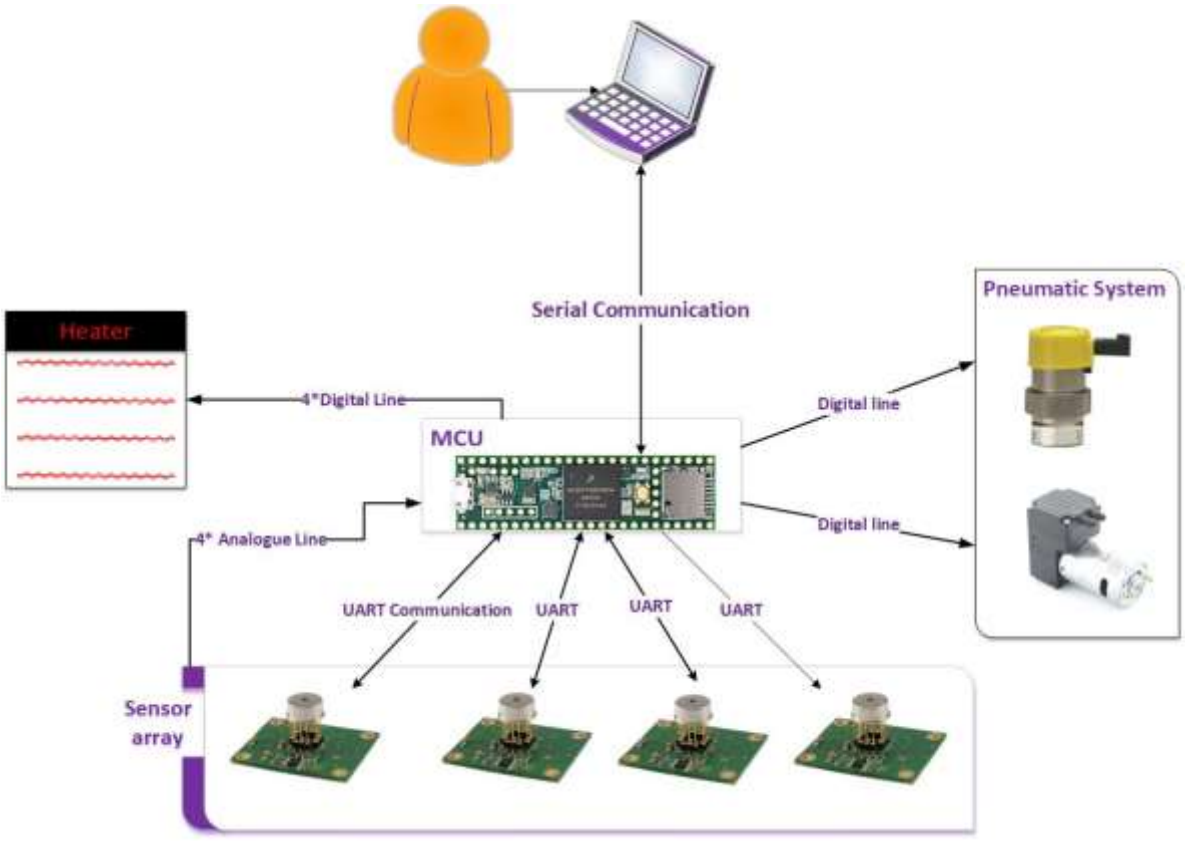

Fig. 6.23 Overview of the optical eNose communication lines

6.11.1 Sensor Board

As described earlier, several on-demand parameters are available from the sensors. To request a parameter information, a five to sixteen-byte package is sent to the sensor board with an appropriate operational code (OPC). These OPCs are the same for all four sensors. The important OPCs, which were used in this software, are listed below in Table 6.2 and Table 6.3 with their descriptions. The OPCs can be divided to two types, request and set categories.

Table 6.2 The list of operational codes, user requested from sensors

Name	OPC	Information Provide	User usage
GET_VERSION	0X00	Sensor boards serial number, hardware and software information.	General information
GET_STATE	0X01	State, module code and error code	Indicates error with sensor
SW_RESET	0X02	Triggers the sensor boards software reset	Reset the board software before each test
NML_GET_DET_INFO	0X10	Sensor's serial and article number, type of sensor, minimum and maximum wavelength of sensor	General information&Indication of each sensor wavelength limit
NML_GET_VDDH	0X11	Minimum voltage requirement for changing the filter central wavelength	General information
NML_GET_TEMP	0X015	Sensor and sensor's board temperature value	Temperature controller feedback inside chamber

Table 6.3 The list of operational codes, user sets to sensors

Name	OPC	Information provide	User usage
NML_SET_POTI_OFFSET	0X12	Sets sensor's output offset	To increase the gain and offset when necessary
NML_SET_POTI_GAIN	0X13	Sets sensor's output gain	
NML_SET_CWL	0X19	Sets sensor's central wavelength	Change the wave length when required

The sensor boards communicate through a UART protocol with speed of 1Mbaud rate with microcontroller. Since these sensor boards work based on an asynchronous serial protocol, it is important to ensure that the data transfer is robust and error-free. For synchronisation of data between MCU and four sensors, a 1 stop bit was defined, and for finding the endianness of transferred data, a least-significant bit (lsb) method was chosen. Sensor's boards communications are package oriented and based on a simple request-reply structure. It means that the MCU can only request one at a time for each sensor and needs to wait for a reply from each sensor board.

To receive any information from the sensor board, the MCU sends a package as shown in Table 6.4. A package includes the header byte, which shows when the package starts. This follows by the OPC and data length (as defined in the datasheet). Each package of N byte data is closed by a 16bit cyclic redundancy check (CRC) value.

Table 6.4 Data package sent from Teensy3.6 to each sensor board

Header		**OPC**	**Data length**	**Data 0**	**Data 1**	**…**	**CRC_Low**	**CRC_High**
1Byte = 0xFF		1 Byte	1Byte = N	<…….. N Byte ……..>			2 Byte	
example	0xFF	0x11	0x00				0x4D	0X2D

The receiving package of information from the sensor board, to the microcontroller has the same structure as the sending package with one more byte called “status” shown in Table 6.5. As stated before, to make sure the package gets to the detector correctly and sent back without error, there is status section in all receiving packages, which shows the correctness of the data package. In all OPCs, if the communication is correct, the status value is 0: ACK, otherwise the status value will be different according to the error.

Table 6.5 Data package sent from each sensor board to Teensy 3.6

Header		**OPC**	**Status**	**Data length**	**Data 0**	**Data 1**	**…**	**CRC_Low**	**CRC_High**
1Byte = 0xFF		1 Byte	1 Byte	1Byte = N	<……. N Byte ……..>			2 Byte	
example	0xFF	0x11	0x00	0x04	0x96	0xDA	0x26	0x47	0X70
					0x42				
					= 41.71				

6.11.2 C++ Library for Microcontroller

The microcontroller is the interface between the Windows software and the other electronic parts inside the eNose instrument. It works as a bridge, it connects the

Windows software with the optical sensors, optical path heater, electronic valve and pump. To achieve all these communications, a new interfacing library protocol was developed in C++ in visual studio software. The Received instructions from Windows software were translated and sent to the corresponding part of the eNose.

The most critical part of microcontroller development was related to the communication part with the sensors, where it translates the instructions from Windows software and sends requests to the sensors with the relevant OPC code. Microcontroller receives all packages from the four sensors, restructures data, and streams them to the Windows software. The MCU checks the status of the receiving packages to see if their values are zero (this means there is no error or mistake) and converts the receiving data (Bytes) to characters. Then it puts all the characters of the four sensors in an array and sends it to the windows platform. Fig. 6.24 shows an example of how MCU restructures every data coming from the four sensors and prepares them to send the package to Windows.

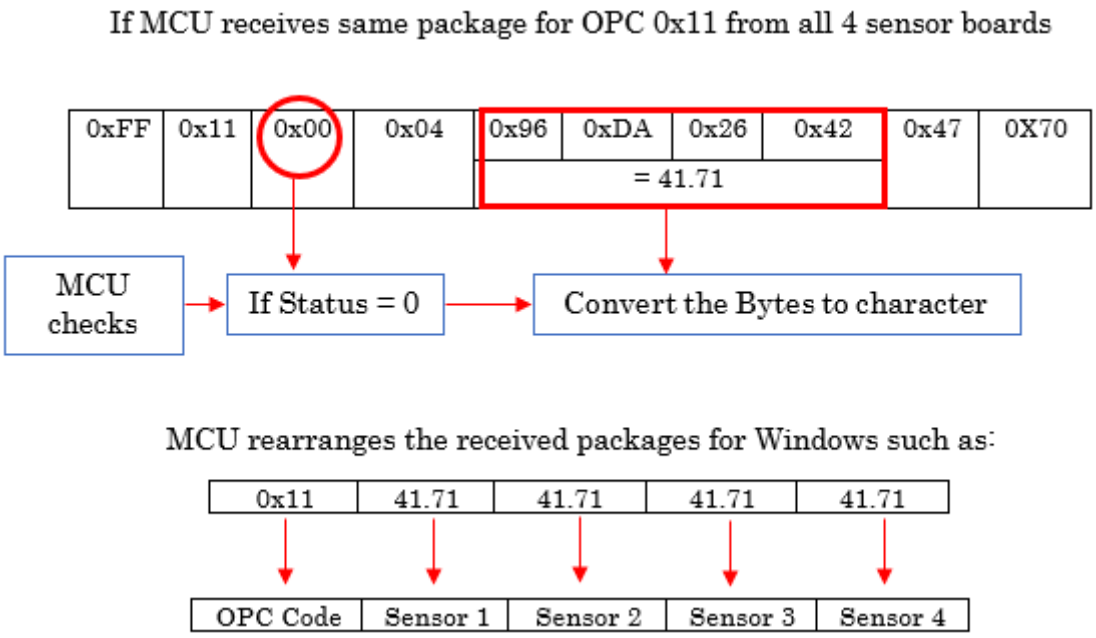

Fig. 6.24 Restructure of the data package in MCU

The sensors outputs are analogue voltage (between 0 and 3.3V) and MCU constantly reads these values. The developed library for MCU also includes control lines on heater, pump and the eNose instrument's valve.

6.11.3 Optical eNose Software

The Optical eNose software manages the experiment timing, sensor states, sensor response, and logs this information to a .csv file. At the start of the analysis, the user connects the optical eNose to a computer running the Windows software via a USB cable. The software detects the optical eNose microcontroller and sends an instruction

requesting sensor information. The wavelengths, voltage range, temperatures, manufacturer information, and states of the sensors are displayed. This step is important as the information from the sensors is used to map the wavelengths and voltage during analysis, ensuring the user does not exceed the prescribed ranges for each sensor. The status information also alerts the user to the health of each sensor before the start of an experiment. Once these checks are complete, the user can set up the software to run an analysis. The software allows two modes of operation:

- Scanning Mode:

In this mode, the user selects a minimum and maximum wavelength with a specified step size. The software ensures all three parameters are within the manufacturer's recommendation for each sensor. During analysis, the software scans from the minimum to maximum wavelength with steps equal to the defined step size. The minimum and maximum wavelength value for each sensor is shown on the screen. The user should select the wavelength values according to what is shown on the detector information section on the screen. Step size cannot be less than $20nm$ and the chosen value has to be multiplication of $20nm$.

- Sequence Mode:

Here the user enters specific wavelengths of interest to monitor each sensor. The software runs a check to ensure each wavelength is within the range of the sensor specified. During analysis, the software only changes the sensor wavelengths to the prescribed wavelengths.

Once a mode is selected and the wavelength is chosen, the user can define the timing of the experiment. The sensor manufacturer defines a minimum of 2ms interval between wavelength changes and the software ensures the user does not go below this limit. The user can specify intervals for changing wavelength, reading sensor response voltage and logging information to a CSV file. The minimum logging interval (Save rate) is 1/2 the wavelength change (Sweep rate) interval. Additionally, the software ensures the logging interval is at least equal to the sensor response reading interval. Fig. 6.25 shows the settings page.

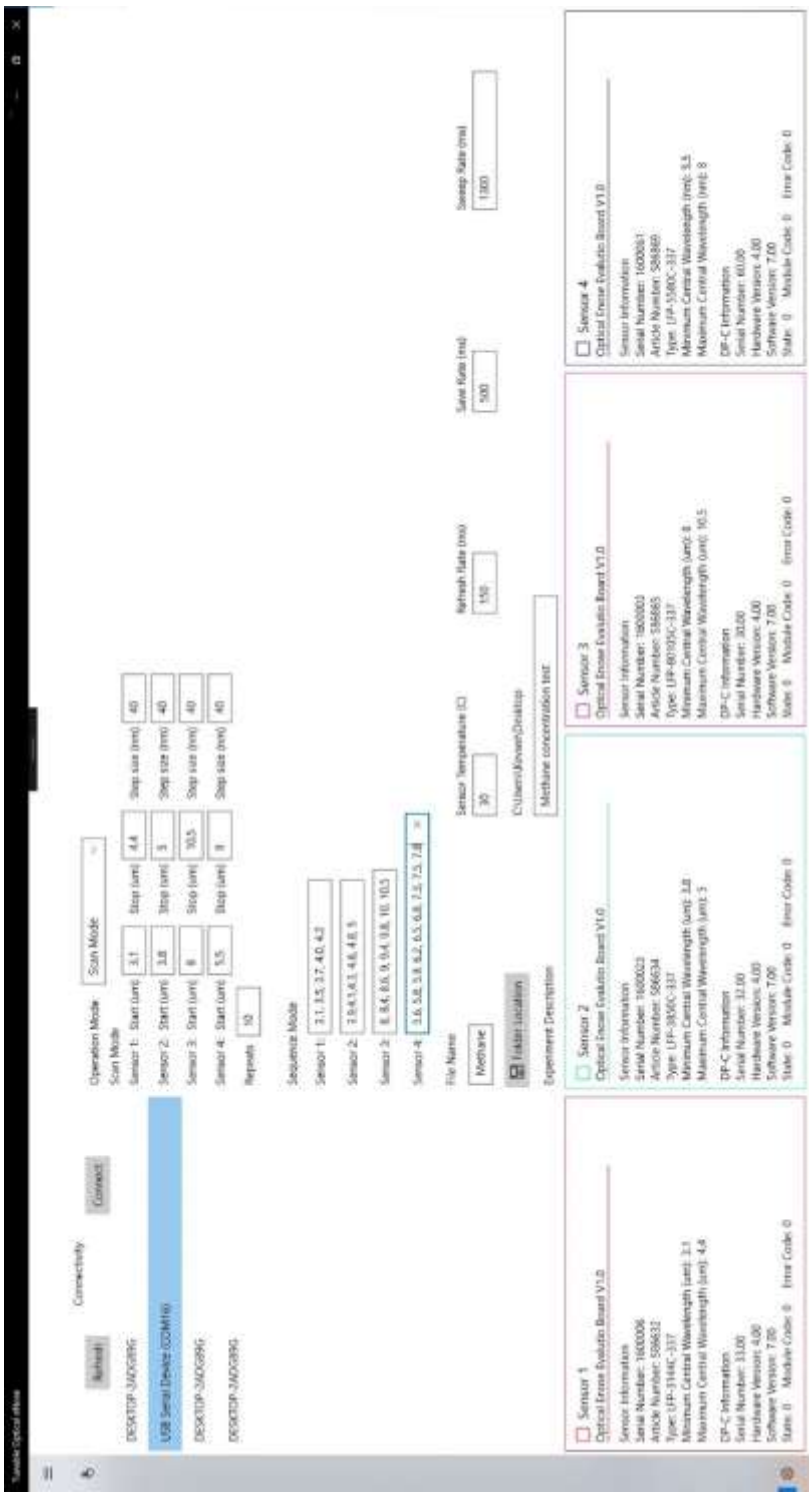

Fig. 6.25 Settings page of the optical eNose software

Once the analysis parameters are entered, the user navigates to the experiment page. Here the user can click to begin the experiment as defined in the settings page. To ensure repeatability across experiments the software creates several system threads to run processes asynchronously. This ensures one process is not blocked by another and each sequence occurs at the predefined time during analysis. Once the experiment begins, the software sends an instruction to the sensors via the microcontroller requesting information on the sensor temperature and voltage response. The information received is graphically plotted and displayed to the user. This step is repeated at the sensor response reading interval specified by the user. At specified sweep interval, the software sends an instruction to the specified sensor requesting to change the wavelength. The software informs the user if the change was successful based on the received sensor status report. The user is also able to change gain and offset of each sensor during an experiment by entering the desired amount in the text box for the particular sensor. Changes to the gain and offset are updated immediately and the software informs the user if the change was successful based on status readback from the sensor. All parameters monitored during the experiment are logged in the CSV file. The experiment page user interface is shown in Fig. 6.26.

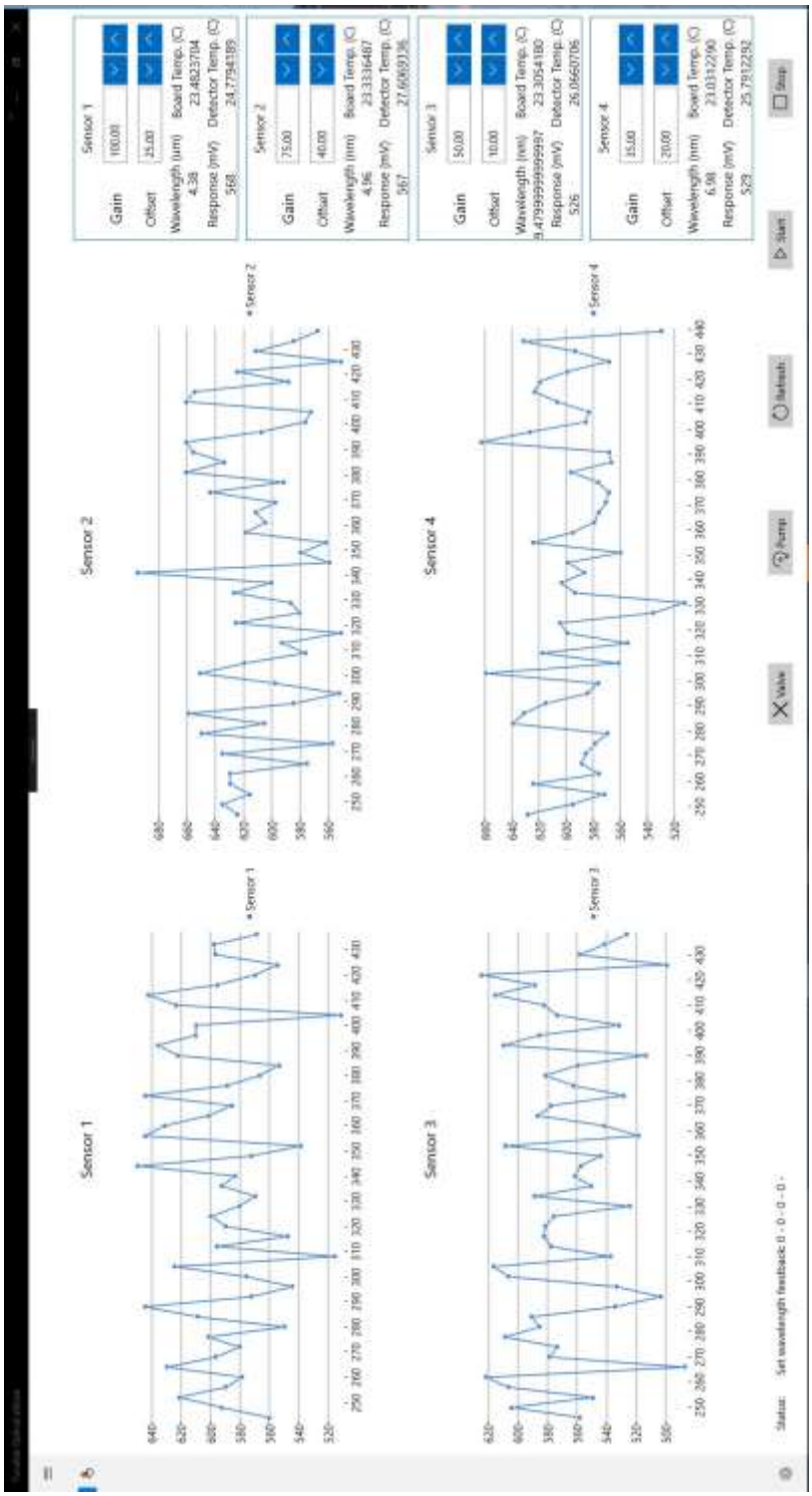

Fig. 6.26 Experiment page of the optical eNose software

6.11.4 Algorithm of Program

Fig. 6.27 shows the flow chart diagram of the optical eNose software. This describes each steps of the windows program process.

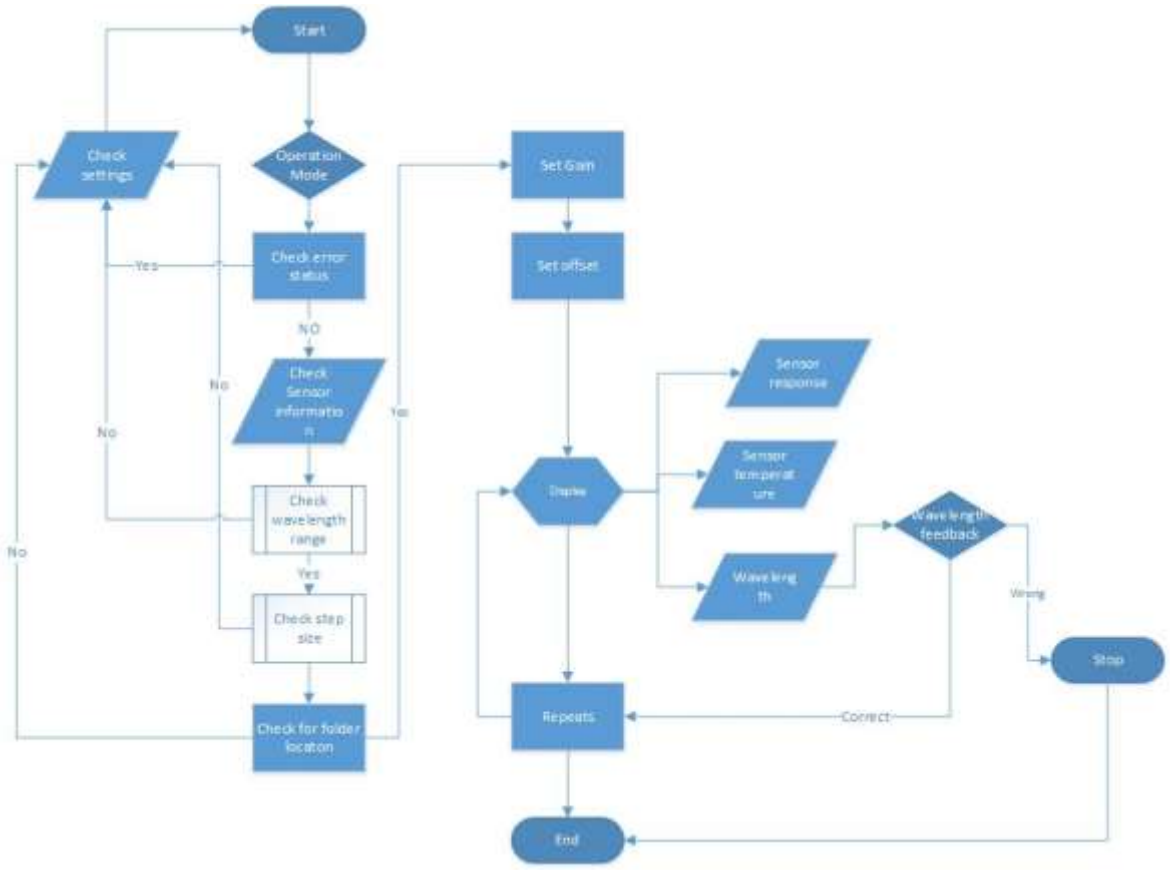

Fig. 6.27 Optical eNose software operation flow chart

6.12 Completed Instrument

This eNose instrument consists of three main parts: electronic design, mechanical system and software implementation. Once electronic system and mechanical parts of the eNose instrument were developed and manufactured, they were tested separately to make sure that each part works satisfactory individually. The software implementation was developed step by step to make sure it is able to control each part independently before everything was assembled together. The last part, after the finalising software implementation, was to assemble the optical eNose. Assembly parts included connecting all the electronics and mechanical parts together by a variety of connectors. The gas line connections on the chambers are Swagelok stainless steel compression fittings. Fig. 6.28 shows the final implementation of the Warwick optical eNose instrument.

Finally, the whole system was fitted in a $47.5 * 23 * 46.8$ cm soundproof white computer case. The case weighs 8.5 kg on its own. After setting up the system inside the case the total weight became 12 kg. This case was chosen because of its large space so that the heat generated from different sections (specially the chamber heaters) won't affect any other part of the system. Fig. 6.29 shows the final fully implemented system of optical eNose instrument.

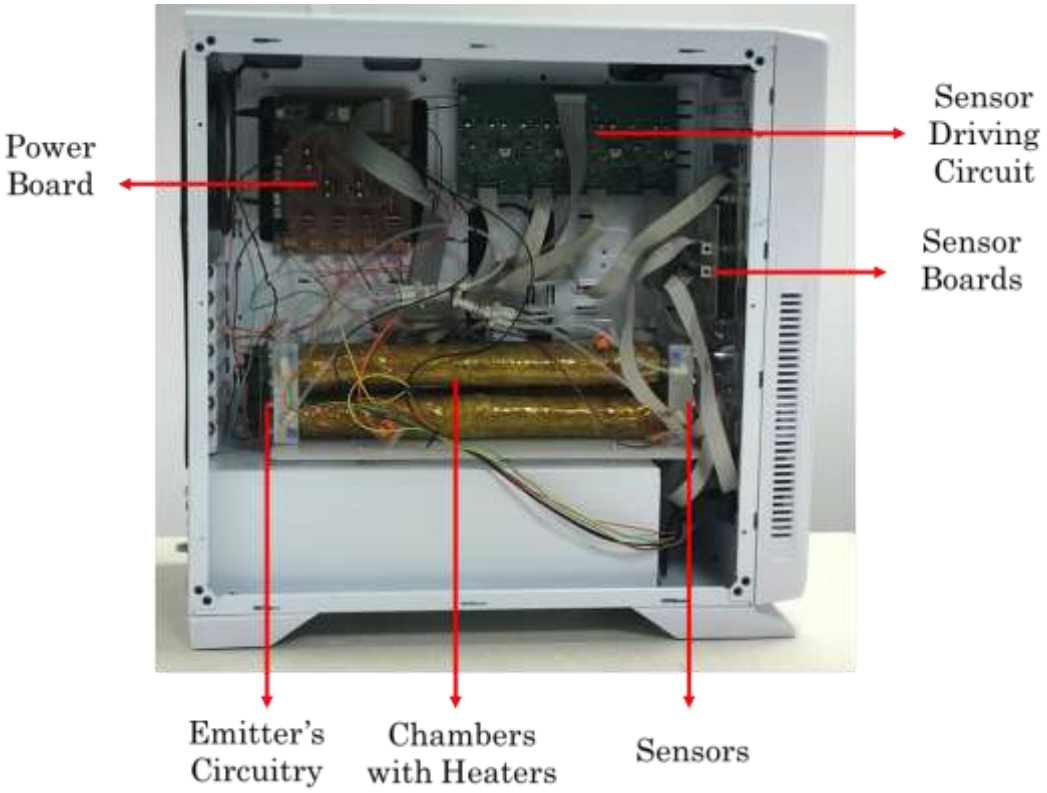

Fig. 6.28 Developed optical eNose setup

Fig. 6.29 Final fully implemented optical eNose

6.13 Conclusions

This chapter reported on the development of an optical electronic nose based on an array of NDIR detectors. The sensor array used in this system were tuneable detectors, which are able to cover the whole infrared range between 3.1μm and 10.5 μm and scan this range to find out the absorption frequencies for a sample.

The emitters used in this system are based on black radiation technology, which emits the infrared beams for the above mentioned range of wavelengths. The microprocessor used in this system was MK66FX1M0VMD18, which acts as a bridge to send the data from sensors to a windows program and vice versa. This system has a stainless-steel gas chamber to avoid any contamination when used in biomedical applications.

The sensors used in this eNose technology provide the opportunity to identify known and unknown substances. In addition, it can measure different substances with multi IR absorption frequency. Chapter 7 will cover the results of comprehensive experiments that were performed using optical eNose to realise its sensitivity and selectivity.

Chapter

7 Experimental Testing of Warwick Optical eNose Instrument

7.1 Introduction

This chapter presents the testing and subsequent application of the optical eNose instrument, which was built and developed for detecting urinary volatile organic compounds to diagnose metabolic and gastro disorders. As discussed in the previous chapter (chapter 6), a novel sensors array was used in the optical eNose which led to the development of the state-of-the-art eNose instrument. This technology has never been used in any other eNose instrument before. Since this is a novel technology, it requires experimentation to evaluate the system. After assessing the system's sensitivity and selectivity with the available test gases, the instrument was then tested using a range of single chemicals and complex odours. At the end, optical eNose instrument was tested on urinary VOCs of diseased and healthy groups. All the aforementioned experiments are explained in detail in this chapter.

7.2 Testing Optical eNose with Single Gases

These tests were designed to use the available gas cylinders in the biomedical laboratory in the School of Engineering at University of Warwick. The tests were aimed to find the sensitivity and selectivity of the optical eNose instrument's sensors array. Discovering the lowest ppm/ppb sensitivity of the instrument is important, because the VOCs emitted from urine samples contain ppm/ppb level of complex odour/gases. The initial experiment was designed to test sensitivity and selectivity of the optical sensors in different wavelength using two single gases such as methane (CH_4) and carbon dioxide (CO_2). These gases were chosen because they are easy to detect due to their large infrared absorption.

7.2.1 Sensors Electronic Driver Board

Table 7.1 shows the information about the gas cylinders used in this experiment.

Table 7.1 Gas cylinders concentration

Gas Cylinder	Concentration
CO_2	1000 ppm in air
CH_4	100 ppm in air

To get different concentration gases out of these cylinders, they were connected to gas mixture part of the gas test rig (explained in chapter 5). In this test each gas was mixed with zero dry air. The total flow rate used in gas mixture was 400ml/min and the lowest achievable flow rate on each gas line was 10ml/min. The temperature of the chamber was 27 ±1 °C during test. Due to the limitation of gas mixture (chapter 5), the lowest achievable concentration of CO_2 and CH_4 gases were 25 ppm and 2.5 ppm respectively. These values were calculated using the equation below:

$$\frac{lowest\ flowrate\ in\ each\ line{=}10\ ml}{Total\ flow{=}400\ ml} = \frac{achievible\ lowest\ concentration}{Total\ cylinder\ concentration} \quad (7.1)$$

For CO_2 test, the concentration of CO_2 was increased linearly from 25 ppm to 250 ppm in 25 ppm steps, additionally 500 ppm, 750 ppm and 1000 ppm were tested along with zero air as a baseline measurement. There was an exposure and recovery time of 25 mins for each concentration step.

For methane test, the second test was performed using CH_4 with a concentration range of 0 to 100 ppm using the developed gas test rig (chapter 5). Similar to the first experiment, the concentration of CH_4 was increased linearly from 2.5 ppm to 25ppm in 2.5ppm steps, additionally 50ppm, 75ppm and 100ppm were tested along with zero air as a baseline measurement. There was an exposure and recovery time of 25 mins for each concentration step.

7.2.2 Results and Discussion

The optical eNose infrared detection range is between 3.1 μm and 10.5 μm. According to the Hitran database[228], CO_2 gas has only one absorption frequency, at 4.2 μm. Fig. 7.1 shows the response of optical sensor at 4.2 μm to variation of CO_2 gas concentration. Fig. 7.2 indicates the changes in concentration of CO_2 vs sensor response. This shows that sensor response is linear to polynomial for same amount of changes in CO_2 concentration. Methane has two absorption frequencies in the IR spectrum frequency. The first one is at 3.4 μm and second one is at 7.8 μm [229]. Two different sensors that cover the mentioned frequencies, were used to demonstrate the system's ability to simultaneously measure the output of multiple sensors at 3.4 μm and 7.88 μm wavelength. The results shown in Fig. 7.3 and Fig. 7.4 indicate that the projected sensitivity to methane was below 1ppm. Fig. 7.5 and Fig. 7.6 show the sensor response vs concentration changes of CH_4 gas in two different wavelengths. Voltage changes is linear for same amount of changes in concentration.

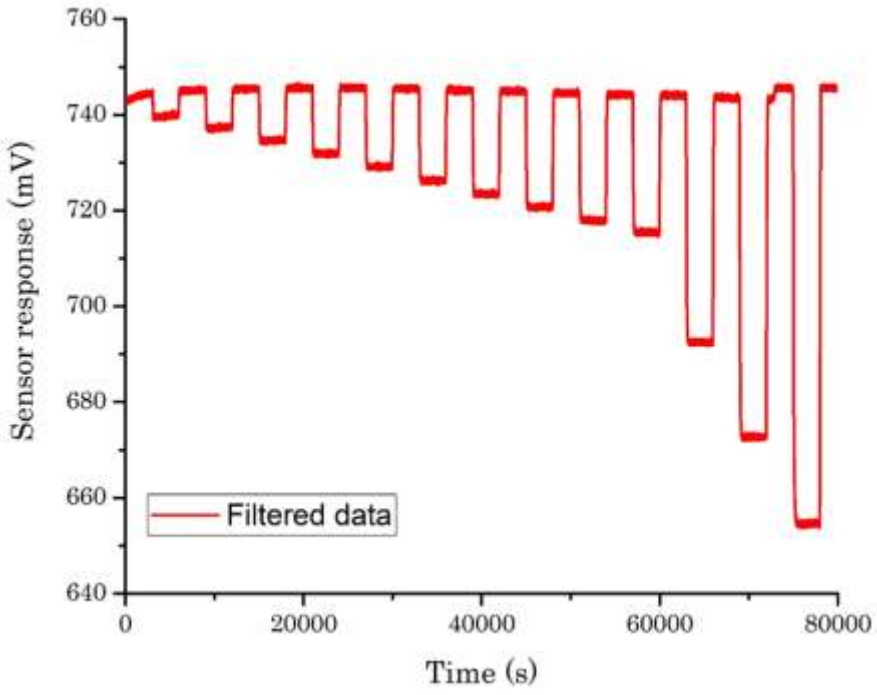

Fig. 7.1 Sensor response to CO2 gas with different concentrations starts from 25 ppm to 1000 ppm at 4.2 μm

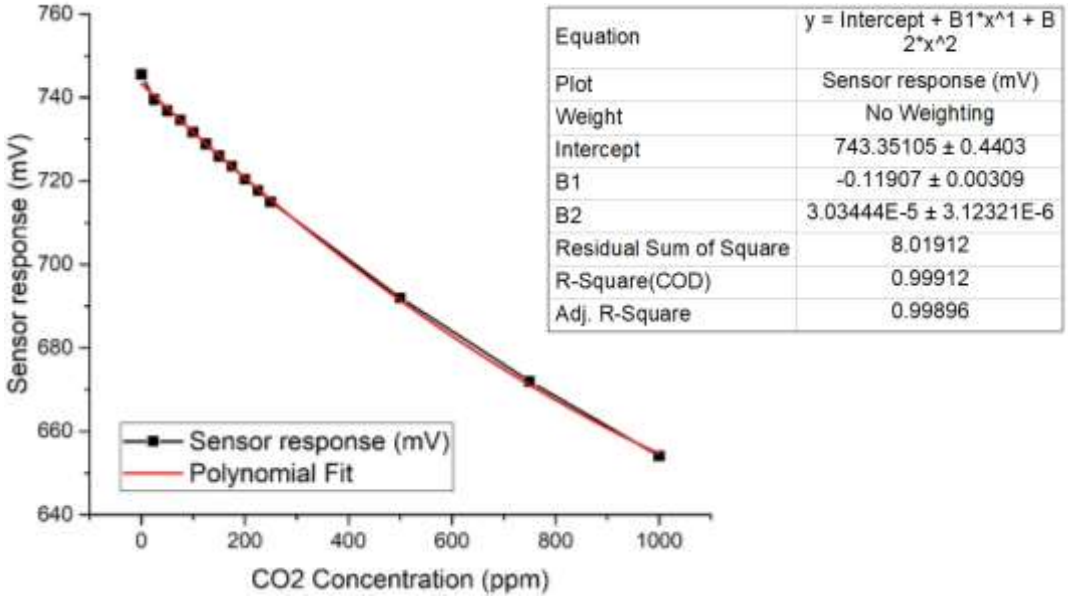

Fig. 7.2 Sensor response vs. CO2 concentration changes at 4.2um

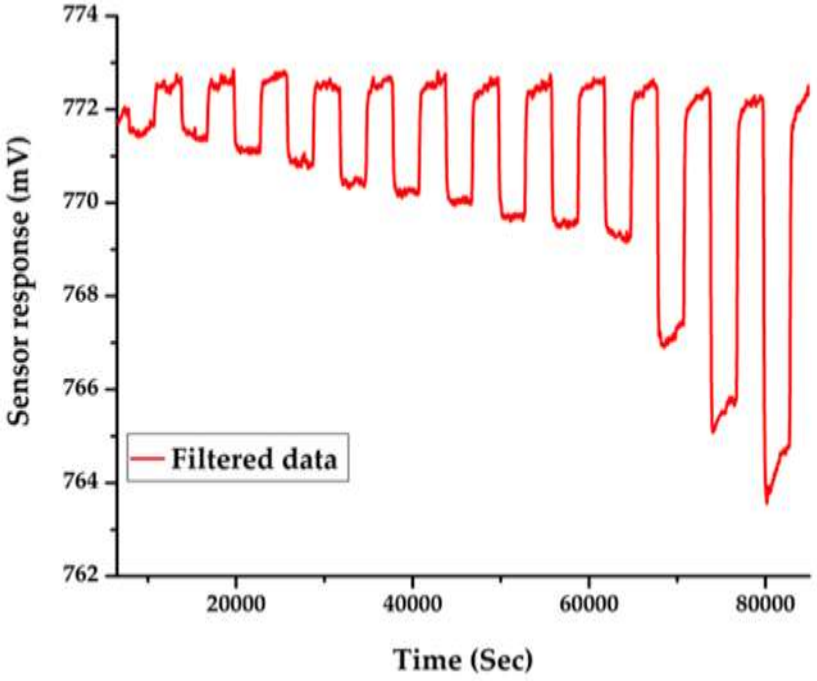

Fig. 7.3 Sensor response to CH4 gas with different concentrations starts from 2.5 ppm to 100 ppm in two different wavelengths 3.4 µm

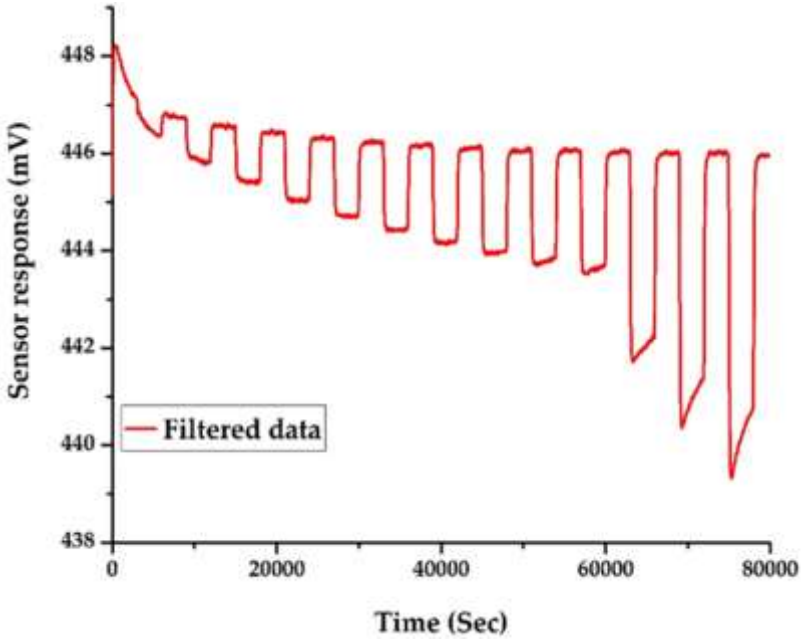

Fig. 7.4 Sensor response to CH4 gas with different concentrations starts from 2.5 ppm to 100 ppm in two different wavelengths 7.88 µm

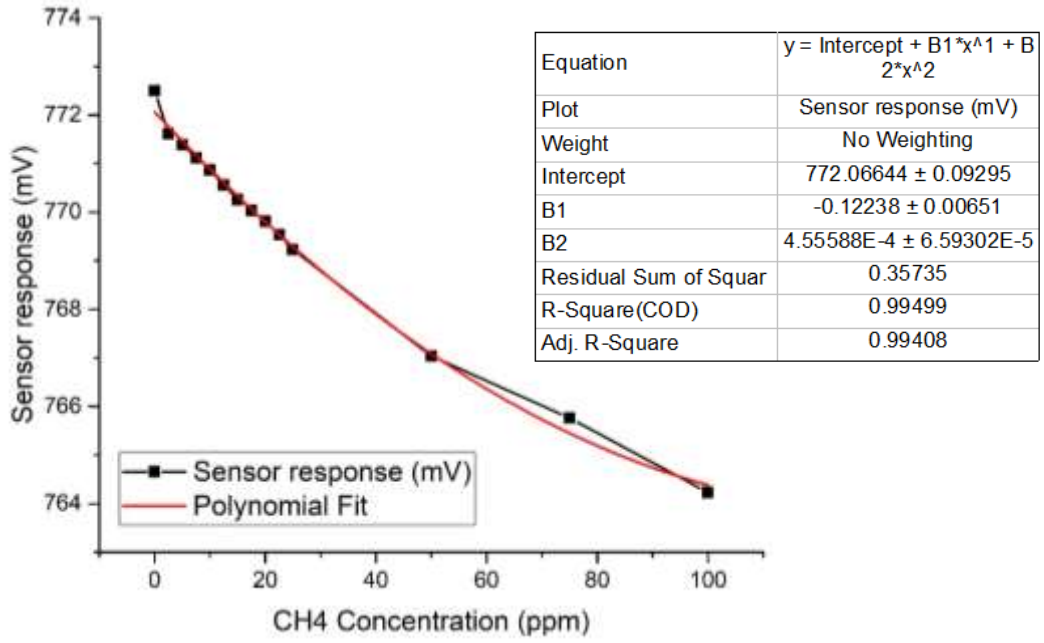

Equation	y = Intercept + B1*x^1 + B 2*x^2
Plot	Sensor response (mV)
Weight	No Weighting
Intercept	772.06644 ± 0.09295
B1	-0.12238 ± 0.00651
B2	4.55588E-4 ± 6.59302E-5
Residual Sum of Squar	0.35735
R-Square(COD)	0.99499
Adj. R-Square	0.99408

Fig. 7.5 Sensor response vs CH4 concentration changes at 3.4 µm

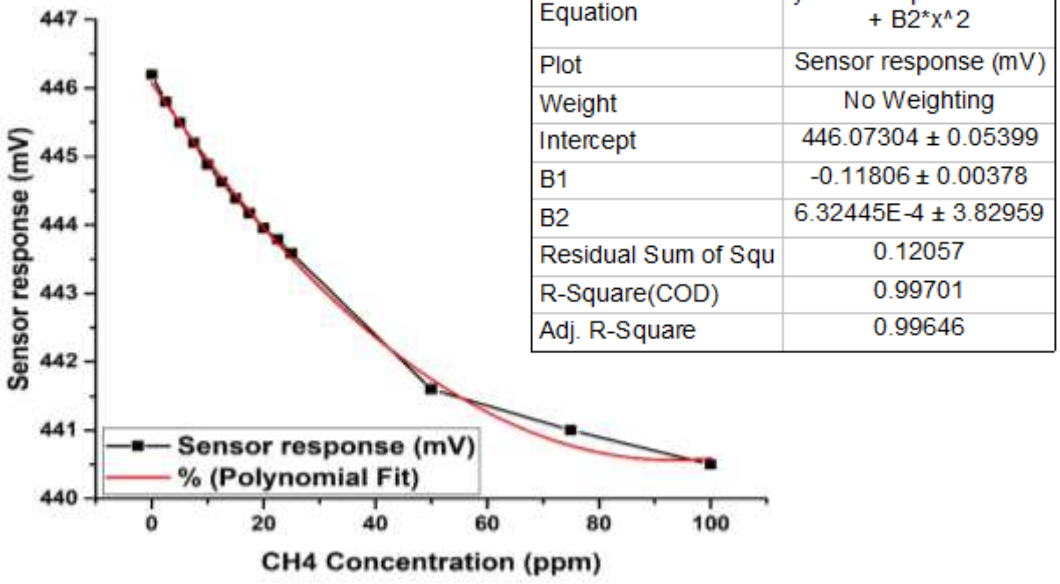

Equation	y = Intercept + B1*x^1 + B2*x^2
Plot	Sensor response (mV)
Weight	No Weighting
Intercept	446.07304 ± 0.05399
B1	-0.11806 ± 0.00378
B2	6.32445E-4 ± 3.82959
Residual Sum of Squ	0.12057
R-Square(COD)	0.99701
Adj. R-Square	0.99646

Fig. 7.6 Sensor response vs CH4 concentration changes at 7.88 µm

7.3 Testing the Optical eNose with Simple and Complex Chemicals

The evaluation of the optical eNose instrument continued by testing it to a range of different single chemicals, acetone, ethanol and isopropanol– some of which are clinically known as relevant biomarkers with recognised absorption frequencies and some complex odours with unknown absorption frequencies.

Each of these single chemicals and complex odours have several absorption frequencies ranging between 3.1 μm and 10.5 μm. For example, acetone and ethanol both have four main big absorption peaks in this range. This means that all four sensors that cover these frequencies were used to show the system's ability to simultaneously measure the output of multiple sensors in different wavelength.

7.3.1 Methods and Materials

One millilitre of 100% single chemicals were mixed with 4 ml of water, cola and orange juice were directly used and 1 gram of coffee was mixed in 4ml of water were prepared for this experiment, then 5 mL of each substance was aliquoted into a 20 mL glass vial. The glass vials were heated to 40 ± 0.1 °C and the headspace of the samples were taken using a 10 ml syringe. The headspace of samples was then injected to gas

chambers. It wasn't possible to calculate concentration of these molecules in this experiment.

7.3.2 Results and Discussion

One of the single chemicals used in this test was acetone. Fig. 7.7 shows the radar plot presentation of the optical eNose response to both acetone and ambient air in the infrared range of 3.1 μm and 10.5 μm. Looking at Fig. 7.7, it is clear that the response of the sensors inside the eNose to the chemical vapour (acetone) is different compared to ambient air. The differences between acetone and ambient air absorption frequencies are mostly between 3.16 μm and 3.7 μm, then 5.56 μm and 9 μm.

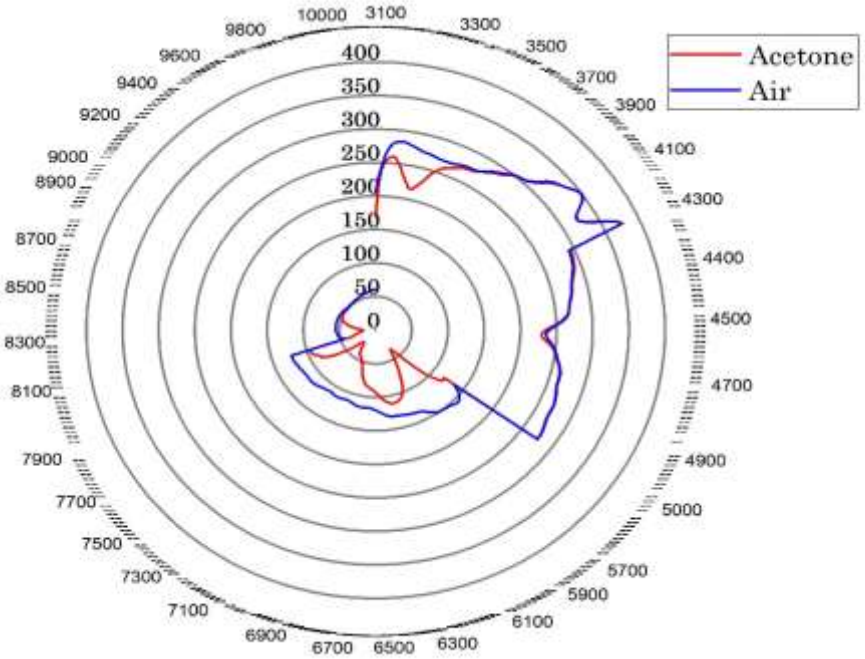

Fig. 7.7 eNose responses to ambient air and Acetone in whole infrared range between 3.1 um and 10.5um.

Fig. 7.8, presence the comparison between the response of the Warwick optical eNose to acetone and the database information (obtained from NIST chemistry book as a reference) [229]. As the optical eNose sensors have different baseline values, the acquired data from sensors were normalised to lie between 0 and 1. The first sensor that covers the range of 3.1 µm to 4.4 µm can detect acetone at 3.34 µm similar to the database. Wavelength of sensors one and two, overlap between 3.8 µm and 4.4 µm. The absorption peak of both sensors was at 4.28 µm. This is due to the existence of CO_2 gas in the zero airline. Sensor three, which covers the wavelength range of 5.5 µm and 8 µm, shows two absorption peaks around 5.88 µm and 7.44 µm close to the absorption frequency of the NIST database. The last sensor, which covers wavelengths from 8 µm to 10.5 µm, detects acetone at around 8.1 µm. Overall, according to Fig. 7.8 it is clear that the optical eNose is able to detect acetone in different wavelengths. Moreover, a satisfactory detection was achieved by comparing test results with database.

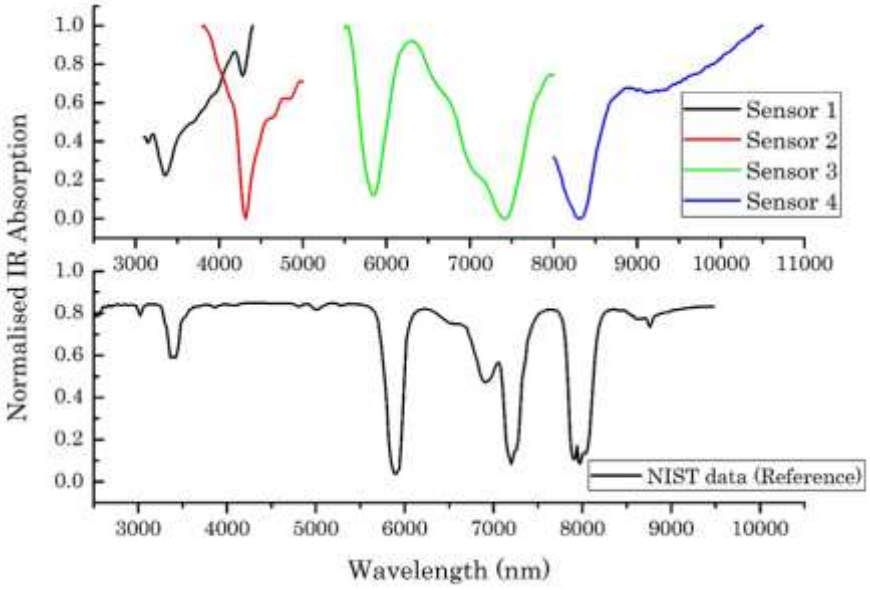

Fig. 7.8 Acetone absorption frequency between 3.1um and 10.5um. Comparing database result with optical eNose

Fig. 7.9, shows the radar plot of the raw responses of sensors at different wavelengths for various chemicals. Some of the chosen wavelengths were based on the known absorption wavelength of single chemicals, and whilst other wavelengths were chosen at equal spacing's for complex chemicals, which they don't have a specific absorption frequency.

A common data analysis approach was applied, where features were extracted from the raw data, based on the maximum voltage drop of the sensor at a predefined wavelength. After these features were extracted, principle component analysis (MultiSense analyser package) was applied. Fig 7.10 shows the LDA classification and Fig 7.11 shows the PCA classification of 6 different classes of samples. Since Isopropanol and ethanol are from the same family of chemicals, they are close to each other in this classification. The results also indicate that cola gave the biggest variation amongst all the samples and that acetone, isopropanol and ethanol are well separated.

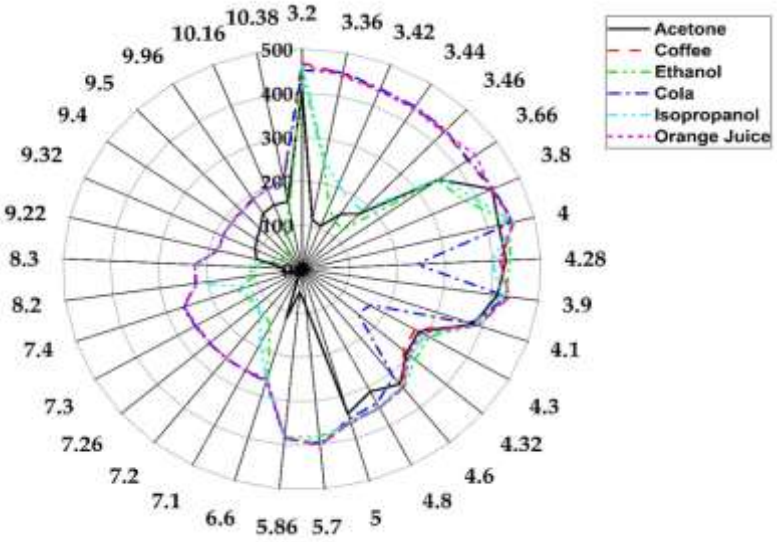

Fig. 7.9 Radar plot of the raw sensors responses at different wavelength for different chemicals

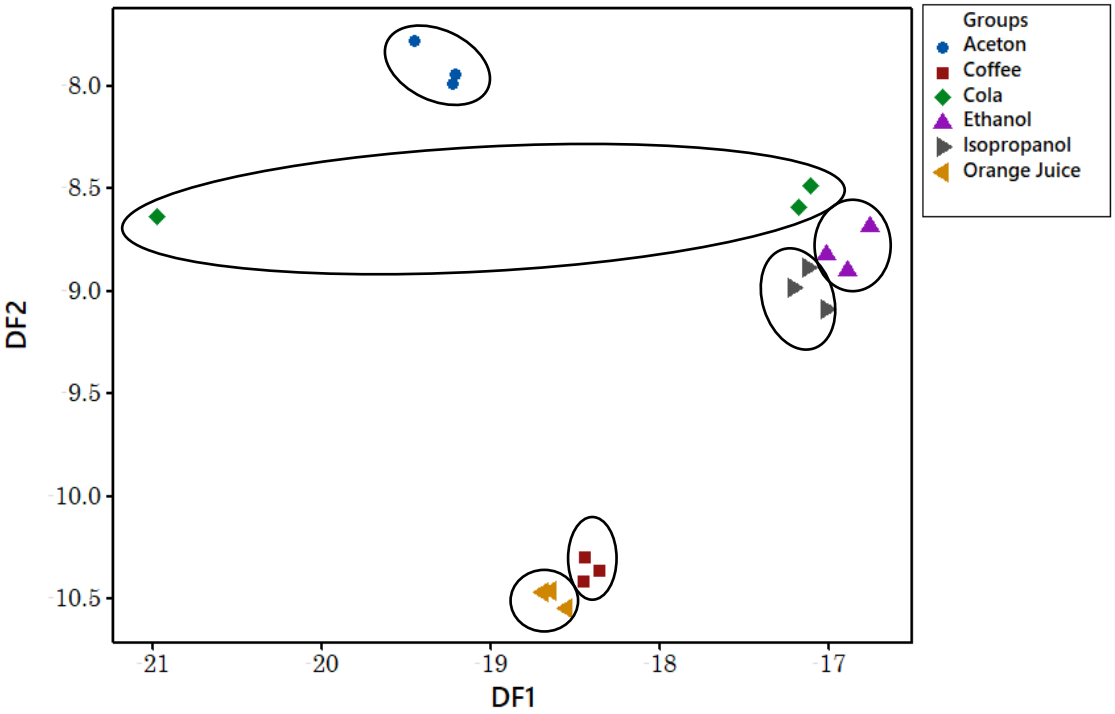

Fig. 7.10 LDA classification separating all 6 groups of Acetone, Isopropanol, Ethanol, Coffee, Cole and Orange juice

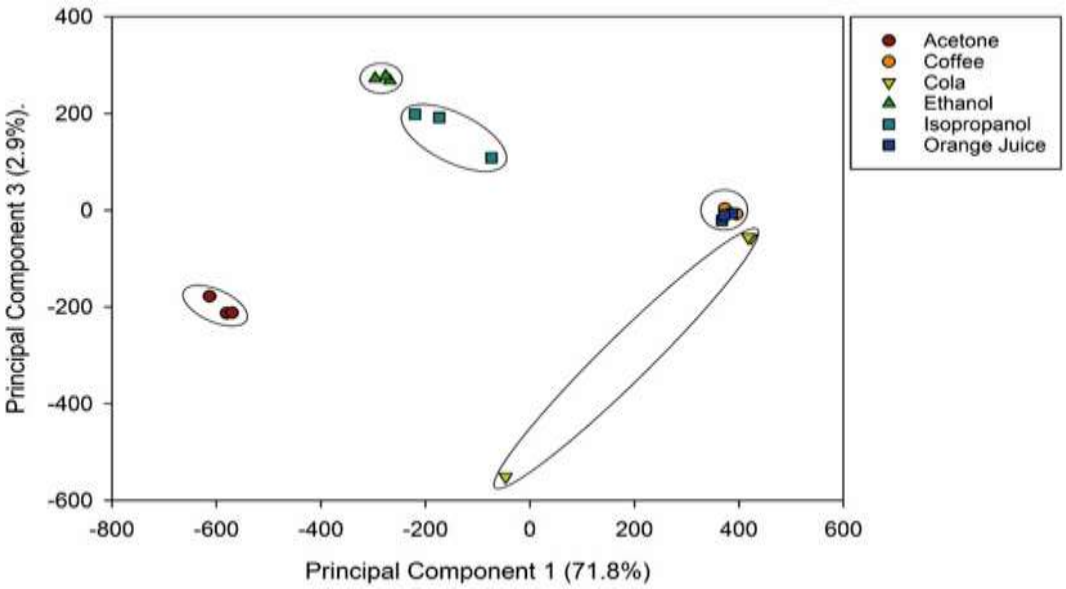

Fig. 7.11 PCA classification separating all 6 groups of Acetone, Isopropanol, Ethanol, Coffee, Cole and Orange juice

7.4 Testing Optical eNose with Urine Sample

After initial experiments were carried out to evaluate the response of the optical eNose instrument to a variety of gases and chemicals and the results showed the ability to reasonably distinguish between groups, testing was undertaken with this technology to a biomedical application.

The aim was to test optical eNose as a diagnostic tool with urine samples from target disease, type 2 diabetes, and control healthy ones. Normally 5 ml of urine sample is required for a VOC source in eNose technology, as it generates enough VOCs which is detectable with eNose. However, the received samples from the hospital only had 1.5 ml of urine from each group. According to previous experiences, 1.5 ml of urine is not a sufficient source of VOCs. Hence, it was decided to buy a synthetic urine sample and make artificial diabetic urines and use these to characterise the instrument.

According to literature review, patients with type 2 diabetes have glucose in their urine[230]. Also, breath studies showed that acetone is considered as a biomarker for diabetes[231]. Therefore, it was decided to simulate a diabetic patient's urine by first adding sugar to the synthetic urine sample and then acetone.

7.4.1 Methods and Materials

For diabetes samples, 3 gr of sugar was dissolved in 9 ml of synthetic urine and 3 mL of it (diabetes control) was aliquoted into a 20 mL glass vial. The glass vials were heated to 50 ± 0.1 °C for 15 minutes to increase the concentration of VOCs on headspace of sample. The headspace of the samples was taken using a 10 ml syringe. The headspace of samples was injected to the gas chambers. After running tests on artificial diabetic samples (with added sugar), 0.2ml of acetone was added to them and they were tested again. A static headspace analysis has been used in the experiment. After heating the samples for 15 minutes, the samples headspace has been extracted by 10 ml of syringe and it is injected to the system. The injection time was 5 seconds. After 20 second the pump starts working for cleaning purposes. The temperature of the chamber was 28 ±1°C during the experiment.

7.4.2 Results and Discussion

Fig. 7.12, shows the radar plot of the raw sensor responses at different wavelengths for different urine samples. Wavelengths were chosen based on the sugar, acetone absorption frequency and some evenly spaced to cover the other wavelengths.

Similar to previous experiments, maximum voltage drops of the sensor at predefined wavelength were extracted as features and after that two common multivariate methods were applied to data. Fig. 7.13 and Fig. 7.14 show the PCA and LDA classification of 3 different classes of urine samples, with sugar and acetone, sugar

and without sugar respectively. In PCA analysis, acetone shows the biggest variation among other groups and it is well separated from others. However, it doesn't show significant separation between a synthetic urine and sweet synthetic urine. LDA classification shows better separation compare to the PCA classification. Separation between all three groups improved over PCA.

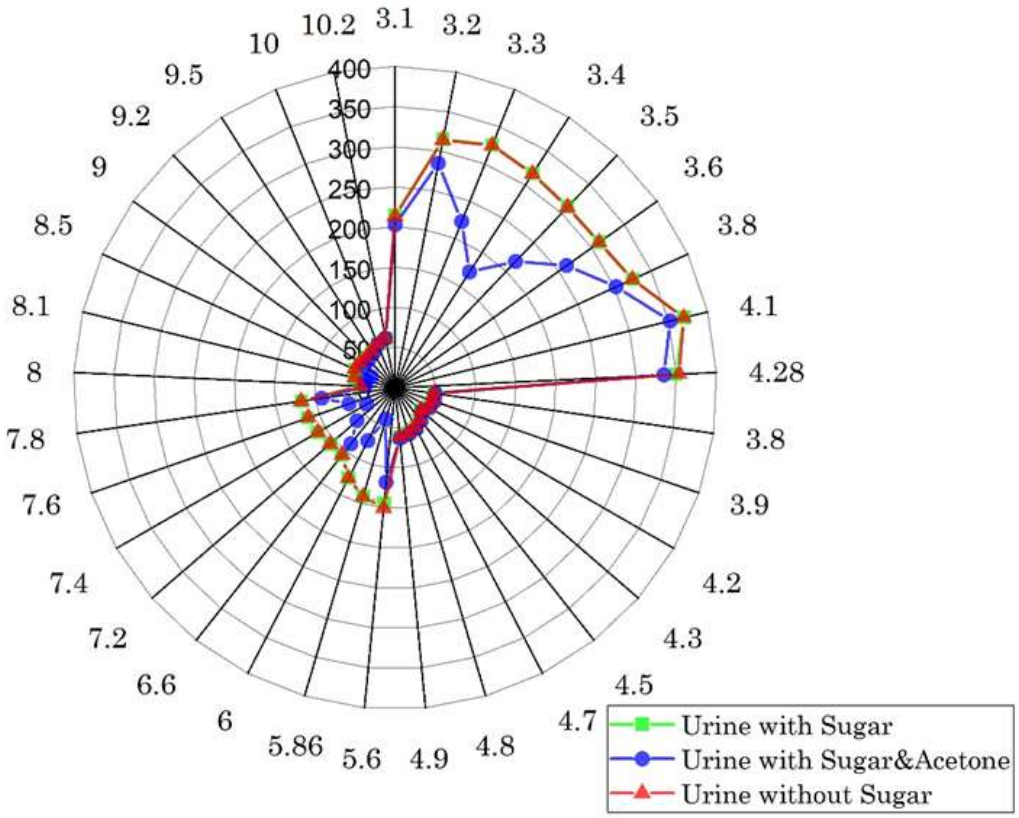

Fig. 7.12 Radar plot of the raw sensors responses at different wavelength for urine samples

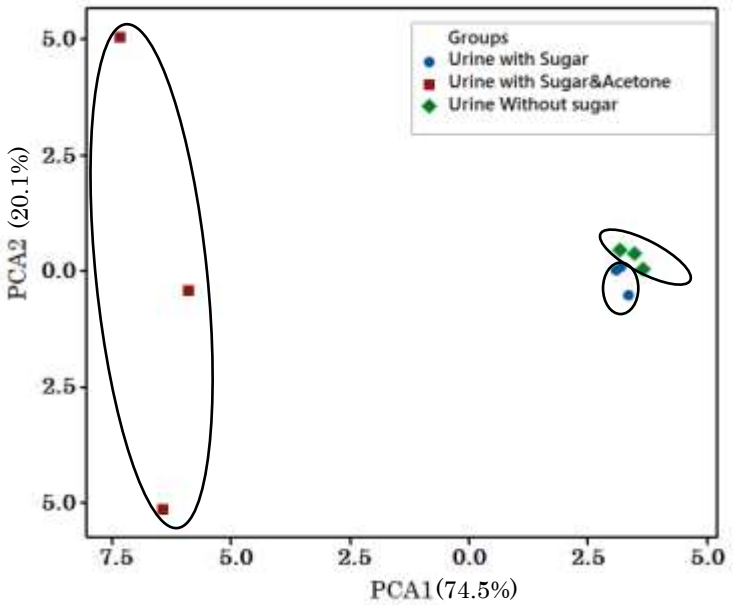

Fig. 7.13 PCA classification separating all 3 groups of urine

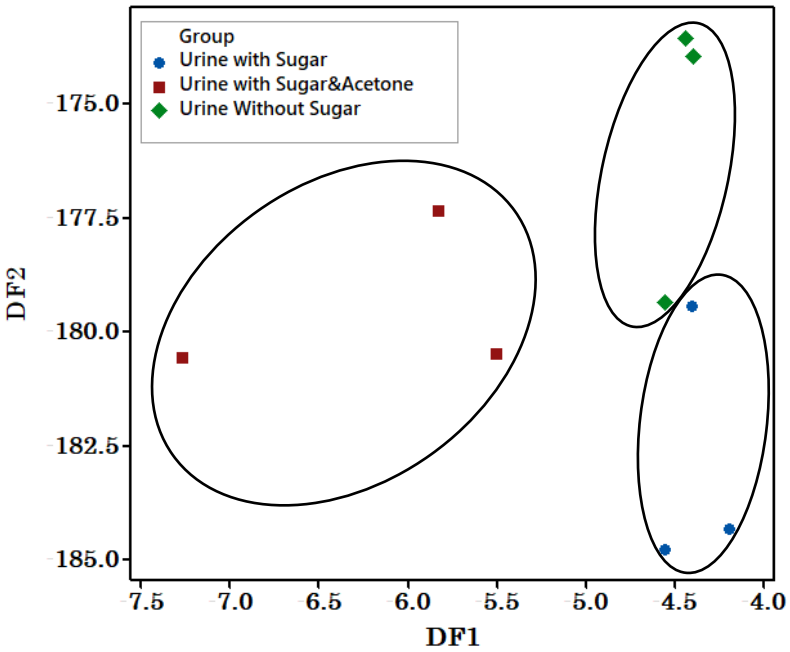

Fig. 7.14 LDA classification separating all 3 groups of urine

7.5 Conclusion

This chapter presented a feasibility study on using an optical based electronic nose based on an array of NDIR detectors as a diagnosing tool for classification of different samples. The initial results indicate that for methane the sensitivity is well below 1 ppm and this sensitivity can be achieved at more than one wavelength. Further testing showed that our system is able to separate more complex vapours and food groups, including acetone and ethanol. Many of the chemicals used here are known biomarkers for different diseases and optical based electronic nose may provide a simple, selective means to detect these chemicals. This study continued by using a synthetic urine and making artificial diabetic samples to be compared with non-diabetic samples. Chemicals that have been used to make artificial diabetic samples, are diabetic biomarkers. The optical eNose was able to distinguish between artificial diabetic and non-diabetic urine samples. The use of an optical tuned filter system has the potential to provide a high dimensional dataset about a sample that could aid in discriminating/identifying disease conditions.

Chapter

8 Conclusion and Further Work

8.1 Conclusions

The main aim of this project was to test if an electronic nose could be used as a point of care diagnostic tool for early stage diagnosis of diabetes and related gastro disorders, using urinary VOCs. The number of diabetic people who have been diagnosed in the UK is on the increase and currently stands at 3.5 million. This number increases further to over 4 million when considering those undiagnosed. Of more concern is the growing rate of diabetic people in the younger generation, who could live with this chronic disease for most of their live. In the UK, diabetes costs the NHS around £14 billion pounds per year, which is 10% of the total NHS budget. Since diabetes can lead to many other conditions, such a kidney disease and heart disease, it is important to diagnose it at an early stage where some form of intervention can be applied (such as life style changes), which reduces the risk of further complications.

The present diagnostic gold standard in diabetes and GI diseases have led to interest in using eNose technology as a clinical tool. eNose technology can be used to analyse gas phase biomarkers emanating from human waste, which makes it patient friendly, low cost per test and non-invasive. According to the literature, there are, and have been, a number of commercial and experimental eNose instruments that have shown promising results in discriminating a disease group from a healthy one, covering a wide range of diseases from cancers to dementia.

One VOCs source from the human body is urine. Urine is one end of the digestion system that directly related to the metabolic system. Chemicals in urine provide valuable information about the body's function. Hence, this study focused on urine as the sample of choice. Due to urine samples being collected and stored for batch testing, first it was important to characterise their stability in storage. The urinary headspace of 137 samples was tested with a commercial field asymmetric ion mobility spectrometry (Lonestar, Owlstone Ltd.), eNose instrument. It was found that as sample's age increased, their stability and the number of VOCs generated from them decreased. This study proposed that urine samples less than 9 months old do not show any significant loss in VOCs emitted from samples. However, the study revealed that samples over 9 months' age begin to experience a relatively rapid decrease in total VOCs.

The study was continued by exploring the discrimination of diabetic from healthy control samples using eNose technology by means of VOCs generated from urine sample. The commercial eNose instruments used in this study were Fox 4000 (Alpha

MOS Ltd.) containing 18 MOX sensors and field asymmetric ion mobility spectrometry (Lonestar from Owlstone Ltd.). To the best of the author's knowledge, this is the only comprehensive study (more than 100 samples) on the diagnosis of diabetes using urinary VOCs and eNose instruments. We were able to successfully discriminate diabetic subjects from healthy volunteers. Samples tested with FAIMS were all less than a year old and it was able to diagnose diabetes with a sensitivity of 100% and a specificity of 89% with a p-value of $9.438 * 10^{-11}$. Samples that were tested using the FOX 4000 instrument, were less than 18 months old and it was possible to separate diabetes and control samples with a sensitivity and a specificity of 98% and 100% respectively.

By reviewing the literature and understanding the weaknesses of the currently available eNose instruments, the idea of designing and developing a novel eNose instrument that could overcome these disadvantages was proposed. The aim was to develop a tuneable optical eNose instrument based on NDIR detectors, which covers a wide range of infrared wavelengths from 3.1 μm and 10.5 μm. This is the first and only eNose instrument that operates based on Fabry-Pérot Interferometer sensor technology with tuneable filter. This technology is based on physical reaction, where chemical molecules absorb certain IR frequencies. The optical eNose technology provides the opportunity to identify known and unknown substances. In addition, it can measure different substances with multi IR absorption frequencies. This means that the optical eNose overcomes the disadvantages of currently available eNose instrument, such as

cross sensitivity and selectivity in addition to removing the effect of humidity and temperature on the sensor array.

To find out the lowest sensitivity of the sensor array inside the eNose, an experimental gas test rig was developed and constructed. The gas test rig included three main parts: gas mixture, VOC generator and humidity generator. An additional gas analyser was developed and added to the system to operate as a test bench. By developing the test rig and a test bench with automated software in-house at the University of Warwick, it was possible to set the exact concentration of a specific gas and humidity that goes into the eNose sensory system. Moreover, by adding a gas analyser to the end of eNose, the user can make sure that the test environment required is delivered. As a result, it was made possible to measure the sensitivity and selectivity of the optical eNose.

At the end of this research project, an optical eNose was tested using single molecules, such as methane that has two absorption wavelengths between 3.1 μm and 10.5 μm, to test the ability of system to detect methane at two different wavelengths simultaneously and the achieved sensitivity was below 1ppm. After that, the eNose system was tested with single and complex chemicals. By using PCA as a statistical method, it was possible to classify 6 different single and complex chemicals. Later on, a synthetic urine was used for simulating the diabetic urine samples. Two diabetic biomarkers, specifically acetone and glucose were added to synthetic urine. PCA and LDA classification methods were used for classifying the groups. The optical eNose showed the satisfactory discrimination of over 95% sensitivity and specificity between

three groups of synthetic urine, synthetic urine with sugar and synthetic urine with acetone and sugar.

8.2 Suggestions for Future work

Suggestions for future work is divided into two main parts. The first part focuses on optical eNose technology and how it can be improved, and the second part addresses medical diagnostics and the further experimentation needed before clinical trials could start.

8.2.1 Optical eNose improvement

For most eNose systems, the sensor array plays the most important role, defined by its sensitivity and selectivity. This optical eNose cover wavelengths from 3.1 μm to 10.5 μm. Even though this is a wide range, in the future new sensors may become available to allow an even wider range of wavelengths to be investigated. Potentially, increasing the functionality of the instrument.

An automatic injection system could also be added to the system. This would help to inject the samples headspace with the same pressure and flow at a specific time. This increases the repeatability and reliability of the experiments.

The windows software for running the optical eNose could also be improved by adding some features such as: controlling emitters switching duty cycle and frequency and adding more check points in sending and receiving the commands from the sensors.

currently the pump and valve are not automatically switching on/off, this can be programmed to be automatic based on injection time.

The optical system could be designed in a way to transfer the data through Bluetooth to the computer system. This could be implemented in the second version of this device.

8.2.2 Medical Diagnosing Improvement

The reliability and evaluation of the optical eNose can be further investigated by testing a variety of single gases with known absorption spectrum. This would help to develop a library for this eNose system that shows the unique absorption spectrum value for each gas. The advantage of building a library is that eNose can detect the existence of an exact vapour when a complex chemical is being tested.

After testing the optical eNose with variety of different single gases, it should be tested with single chemicals. Since single chemicals have several absorption wavelengths (between 3.1 μm and 10.5 μm), they can help to demonstrate the detection capability of the optical eNose in different wavelength ranges. The same experiment can be performed by testing different concentrations of the tested single chemicals to discover the sensor's lowest sensitivity at different wavelengths.

To build up the library for different diseases, it is suggested to choose chemicals that are linked to certain disease biomarkers. For example, Isobutylamine, acetic acid and butyric acid can be used as urine biomarkers for diagnosing Anaerobic bacterial

infections. Isovaleric acid biomarkers can be used for metabolic disorders. Isovaleric acid, alkanes and specific complex mixtures of VOCs are the biomarkers used to detect urinary tract infection.

The developed optical eNose is designed in a way that makes it capable to diagnose diseases from other source of human wastes such as breath. Hence, biomarkers from other VOCs sources could be tested.

To bench mark this optical eNose as a diagnostic tool, more samples from different disease groups should be tested to discover the system's diagnosing capability and its weakness before any clinical trials could be started.

References

[1] K. Persaud and G. Dodd, "Analysis of discrimination mechanisms in the mammalian olfactory system using a model nose," *Nature,* vol. 299, no. 5881, p. 352, 1982.

[2] A. D. Wilson and M. Baietto, "Applications and advances in electronic-nose technologies," *Sensors,* vol. 9, no. 7, pp. 5099-5148, 2009.

[3] T. Aguilera, J. Lozano, J. A. Paredes, F. J. Alvarez, and J. I. Suárez, "Electronic nose based on independent component analysis combined with partial least squares and artificial neural networks for wine prediction," *Sensors,* vol. 12, no. 6, pp. 8055-8072, 2012.

[4] N. Davis. (2014). *Electronic noses explained: in future we will be sniffing out disease*. Available: https://www.theguardian.com/science/2014/apr/02/electronic-noses-explainer-sniffing-disease

[5] Sensigent. *Cyranose Electronic Nose*. Available: http://www.sensigent.com/index.html

[6] A. A. GmbH. (2014). *Portable Electronic Nose*. Available: https://airsense.com/en/products/portable-electronic-nose

[7] RoboScientificLtd. (2016). *Model 307 Analyser*. Available: http://www.roboscientific.com/307.html

[8] F. Adams. (1994). *Aphorisms By Hippocrates* Available: http://classics.mit.edu/Hippocrates/aphorisms.html

[9] G. Tsoucalas and M. Sgantzos, "Hippocrates, on the Infection of the Lower Respiratory Tract among the General Population in Ancient Greece," *Gen Med (Los Angeles),* vol. 4, no. 272, p. 2, 2016.

[10] A. D. Wilson and M. Baietto, "Advances in electronic-nose technologies developed for biomedical applications," *Sensors,* vol. 11, no. 1, pp. 1105-1176, 2011.

[11] D. L. García-González and R. Aparicio, "Sensors: From biosensors to the electronic nose," *Grasas y Aceites,* vol. 53, no. 1, pp. 96-114, 2002.

[12] A. Wilson, "Electronic-nose devices—Potential for noninvasive early disease-detection applications," *Ann Clin Case Rep. 2017; 2,* vol. 1401, 2017.

[13] N. Kahn, O. Lavie, M. Paz, Y. Segev, and H. Haick, "Dynamic nanoparticle-based flexible sensors: Diagnosis of ovarian carcinoma from exhaled breath," *Nano letters,* vol. 15, no. 10, pp. 7023-7028, 2015.

[14] D. UK, "Diabetes UK: key facts and stats," 2016, Available: https://diabetes-resources-production.s3-eu-west-1.amazonaws.com/diabetes-storage/migration/pdf/DiabetesUK_Facts_Stats_Oct16.pdf.

[15] D. UK. (2016). *Diabetes Prevalence 2016 (November 2016)*. Available: https://www.diabetes.org.uk/professionals/position-statements-reports/statistics/diabetes-prevalence-2016

[16] N. D. A. (NDA), "National Diabetes Audit Complications and Mortality 2015-2016," NHS Digital2017, Available: https://digital.nhs.uk/catalogue/PUB30030.

[17] N. Hex, C. Bartlett, D. Wright, M. Taylor, and D. Varley, "Estimating the current and future costs of Type 1 and Type 2 diabetes in the UK, including direct health costs and indirect societal and productivity costs," *Diabetic Medicine,* vol. 29, no. 7, pp. 855-862, 2012.

[18] A. Shakil, R. J. Church, and S. S. Rao, "Gastrointestinal complications of diabetes," *American family physician,* vol. 77, no. 12, 2008.

[19] B. Montgomery. (2018). *Diabetes and Gastrointestinal Issues*. Available: https://www.thediabetescouncil.com/diabetes-and-gastrointestinal-issues/

[20] J. D. Wolosin and S. V. Edelman, "Diabetes and the gastrointestinal tract," *Clinical diabetes,* vol. 18, no. 4, p. 148, 2000.

[21] T. N. I. o. D. a. D. a. K. Diseases. *Digestive Diseases*. Available: https://www.niddk.nih.gov/health-information/digestive-diseases

[22] E. Westenbrink *et al.*, "Development and application of a new electronic nose instrument for the detection of colorectal cancer," *Biosensors and Bioelectronics,* vol. 67, pp. 733-738, 2015.

[23] A. D. Wilson, "Recent Applications of Electronic-Nose Technologies for the Noninvasive Early Diagnosis of Gastrointestinal Diseases," in *Multidisciplinary Digital Publishing Institute Proceedings*, 2017, vol. 2, no. 3, p. 147.

[24] D. K. Chan, C. L. Leggett, and K. K. Wang, "Diagnosing gastrointestinal illnesses using fecal headspace volatile organic compounds," *World journal of gastroenterology,* vol. 22, no. 4, p. 1639, 2016.

[25] W. H. Herman *et al.*, "Early detection and treatment of type 2 diabetes reduce cardiovascular morbidity and mortality: a simulation of the results of the Anglo-Danish-Dutch Study of Intensive Treatment in People With Screen-Detected Diabetes in Primary Care (ADDITION-Europe)," *Diabetes care,* vol. 38, no. 8, pp. 1449-1455, 2015.

[26] M. E. Cox and D. Edelman, "Tests for screening and diagnosis of type 2 diabetes," *Clinical diabetes,* vol. 27, no. 4, pp. 132-138, 2009.

[27] NIDDK. (2014). *The A1C Test & Diabetes*. Available: https://www.niddk.nih.gov/health-information/diabetes/overview/tests-diagnosis/a1c-test

[28] D. U. charity. (2017). *Diagnostic criteria for diabetes*. Available: https://www.diabetes.org.uk/professionals/position-statements-reports/diagnosis-ongoing-management-monitoring/new_diagnostic_criteria_for_diabetes

[29] L. Capelli *et al.*, "Application and uses of electronic noses for clinical diagnosis on urine samples: A review," *Sensors,* vol. 16, no. 10, p. 1708, 2016.

[30] S. Bouatra *et al.*, "The human urine metabolome," *PloS one,* vol. 8, no. 9, p. e73076, 2013.

[31] K. Arshak, E. Moore, G. Lyons, J. Harris, and S. Clifford, "A review of gas sensors employed in electronic nose applications," *Sensor review,* vol. 24, no. 2, pp. 181-198, 2004.

[32] H. Shi, M. Zhang, and B. Adhikari, "Advances of electronic nose and its application in fresh foods: A review," *Critical Reviews in Food Science and Nutrition,* pp. 1-11, 2017.

[33] L. Jirovetz, G. Buchbauer, A. Stoyanova, A. Balinova, Z. Guangjiun, and M. Xihan, "Solid phase microextraction/gas chromatographic and olfactory analysis of the scent and fixative properties of the essential oil of Rosa damascena L. from China," *Flavour and fragrance journal,* vol. 20, no. 1, pp. 7-12, 2005.

[34] H. T. Nagle, R. Gutierrez-Osuna, and S. S. Schiffman, "The how and why of electronic noses," *IEEE spectrum,* vol. 35, no. 9, pp. 22-31, 1998.

[35] K. Persaud and G. Dodd, "Analysis of discrimination mechanisms in the mammalian olfactory system using a model nose," *Nature,* vol. 299, no. 5881, pp. 352-355, 1982.

[36] H.-G. Byun, K. C. Persaud, and A. M. Pisanelli, "Wound-state monitoring for burn patients using E-nose/SPME system," *ETRI Journal,* vol. 32, no. 3, pp. 440-446, 2010.

[37] V. Y. Musatov, V. Sysoev, M. Sommer, and I. Kiselev, "Assessment of meat freshness with metal oxide sensor microarray electronic nose: A practical approach," *Sensors and Actuators B: Chemical,* vol. 144, no. 1, pp. 99-103, 2010.

[38] T. Anderson *et al.*, "Advances in hydrogen, carbon dioxide, and hydrocarbon gas sensor technology using GaN and ZnO-based devices," *Sensors,* vol. 9, no. 6, pp. 4669-4694, 2009.

[39] Y.-C. Chang, H. Bai, S.-N. Li, and C.-N. Kuo, "Bromocresol green/mesoporous silica adsorbent for ammonia gas sensing via an optical sensing instrument," *Sensors,* vol. 11, no. 4, pp. 4060-4072, 2011.

[40] Y. Wang, M. M. Tong, D. Zhang, and Z. Gao, "Improving the performance of catalytic combustion type methane gas sensors using nanostructure elements doped with rare earth cocatalysts," *Sensors,* vol. 11, no. 1, pp. 19-31, 2010.

[41] M. Duval, "New techniques for dissolved gas-in-oil analysis," *IEEE Electrical Insulation Magazine,* vol. 19, no. 2, pp. 6-15, 2003.

[42] N. Tamaekong, C. Liewhiran, A. Wisitsoraat, and S. Phanichphant, "Flame-spray-made undoped zinc oxide films for gas sensing applications," *Sensors,* vol. 10, no. 8, pp. 7863-7873, 2010.

[43] C. Caucheteur, M. Debliquy, D. Lahem, and P. Mégret, "Catalytic fiber Bragg grating sensor for hydrogen leak detection in air," *IEEE Photonics Technology Letters,* vol. 20, no. 2, pp. 96-98, 2008.

[44] H.-E. Endres *et al.*, "A thin-film SnO2 sensor system for simultaneous detection of CO and NO2 with neural signal evaluation," *Sensors and Actuators B: Chemical,* vol. 36, no. 1-3, pp. 353-357, 1996.

[45] E. Billi, J.-P. Viricelle, L. Montanaro, and C. Pijolat, "Development of a protected gas sensor for exhaust automotive applications," *IEEE Sensors Journal,* vol. 2, no. 4, pp. 342-348, 2002.

[46] W. J. Fleming, "Overview of automotive sensors," *IEEE sensors journal,* vol. 1, no. 4, pp. 296-308, 2001.

[47] J. Vink, H. Verhoeven, and J. Huijsing, "Response Speed Optimization of Thermal Gas-Flow Sensors for Medical Application," in *Solid-State Sensors and Actuators, 1995 and Eurosensors IX.. Transducers' 95. The 8th International Conference on*, 1995, vol. 1, pp. 524-527: IEEE.

[48] R. P. Arasaradnam, J. A. Covington, and K. D. Bardhan, "Detecting inflammatory bowel disease through an electronic nose," *gastrointestinal nursing,* vol. 8, no. 9, 2010.

[49] E. Westenbrink *et al.*, "PWE-116 Detection of Colorectal Cancer from Urinary Volatile Organic Compounds Using a New Chromatograph/Electronic-Nose Instrument–Wolf System," ed: BMJ Publishing Group, 2016.

[50] S. Esfahani *et al.*, "A RAPID DISCRIMINATION OF DIABETIC PATIENTS FROM VOLUNTEERS USING URINARY VOLATILE AND AN ELECTRONIC NOSE."

[51] S. Scarlata, G. Pennazza, M. Santonico, C. Pedone, and R. Antonelli Incalzi, "Exhaled breath analysis by electronic nose in respiratory diseases," *Expert review of molecular diagnostics,* vol. 15, no. 7, pp. 933-956, 2015.

[52] G. Xiao *et al.*, "Trace amount formaldehyde gas detection for indoor air quality monitoring," in *Instrumentation and Measurement Technology Conference (I2MTC), 2011 IEEE*, 2011, pp. 1-4: IEEE.

[53] T. A. Emadi, C. Shafai, M. S. Freund, D. J. Thomson, D. S. Jayas, and N. D. White, "Development of a polymer-based gas sensor-humidity and CO 2

sensitivity," in *Microsystems and Nanoelectronics Research Conference, 2009. MNRC 2009. 2nd*, 2009, pp. 112-115: IEEE.

[54] D. Lazik, S. Ebert, M. Leuthold, J. Hagenau, and H. Geistlinger, "Membrane based measurement technology for in situ monitoring of gases in soil," *Sensors,* vol. 9, no. 2, pp. 756-767, 2009.

[55] G. F. Fine, L. M. Cavanagh, A. Afonja, and R. Binions, "Metal oxide semi-conductor gas sensors in environmental monitoring," *Sensors,* vol. 10, no. 6, pp. 5469-5502, 2010.

[56] S. M. Kanan, O. M. El-Kadri, I. A. Abu-Yousef, and M. C. Kanan, "Semiconducting metal oxide based sensors for selective gas pollutant detection," *Sensors,* vol. 9, no. 10, pp. 8158-8196, 2009.

[57] L. Capelli, L. Dentoni, S. Sironi, and R. Del Rosso, "The need for electronic noses for environmental odour exposure assessment," *Water Science and Technology,* vol. 69, no. 1, pp. 135-141, 2014.

[58] T. Dymerski, J. Gębicki, W. Wardencki, and J. Namieśnik, "Quality evaluation of agricultural distillates using an electronic nose," *Sensors,* vol. 13, no. 12, pp. 15954-15967, 2013.

[59] A. D. Wilson, "Diverse applications of electronic-nose technologies in agriculture and forestry," *Sensors,* vol. 13, no. 2, pp. 2295-2348, 2013.

[60] K. Brudzewski, S. Osowski, and W. Pawlowski, "Metal oxide sensor arrays for detection of explosives at sub-parts-per million concentration levels by the

differential electronic nose," *Sensors and Actuators B: Chemical,* vol. 161, no. 1, pp. 528-533, 2012.

[61] J. W. Gardner and P. N. Bartlett, "A brief history of electronic noses," *Sensors and Actuators B: Chemical,* vol. 18, no. 1-3, pp. 210-211, 1994.

[62] K. C. Persaud, S. M. Khaffaf, J. S. Payne, A. M. Pisanelli, D.-H. Lee, and H.-G. Byun, "Sensor array techniques for mimicking the mammalian olfactory system," *Sensors and Actuators B: Chemical,* vol. 36, no. 1-3, pp. 267-273, 1996.

[63] F. A. Davide, C. Di Natale, and A. D'Amico, "Self-organising sensory maps in odour classification mimicking," *Biosensors and Bioelectronics,* vol. 10, no. 1, pp. 203-218, 1995.

[64] P. Pelosi and K. Persaud, "Gas sensors: towards an artificial nose," in *Sensors and sensory systems for advanced robots*: Springer, 1988, pp. 361-381.

[65] K. C. Persaud, "Electronic gas and odour detectors that mimic chemoreception in animals," *TRAC Trends in Analytical Chemistry,* vol. 11, no. 2, pp. 61-67, 1992.

[66] J. W. Gardner, "Detection of vapours and odours from a multisensor array using pattern recognition Part 1. Principal component and cluster analysis," *Sensors and Actuators B: Chemical,* vol. 4, no. 1-2, pp. 109-115, 1991.

[67] A. Berna, "Metal oxide sensors for electronic noses and their application to food analysis," *Sensors,* vol. 10, no. 4, pp. 3882-3910, 2010.

[68] B. Kowalski and C. Bender, "Pattern recognition. Powerful approach to interpreting chemical data," *Journal of the American Chemical Society,* vol. 94, no. 16, pp. 5632-5639, 1972.

[69] T. C. Pearce, S. S. Schiffman, H. T. Nagle, and J. W. Gardner, *Handbook of machine olfaction: electronic nose technology*. John Wiley & Sons, 2006.

[70] S. M. Scott, D. James, and Z. Ali, "Data analysis for electronic nose systems," *Microchimica Acta,* vol. 156, no. 3-4, pp. 183-207, 2006.

[71] S. Capone, P. Siciliano, F. Quaranta, R. Rella, M. Epifani, and L. Vasanelli, "Analysis of vapours and foods by means of an electronic nose based on a sol–gel metal oxide sensors array," *Sensors and Actuators B: Chemical,* vol. 69, no. 3, pp. 230-235, 2000.

[72] S. E. Zohora, A. Khan, A. Srivastava, and N. Hundewale, "Electronic noses application to food analysis using metal oxide sensors: a review," *International Journal of Soft Computing and Engineering,* vol. 3, pp. 199-205, 2013.

[73] M. Egashira and Y. Shimizu, "Odor sensing by semiconductor metal oxides," *Sensors and Actuators B: Chemical,* vol. 13, no. 1-3, pp. 443-446, 1993.

[74] H. Shurmer, J. Gardner, and H. Chan, "The application of discrimination technique to alcohols and tobaccos using tin-oxide sensors," *Sensors and Actuators,* vol. 18, no. 3-4, pp. 361-371, 1989.

[75] J. W. Gardner and P. N. Bartlett, *Electronic noses: principles and applications*. Oxford University Press, USA, 1999.

[76] H.-S. Yim *et al.*, "Polymer membrane-based ion-, gas-and bio-selective potentiometric sensors," *Biosensors and Bioelectronics,* vol. 8, no. 1, pp. 1-38, 1993.

[77] A. Pisanelli, A. Qutob, P. Travers, S. Szyszko, and K. Persaud, "Applications of multi-array polymer sensors to food industries," *Life Chemistry Reports,* vol. 11, pp. 303-308, 1994.

[78] P. Verma and R. Yadava, "Polymer selection for SAW sensor array based electronic noses by fuzzy c-means clustering of partition coefficients: Model studies on detection of freshness and spoilage of milk and fish," *Sensors and Actuators B: Chemical,* vol. 209, pp. 751-769, 2015.

[79] E. J. Staples, "Electronic nose simulation of olfactory response containing 500 orthogonal sensors in 10 seconds," in *Ultrasonics Symposium, 1999. Proceedings. 1999 IEEE*, 1999, vol. 1, pp. 417-423: IEEE.

[80] Z. Zhao, F. Tian, H. Liao, X. Yin, Y. Liu, and B. Yu, "A novel spectrum analysis technique for odor sensing in optical electronic nose," *Sensors and Actuators B: Chemical,* vol. 222, pp. 769-779, 2016.

[81] G. Harsányi, "Polymer films in sensor applications: a review of present uses and future possibilities," *Sensor Review,* vol. 20, no. 2, pp. 98-105, 2000.

[82] H. V. Shurmer and J. W. Gardner, "Odour discrimination with an electronic nose," *Sensors and Actuators B: Chemical,* vol. 8, no. 1, pp. 1-11, 1992.

[83] S. M. van Ruth, "Evaluation of two gas chromatography–olfactometry methods: The detection frequency and perceived intensity method," *Journal of Chromatography A,* vol. 1054, no. 1, pp. 33-37, 2004.

[84] X. Liu, S. Cheng, H. Liu, S. Hu, D. Zhang, and H. Ning, "A survey on gas sensing technology," *Sensors,* vol. 12, no. 7, pp. 9635-9665, 2012.

[85] O. S. Papadopoulou, E. Z. Panagou, F. R. Mohareb, and G.-J. E. Nychas, "Sensory and microbiological quality assessment of beef fillets using a portable electronic nose in tandem with support vector machine analysis," *Food Research International,* vol. 50, no. 1, pp. 241-249, 2013.

[86] Y. G. Martın, M. C. C. Oliveros, J. L. P. Pavón, C. G. Pinto, and B. M. Cordero, "Electronic nose based on metal oxide semiconductor sensors and pattern recognition techniques: characterisation of vegetable oils," *Analytica Chimica Acta,* vol. 449, no. 1-2, pp. 69-80, 2001.

[87] W. Göpel and K. D. Schierbaum, "SnO2 sensors: current status and future prospects," *Sensors and Actuators B: Chemical,* vol. 26, no. 1-3, pp. 1-12, 1995.

[88] C. Wang, L. Yin, L. Zhang, D. Xiang, and R. Gao, "Metal oxide gas sensors: sensitivity and influencing factors," *Sensors,* vol. 10, no. 3, pp. 2088-2106, 2010.

[89] E. Kanazawa *et al.*, "Metal oxide semiconductor N 2 O sensor for medical use," *Sensors and Actuators B: Chemical,* vol. 77, no. 1, pp. 72-77, 2001.

[90] G. Korotcenkov, "Metal oxides for solid-state gas sensors: What determines our choice?," *Materials Science and Engineering: B,* vol. 139, no. 1, pp. 1-23, 2007.

[91] L. Fraiwan, K. Lweesy, A. Bani-Salma, and N. Mani, "A wireless home safety gas leakage detection system," in *Biomedical Engineering (MECBME), 2011 1st Middle East Conference on*, 2011, pp. 11-14: IEEE.

[92] F. E. Inc. *MOS type Operating principle*. Available: http://www.figaro.co.jp/en/technicalinfo/principle/mos-type.html

[93] H. Steffes, C. Imawan, F. Solzbacher, and E. Obermeier, "Enhancement of NO 2 sensing properties of In 2 O 3-based thin films using an Au or Ti surface modification," *Sensors and Actuators B: Chemical,* vol. 78, no. 1, pp. 106-112, 2001.

[94] M. Batzill and U. Diebold, "The surface and materials science of tin oxide," *Progress in surface science,* vol. 79, no. 2, pp. 47-154, 2005.

[95] B. J. Doleman, M. C. Lonergan, E. J. Severin, T. P. Vaid, and N. S. Lewis, "Quantitative study of the resolving power of arrays of carbon black− polymer composites in various vapor-sensing tasks," *Analytical Chemistry,* vol. 70, no. 19, pp. 4177-4190, 1998.

[96] K. J. Albert *et al.*, "Cross-reactive chemical sensor arrays," *Chemical reviews,* vol. 100, no. 7, pp. 2595-2626, 2000.

[97] D. Strike, M. Meijerink, and M. Koudelka-Hep, "Electronic noses–A mini-review," *Fresenius' journal of analytical chemistry,* vol. 364, no. 6, pp. 499-505, 1999.

[98] M. S. Freund and N. S. Lewis, "A chemically diverse conducting polymer-based" electronic nose"," *Proceedings of the National Academy of Sciences,* vol. 92, no. 7, pp. 2652-2656, 1995.

[99] J. M. Slater, J. Paynter, and E. Watt, "Multi-layer conducting polymer gas sensor arrays for olfactory sensing," *Analyst,* vol. 118, no. 4, pp. 379-384, 1993.

[100] P. N. Bartlett, P. B. Archer, and S. K. Ling-Chung, "Conducting polymer gas sensors part I: fabrication and characterization," *Sensors and Actuators,* vol. 19, no. 2, pp. 125-140, 1989.

[101] T. C. Pearce, J. W. Gardner, S. Friel, P. N. Bartlett, and N. Blair, "Electronic nose for monitoring the flavour of beers," *Analyst,* vol. 118, no. 4, pp. 371-377, 1993.

[102] T. Gibson *et al.*, "Detection and simultaneous identification of microorganisms from headspace samples using an electronic nose," *Sensors and Actuators B: Chemical,* vol. 44, no. 1, pp. 413-422, 1997.

[103] C. Ridgway, J. Chambers, E. Portero-Larragueta, and O. Prosser, "Detection of mite infestation in wheat by electronic nose with transient flow sampling," *Journal of the Science of Food and Agriculture,* vol. 79, no. 15, pp. 2067-2074, 1999.

[104] R. Dutta, E. L. Hines, J. W. Gardner, and P. Boilot, "Bacteria classification using Cyranose 320 electronic nose," *Biomedical engineering online,* vol. 1, no. 1, p. 4, 2002.

[105] D. Luo, H. G. Hosseini, and J. R. Stewart, "Application of ANN with extracted parameters from an electronic nose in cigarette brand identification," *Sensors and Actuators B: Chemical,* vol. 99, no. 2, pp. 253-257, 2004.

[106] D. Hodgins, "The development of an electronic 'nose'for industrial and environmental applications," *Sensors and Actuators B: Chemical,* vol. 27, no. 1-3, pp. 255-258, 1995.

[107] A. Partridge, P. Harris, and M. Andrews, "High sensitivity conducting polymer sensors," *Analyst,* vol. 121, no. 9, pp. 1349-1353, 1996.

[108] P. Si, J. Mortensen, A. Komolov, J. Denborg, and P. J. Møller, "Polymer coated quartz crystal microbalance sensors for detection of volatile organic compounds in gas mixtures," *Analytica chimica acta,* vol. 597, no. 2, pp. 223-230, 2007.

[109] A. Bougharouat, A. Bellel, S. Sahli, Y. Segui, and P. Raynaud, "Polymer coated quartz crystal microbalance sensors for the detection of volatile organic compounds," *Journal of New Technology and Materials,* vol. 3, no. 1, pp. 8-11, 2013.

[110] M. Abbas, G. Moustafa, J. Mitrovics, and W. Gopel, "Multicomponent gas analysis of a mixture of chloroform, octane and toluene using a piezoelectric quartz crystal sensor array," *Analytica chimica acta,* vol. 393, no. 1, pp. 67-76, 1999.

[111] T. C. Office. *A Surface Acoustic Wave (SAW)-Based Sensor for VLSI Circuits*. Available: http://technologies.research.gwu.edu/technologies/06-00x-zaghloul_a-surface-acoustic-wave-saw-based-sensor-for-vlsi-circuits

[112] S. S. Schiffman and T. C. Pearce, "Introduction to olfaction: perception, anatomy, physiology, and molecular biology," *Handbook of Machine Olfaction: Electronic Nose Technology,* pp. 1-31, 2003.

[113] N. Barié, M. Bücking, and M. Rapp, "A novel electronic nose based on miniaturized SAW sensor arrays coupled with SPME enhanced headspace-analysis and its use for rapid determination of volatile organic compounds in food quality monitoring," *Sensors and Actuators B: Chemical,* vol. 114, no. 1, pp. 482-488, 2006.

[114] X. Chen *et al.*, "A study of an electronic nose for detection of lung cancer based on a virtual SAW gas sensors array and imaging recognition method," *Measurement Science and Technology,* vol. 16, no. 8, p. 1535, 2005.

[115] A. Marina, Y. C. Man, and I. Amin, "Use of the SAW sensor electronic nose for detecting the adulteration of virgin coconut oil with RBD palm kernel olein," *Journal of the American Oil Chemists' Society,* vol. 87, no. 3, pp. 263-270, 2010.

[116] E. Bakker and M. Telting-Diaz, "Electrochemical sensors," *Analytical chemistry,* vol. 74, no. 12, pp. 2781-2800, 2002.

[117] I. Custom Sensor Solutions. (2009). *Why Do Some Electrochemical Gas Sensors Have Two Electrodes, and Some Have Three?* Available: http://www.customsensorsolutions.com/ap-TwoAndThreeElectrode.html

[118] H. Kiesele and M. Wittich, "Electrochemical gas sensors for use under extreme climatic conditions," *Dräger Rev,* vol. 85, pp. 10-13, 2000.

[119] B. Szulczyński and J. Gębicki, "Currently Commercially Available Chemical Sensors Employed for Detection of Volatile Organic Compounds in Outdoor and Indoor Air," *Environments,* vol. 4, no. 1, p. 21, 2017.

[120] D. L. S. Rothman. (09/12/2017). *The HITRAN Database*. Available: https://www.cfa.harvard.edu/hitran/

[121] D. Calloway, "Beer-lambert law," *J. Chem. Educ,* vol. 74, no. 7, p. 744, 1997.

[122] Z. Haiming, "Experiment study of continuous emission monitoring system based on differential optical absorption spectroscopy," in *Education Technology and Training, 2008. and 2008 International Workshop on Geoscience and Remote Sensing. ETT and GRS 2008. International Workshop on*, 2008, vol. 1, pp. 175-177: IEEE.

[123] C. Charlton, B. Temelkuran, G. Dellemann, and B. Mizaikoff, "Midinfrared sensors meet nanotechnology: Trace gas sensing with quantum cascade lasers inside photonic band-gap hollow waveguides," *Applied Physics Letters,* vol. 86, no. 19, p. 194102, 2005.

[124] H. Miya *et al.*, "Compact Raman Lidar for hydrogen gas leak detection," in *Conference on Lasers and Electro-Optics/Pacific Rim*, 2009, p. ME1_3: Optical Society of America.

[125] T. F. Refaat *et al.*, "Backscatter 2-$\mu\hbox {m} $ Lidar Validation for Atmospheric $\hbox {CO} _ {2} $ Differential Absorption Lidar Applications," *IEEE Transactions on Geoscience and Remote Sensing,* vol. 49, no. 1, pp. 572-580, 2011.

[126] K. Liu *et al.*, "Investigation of wavelength modulation and wavelength sweep techniques in intracavity fiber laser for gas detection," *Journal of Lightwave Technology,* vol. 29, no. 1, pp. 15-21, 2011.

[127] M. Vainio and L. Halonen, "Mid-infrared optical parametric oscillators and frequency combs for molecular spectroscopy," *Physical Chemistry Chemical Physics,* vol. 18, no. 6, pp. 4266-4294, 2016.

[128] W. Baetz, A. Kroll, and G. Bonow, "Mobile robots with active IR-optical sensing for remote gas detection and source localization," in *Robotics and Automation, 2009. ICRA'09. IEEE International Conference on*, 2009, pp. 2773-2778: IEEE.

[129] J. Kwon, G. Ahn, G. Kim, J. C. Kim, and H. Kim, "A study on NDIR-based CO2 sensor to apply remote air quality monitoring system," in *ICCAS-SICE, 2009*, 2009, pp. 1683-1687: IEEE.

[130] A. Mills, A. Lepre, and L. Wild, "Breath-by-breath measurement of carbon dioxide using a plastic film optical sensor," *Sensors and Actuators B: Chemical,* vol. 39, no. 1, pp. 419-425, 1997.

[131] A. De Luca, S. Z. Ali, R. Hopper, S. Boual, J. W. Gardner, and F. Udrea, "Filterless non-dispersive infra-red gas detection: A proof of concept," in *Micro Electro Mechanical Systems (MEMS), 2017 IEEE 30th International Conference on*, 2017, pp. 1220-1223: IEEE.

[132] W. Ma *et al.*, "CO $ _ {2} $ Gas Sensing Using Optical Fiber Fabry–Perot Interferometer Based on Polyethyleneimine/Poly (Vinyl Alcohol) Coating," *IEEE Photonics Journal,* vol. 9, no. 3, pp. 1-8, 2017.

[133] J. Covington, M. v. der Schee, A. Edge, B. Boyle, R. Savage, and R. Arasaradnam, "The application of FAIMS gas analysis in medical diagnostics," *Analyst,* vol. 140, no. 20, pp. 6775-6781, 2015.

[134] OWLSTONE. (2014). *A Comparison of the 3 Main Forms of Ion Mobility Spectrometry*. Available: https://www.owlstonemedical.com/media/uploads/files/UMC0044-At-A-Glance-Guide-Main-Forms-IMS.pdf

[135] O. MEDICAL. (2017). *Why is ultraFAIMS orthogonal to other forms of IMS and MS?* Available: https://www.owlstonemedical.com/about/blog/2017/apr/3/why-ultrafaims-orthogonal/

[136] I. Buryakov, E. Krylov, A. Makas, E. Nazarov, V. Pervukhin, and U. Rasulev, "Ion division by their mobility in high tension alternating electric-field," *Pisma V Zhurnal Tekhnicheskoi Fiziki,* vol. 17, no. 12, pp. 60-65, 1991.

[137] R. Guevremont, "High-field asymmetric waveform ion mobility spectrometry: a new tool for mass spectrometry," *Journal of Chromatography A,* vol. 1058, no. 1, pp. 3-19, 2004.

[138] D. Guo, Y. Wang, L. Li, X. Wang, and J. Luo, "Precise determination of nonlinear function of ion mobility for explosives and drugs at high electric fields for microchip FAIMS," *Journal of Mass Spectrometry,* vol. 50, no. 1, pp. 198-205, 2015.

[139] Q. Wang, Y.-F. Xie, W.-J. Zhao, P. Li, H. Qian, and X.-Z. Wang, "Rapid microchip-based FAIMS determination of trimethylamine, an indicator of pork deterioration," *Analytical Methods,* vol. 6, no. 9, pp. 2965-2972, 2014.

[140] Y.-Q. Xia, S. T. Wu, and M. Jemal, "LC-FAIMS-MS/MS for quantification of a peptide in plasma and evaluation of FAIMS global selectivity from plasma components," *Analytical chemistry,* vol. 80, no. 18, pp. 7137-7143, 2008.

[141] G. R. Lambertus *et al.*, "Silicon microfabricated column with microfabricated differential mobility spectrometer for GC analysis of volatile organic compounds," *Analytical Chemistry,* vol. 77, no. 23, pp. 7563-7571, 2005.

[142] A. Wilks, M. Hart, A. Koehl, J. Somerville, B. Boyle, and D. Ruiz-Alonso, "Characterization of a miniature, ultra-high-field, ion mobility spectrometer," *International Journal for Ion Mobility Spectrometry,* vol. 15, no. 3, pp. 199-222, 2012.

[143] W. Gabryelski, F. Wu, and K. L. Froese, "Comparison of high-field asymmetric waveform ion mobility spectrometry with GC methods in analysis of haloacetic acids in drinking water," *Analytical chemistry,* vol. 75, no. 10, pp. 2478-2486, 2003.

[144] E. Krylov, "Comparison of the planar and coaxial field asymmetrical waveform ion mobility spectrometer (FAIMS)," *International Journal of Mass Spectrometry,* vol. 225, no. 1, pp. 39-51, 2003.

[145] A. M. Helmenstine. (2017, 14/12/2017). *Gas Chromatography - What It Is and How It Works*. Available: https://www.thoughtco.com/gas-chromatography-4138098

[146] BBC. (2014, 15/12/2017). *Gas chromatography*. Available: http://www.bbc.co.uk/schools/gcsebitesize/science/triple_ocr_21c/further_chemistry/chromatography/revision/5/

[147] (April 2016). *Gas Chromatography Theory*. Available: http://www.chem.ucla.edu/~bacher/General/30BL/gc/theory.html

[148] I. D. Ltd. (2017). *IMSPEX DIAGNOSTICS Ltd*. Available: http://imspex.com/products/

[149] O. M. Ltd. (2017). *Owlstone Medical*. Available: https://www.owlstonemedical.com/products/

[150] H. J. G. E. Vanneste, "Advanced Instrumentation: Commercial Electronic Nose Instruments," in *Handbook of Machine Olfaction: Electronic Nose Technology*, S. S. S. T.C. Pearce, H.T. Nagle, J.W. Gardner, Ed., 2003.

[151] F. Röck, N. Barsan, and U. Weimar, "Electronic nose: current status and future trends," *Chemical reviews,* vol. 108, no. 2, pp. 705-725, 2008.

[152] M. Shirasu and K. Touhara, "The scent of disease: volatile organic compounds of the human body related to disease and disorder," *The Journal of Biochemistry,* vol. 150, no. 3, pp. 257-266, 2011.

[153] F. Adams, "Hippocratic writings: Aphorisms IV, V," *The Internet Classic Archive,* pp. 1-10, 1994.

[154] R. Porter, "The early years," ed: Harper Collins: London, UK, 1977, pp. 147-162.

[155] A. Manolis, "The diagnostic potential of breath analysis," *Clinical chemistry,* vol. 29, no. 1, pp. 5-15, 1983.

[156] M. Phillips, "Method for the collection and assay of volatile organic compounds in breath," *Analytical biochemistry,* vol. 247, no. 2, pp. 272-278, 1997.

[157] S. Chandiok, B. Crawley, B. Oppenheim, P. Chadwick, S. Higgins, and K. Persaud, "Screening for bacterial vaginosis: a novel application of artificial nose technology," *Journal of clinical pathology,* vol. 50, no. 9, pp. 790-791, 1997.

[158] R. Dutta, D. Morgan, N. Baker, J. W. Gardner, and E. L. Hines, "Identification of Staphylococcus aureus infections in hospital environment: electronic nose based approach," *Sensors and Actuators B: Chemical,* vol. 109, no. 2, pp. 355-362, 2005.

[159] J. Gardner, M. Craven, C. Dow, and E. Hines, "The prediction of bacteria type and culture growth phase by an electronic nose with a multi-layer perceptron network," *Measurement Science and Technology,* vol. 9, no. 1, p. 120, 1998.

[160] R. Fend, A. H. Kolk, C. Bessant, P. Buijtels, P. R. Klatser, and A. C. Woodman, "Prospects for clinical application of electronic-nose technology to early detection of Mycobacterium tuberculosis in culture and sputum," *Journal of Clinical Microbiology,* vol. 44, no. 6, pp. 2039-2045, 2006.

[161] A. K. Pavlou *et al.*, "Use of an electronic nose system for diagnoses of urinary tract infections," *Biosensors and Bioelectronics,* vol. 17, no. 10, pp. 893-899, 2002.

[162] C. W. Hanson and E. R. Thaler, "Electronic nose prediction of a clinical pneumonia score: biosensors and microbes," *Anesthesiology: The Journal of the American Society of Anesthesiologists,* vol. 102, no. 1, pp. 63-68, 2005.

[163] R. F. Machado *et al.*, "Detection of lung cancer by sensor array analyses of exhaled breath," *American journal of respiratory and critical care medicine,* vol. 171, no. 11, pp. 1286-1291, 2005.

[164] J. W. Yates *et al.*, "Data reduction in headspace analysis of blood and urine samples for robust bacterial identification," *Computer methods and programs in biomedicine,* vol. 79, no. 3, pp. 259-271, 2005.

[165] A. Voss *et al.*, "Smelling renal dysfunction via electronic nose," *Annals of biomedical engineering,* vol. 33, no. 5, pp. 656-660, 2005.

[166] J. W. Gardner, H. W. Shin, and E. L. Hines, "An electronic nose system to diagnose illness," *Sensors and Actuators B: Chemical,* vol. 70, no. 1, pp. 19-24, 2000.

[167] R. P. Arasaradnam *et al.*, "Detection of colorectal cancer (CRC) by urinary volatile organic compound analysis," *PLoS One,* vol. 9, no. 9, p. e108750, 2014.

[168] R. P. Arasaradnam *et al.*, "A novel tool for noninvasive diagnosis and tracking of patients with inflammatory bowel disease," *Inflammatory bowel diseases,* vol. 19, no. 5, pp. 999-1003, 2013.

[169] J. A. Covington *et al.*, "The detection of patients at risk of gastrointestinal toxicity during pelvic radiotherapy by electronic nose and FAIMS: a pilot study," *Sensors,* vol. 12, no. 10, pp. 13002-13018, 2012.

[170] A. Zlatkis, R. S. Brazell, and C. F. Poole, "The role of organic volatile profiles in clinical diagnosis," *Clinical Chemistry,* vol. 27, no. 6, pp. 789-797, 1981.

[171] G. A. Mills and V. Walker, "Headspace solid-phase microextraction profiling of volatile compounds in urine: application to metabolic investigations," *Journal of Chromatography B: Biomedical Sciences and Applications,* vol. 753, no. 2, pp. 259-268, 2001.

[172] D. Samudrala *et al.*, "Changes in urine headspace composition as an effect of strenuous walking," *Metabolomics,* vol. 11, no. 6, pp. 1656-1666, 2015.

[173] B. de Lacy Costello, N. M. Ratcliffe, A. Amann, and D. Smith, "Volatile organic compounds (VOCs) found in urine and stool," *Volatile biomarkers: non-invasive diagnosis in physiology and medicine 1st edn. Amann A, Smith D, Editors Amsterdam: Elsevier,* pp. 405-62, 2013.

[174] C. M. Willis *et al.*, "Olfactory detection of human bladder cancer by dogs: proof of principle study," *Bmj,* vol. 329, no. 7468, p. 712, 2004.

[175] J.-N. Cornu, G. Cancel-Tassin, V. Ondet, C. Girardet, and O. Cussenot, "Olfactory detection of prostate cancer by dogs sniffing urine: a step forward in early diagnosis," *European urology,* vol. 59, no. 2, pp. 197-201, 2011.

[176] G. Taverna *et al.*, "Olfactory system of highly trained dogs detects prostate cancer in urine samples," *The Journal of urology,* vol. 193, no. 4, pp. 1382-1387, 2015.

[177] A. Pavlou and A. Turner, "Sniffing out the truth: clinical diagnosis using the electronic nose," *Clinical chemistry and laboratory medicine,* vol. 38, no. 2, pp. 99-112, 2000.

[178] K. Liddell, "Smell as a diagnostic marker," *Postgraduate medical journal,* vol. 52, no. 605, pp. 136-138, 1976.

[179] K. Tanaka, J. Orr, and K. Isselbacher, "Identification of β-hydroxyisovaleric acid in the urine of a patient with isovaleric acidemia," *Biochimica et Biophysica Acta (BBA)-Lipids and Lipid Metabolism,* vol. 152, no. 3, pp. 638-641, 1968.

[180] A. P. Turner and N. Magan, "Electronic noses and disease diagnostics," *Nature Reviews Microbiology,* vol. 2, no. 2, pp. 161-166, 2004.

[181] A. K. Pavlou, N. Magan, D. Sharp, J. Brown, H. Barr, and A. P. F. Turner, "An intelligent rapid odour recognition model in discrimination of Helicobacter pylori and other gastroesophageal isolates in vitro," *Biosensors and Bioelectronics,* vol. 15, no. 7, pp. 333-342, 2000.

[182] S. Aathithan, J. Plant, A. Chaudry, and G. French, "Diagnosis of bacteriuria by detection of volatile organic compounds in urine using an automated headspace analyzer with multiple conducting polymer sensors," *Journal of clinical microbiology,* vol. 39, no. 7, pp. 2590-2593, 2001.

[183] C. Di Natale, A. Mantini, A. Macagnano, D. Antuzzi, R. Paolesse, and A. D'Amico, "Electronic nose analysis of urine samples containing blood," *Physiological Measurement,* vol. 20, no. 4, p. 377, 1999.

[184] N. Guernion, N. M. Ratcliffe, P. T. Spencer-Phillips, and R. A. Howe, "Identifying bacteria in human urine: current practice and the potential for rapid, near-patient diagnosis by sensing volatile organic compounds," *Clinical chemistry and laboratory medicine,* vol. 39, no. 10, pp. 893-906, 2001.

[185] J. Sidbury, E. K. Smith, and W. Harlan, "An inborn error of short-chain fatty acid metabolism: the odor-of-sweaty-feet syndrome," *The Journal of pediatrics,* vol. 70, no. 1, pp. 8-15, 1967.

[186] V. S. Kodogiannis, J. N. Lygouras, A. Tarczynski, and H. S. Chowdrey, "Artificial odor discrimination system using electronic nose and neural networks for the identification of urinary tract infection," *IEEE Transactions on Information Technology in Biomedicine,* vol. 12, no. 6, pp. 707-713, 2008.

[187] N. Hayward, T. Jeavons, A. Nicholson, and A. Thornton, "Methyl mercaptan and dimethyl disulfide production from methionine by Proteus species detected by head-space gas-liquid chromatography," *Journal of clinical microbiology,* vol. 6, no. 3, pp. 187-194, 1977.

[188] T. Davies and N. Hayward, "Volatile products from acetylcholine as markers in the rapid urine test using head-space gas—liquid chromatography," *Journal of Chromatography B: Biomedical Sciences and Applications,* vol. 307, pp. 11-21, 1984.

[189] J. M. Zechman, S. Aldinger, and J. N. Labows, "Characterization of pathogenic bacteria by automated headspace concentration—gas chromatography," *Journal*

of Chromatography B: Biomedical Sciences and Applications, vol. 377, pp. 49-57, 1986.

[190] J. Najarian, "The diagnostic importance of the odor of urine," *The New England journal of medicine,* vol. 303, no. 19, p. 1128, 1980.

[191] E. Expert Panel on Detection, "Executive summary of the Third Report of the National Cholesterol Education Program (NCEP) expert panel on detection, evaluation, and treatment of high blood cholesterol in adults (Adult Treatment Panel III)," *Jama,* vol. 285, no. 19, p. 2486, 2001.

[192] S. Watanabe, M. Hojo, and A. Nagahara, "Metabolic syndrome and gastrointestinal diseases," *Journal of gastroenterology,* vol. 42, no. 4, pp. 267-274, 2007.

[193] G. r. Locke, N. J. Talley, S. L. Fett, A. R. Zinsmeister, and L. r. Melton, "Prevalence and clinical spectrum of gastroesophageal reflux: a population-based study in Olmsted County, Minnesota," *Gastroenterology,* vol. 112, no. 5, pp. 1448-1456, 1997.

[194] L. Murray *et al.*, "Relationship between body mass and gastro-oesophageal reflux symptoms: The Bristol Helicobacter Project," *International Journal of Epidemiology,* vol. 32, no. 4, pp. 645-650, 2003.

[195] C. Clinic. (2017). *Gastrointestinal Disorders*. Available: https://my.clevelandclinic.org/health/articles/7040-gastrointestinal-disorders

[196] A. D. Wilson, "Recent Applications of Electronic-Nose Technologies for the Noninvasive Early Diagnosis of Gastrointestinal Diseases."

[197] A. Roine *et al.*, "Detection of prostate cancer by an electronic nose: a proof of principle study," *The Journal of urology,* vol. 192, no. 1, pp. 230-235, 2014.

[198] J. A. Covington *et al.*, "Application of a novel tool for diagnosing bile acid diarrhoea," *Sensors,* vol. 13, no. 9, pp. 11899-11912, 2013.

[199] A. Pavlou, A. Turner, and N. Magan, "Recognition of anaerobic bacterial isolates in vitro using electronic nose technology," *Letters in applied microbiology,* vol. 35, no. 5, pp. 366-369, 2002.

[200] M. Bruins *et al.*, "Device-independent, real-time identification of bacterial pathogens with a metal oxide-based olfactory sensor," *European journal of clinical microbiology & infectious diseases,* vol. 28, no. 7, pp. 775-780, 2009.

[201] V. Kodogiannis and E. Wadge, "The use of gas-sensor arrays to diagnose urinary tract infections," *International journal of neural systems,* vol. 15, no. 05, pp. 363-376, 2005.

[202] A. Roine *et al.*, "Rapid and accurate detection of urinary pathogens by mobile IMS-based electronic nose: a proof-of-principle study," *PLoS One,* vol. 9, no. 12, p. e114279, 2014.

[203] R. P. Arasaradnam *et al.*, "Differentiating Coeliac disease from irritable bowel syndrome by urinary volatile organic compound analysis–a pilot study," *PloS one,* vol. 9, no. 10, p. e107312, 2014.

[204] R. Arasaradnam *et al.*, "Evaluation of gut bacterial populations using an electronic e-nose and field asymmetric ion mobility spectrometry: further

insights into 'fermentonomics'," *Journal of medical engineering & technology,* vol. 36, no. 7, pp. 333-337, 2012.

[205] J. Kwak, C. C. Grigsby, B. R. Smith, M. M. Rizki, and G. Preti, "Changes in volatile compounds of human urine as it ages: Their interaction with water," *Journal of Chromatography B,* vol. 941, pp. 50-53, 2013.

[206] J. Kwak, C. C. Grigsby, G. Preti, M. M. Rizki, K. Yamazaki, and G. K. Beauchamp, "Changes in volatile compounds of mouse urine as it ages: Their interactions with water and urinary proteins," *Physiology & behavior,* vol. 120, pp. 211-219, 2013.

[207] O. M. Ltd. (2017). *ATLAS Headspace Sampler*. Available: https://www.owlstonemedical.com/products/atlas/

[208] I. Federation, "IDF diabetes atlas: International Diabetes Federation," *Executive Office,* 2011.

[209] W. Ping, T. Yi, X. Haibao, and S. Farong, "A novel method for diabetes diagnosis based on electronic nose," *Biosensors and Bioelectronics,* vol. 12, no. 9, pp. 1031-1036, 1997.

[210] H. Lin *et al.*, "Rapid discrimination of Apiaceae plants by electronic nose coupled with multivariate statistical analyses," *Journal of pharmaceutical and biomedical analysis,* vol. 84, pp. 1-4, 2013.

[211] S. Dragonieri *et al.*, "An electronic nose in the discrimination of patients with asthma and controls," *Journal of Allergy and Clinical Immunology,* vol. 120, no. 4, pp. 856-862, 2007.

[212] M. B. Kursa and W. R. Rudnicki, "Feature selection with the Boruta package," *J Stat Softw,* vol. 36, no. 11, pp. 1-13, 2010.

[213] E. Schaller, J. O. Bosset, and F. Escher, "'Electronic noses' and their application to food," *LWT-Food Science and Technology,* vol. 31, no. 4, pp. 305-316, 1998.

[214] Owlstone. (2017, 21/08). *OVG-4*. Available: https://www.owlstoneinc.com/products/ovg-4/

[215] O. Ltd. (2008, 21/08). *GEN-SYS User Manual* Available: https://www.owlstoneinc.com/products/gen-sys-products/

[216] F. S. Company. (2017, 23/08/2017). *Understanding the difference between absolute, gage and differential pressure*. Available: https://www.first-sensor.com/en/products/pressure-sensors/pressure-sensors-and-transmitters/pressure-types.html

[217] F. Semiconductor. (2012, 24/08/2017). *50 kPa On-Chip Temperature Compensated and Calibrated Silicon Pressure Sensors*. Available: http://www.farnell.com/datasheets/2291656.pdf?_ga=2.81494039.1427935608.1503530701-190300071.1500997265

[218] V. Oyj. (2013, 24/08/2017). *HUMIDITY CONVERSION FORMULAS*. Available: http://www.vaisala.com/Vaisala%20Documents/Application%20notes/Humidity_Conversion_Formulas_B210973EN-F.pdf

[219] Clairair. (09/09/2017). *Prime IR sensors*. Available: http://www.clairair.co.uk/products/prime-ir-sensors/

[220] Clairair. (09/09/2017). *OEM Transmitters*. Available: http://www.clairair.co.uk/products/oem-transmitters/

[221] A. air. (2013, 09/09/2017). *NDIR*. Available: http://www.alphasense.com/index.php/products/ndir-air/

[222] Alphasense. (2013, 10/09/2017). *Analogue Front End (AFE); Alphasense A4 Air Quality Gas Sensor Alphasense A4 Air Quality Gas Sensors*. Available: http://www.alphasense.com/WEB1213/wp-content/uploads/2015/11/AFE.pdf

[223] (2015). *The HITRAN Database*. Available: https://www.cfa.harvard.edu/hitran/

[224] INFRATEC. *Tunable detectors (FPI detectors)*. Available: http://www.infratec.co.uk/sensor-division/products/variable-color-detectors.html

[225] N. Neumann, M. Ebermann, S. Kurth, and K. Hiller, "Tunable infrared detector with integrated micromachined Fabry-Perot filter," *Journal of Micro/Nanolithography, MEMS, and MOEMS,* vol. 7, no. 2, pp. 021004-021004-9, 2008.

[226] A. AG. (2017). *EMIRS200*. Available: https://www.axetris.com/en/irs/products/emirs200/to39-with-reflector1#country-list

[227] PJRC. *Teensy 3.6 USB Development Board*. Available: https://www.pjrc.com/store/teensy36.html

[228] D. L. S. R. D. I. E. Gordon., "High-resolution transmission molecular absorption database.," in *The HITRAN database*, ed. Atomic and Molecular Physics Division, Harvard-Smithsonian Center, 2015.

[229] N. I. o. S. a. T. (NIST). (2017). *NIST Standard Reference Database Number 69*. Available: http://webbook.nist.gov/cgi/cbook.cgi?ID=C74828&Type=IR-SPEC&Index=1

[230] S. Siyang, C. Wongchoosuk, and T. Kerdcharoen, "Diabetes diagnosis by direct measurement from urine odor using electronic nose," in *Biomedical Engineering International Conference (BMEiCON), 2012*, 2012, pp. 1-4: IEEE.

[231] Z. Wang and C. Wang, "Is breath acetone a biomarker of diabetes? A historical review on breath acetone measurements," *Journal of breath research,* vol. 7, no. 3, p. 037109, 2013.